

1  
2  
3  
4  
5  
6  
7  
8  
9  
10  
11  
12  
13  
14  
15  
16  
17  
18  
19  
20  
21  
22  
23  
24  
25  
26  
27  
28  
29  
30  
31  
32  
33  
34  
35  
36  
37  
38  
39  
40  
41  
42  
43  
44  
45  
46  
47  
48  
49  
50  
51  
52  
53  
54  
55  
56  
57  
58  
59  
60  
61  
62  
63  
64  
65

**U-Pb, Re-Os, AND Ar/Ar GEOCHRONOLOGY OF REE-RICH BRECCIA PIPES  
AND ASSOCIATED HOST ROCKS FROM THE MESOPROTEROZOIC PEA  
RIDGE Fe-REE-Au DEPOSIT, ST. FRANCOIS MOUNTAINS, MISSOURI, USA**

J.N. Aleinikoff<sup>1</sup>, D. Selby<sup>2</sup>, J.F. Slack<sup>3</sup>, W.C. Day<sup>1</sup>, R.M. Pillers<sup>1</sup>, M.A. Cosca<sup>1</sup>, C.M. Seeger<sup>4</sup>, C.M. Fanning<sup>5</sup>, I.M. Samson<sup>6</sup>

<sup>1</sup> U.S. Geological Survey, Denver Federal Center, Box 25046, Denver, CO 80225

<sup>2</sup> Department of Earth Sciences, University of Durham, Durham United Kingdom DH1 3LE

<sup>3</sup> U.S. Geological Survey, National Center, MS 954, Reston, VA 20192

<sup>4</sup> Missouri Department of Natural Resources, Rolla, MO 65402

<sup>5</sup> Research School of Earth Sciences The Australian National University, Canberra, ACT, Australia 0200

<sup>6</sup> Department of Earth and Environmental Sciences, University of Windsor, Windsor, ON, Canada N9B 3P4

---

Corresponding author; e-mail: [jaleinikoff@usgs.gov](mailto:jaleinikoff@usgs.gov)

1  
2  
3  
4  
5  
6  
7  
8  
9  
10  
11  
12  
13  
14  
15  
16  
17  
18  
19  
20  
21  
22  
23  
24  
25  
26  
27  
28  
29  
30  
31  
32  
33  
34  
35  
36  
37  
38  
39  
40  
41  
42  
43  
44  
45  
46  
47  
48  
49  
50  
51  
52  
53  
54  
55  
56  
57  
58  
59  
60  
61  
62  
63  
64  
65

## ABSTRACT

Rare earth element (REE)-rich breccia pipes (600,000 t @ 12% REO) are preserved along the margins of the 136 Mt Pea Ridge magnetite-apatite deposit, within Mesoproterozoic (~1.47 Ga) volcanic-plutonic rocks of the St. Francois Mountains terrane in southeastern Missouri, USA. The breccia pipes cut the rhyolite-hosted magnetite deposit, and contain clasts of nearly all local bedrock and mineralized lithologies.

Grains of monazite and xenotime were extracted from breccia pipe samples for SHRIMP U-Pb geochronology; both minerals were also dated in one polished thin section. Monazite forms two morphologies: (1) matrix granular grains composed of numerous small (<50  $\mu\text{m}$ ) crystallites intergrown with rare xenotime, thorite, apatite, and magnetite; and (2) coarse euhedral, glassy, bright yellow grains similar to typical igneous or metamorphic monazite. Trace element abundances (including REE patterns) were determined on selected grains of monazite (both morphologies) and xenotime. Zircon grains from two samples of host rhyolite and two late felsic dikes collected underground at Pea Ridge were also dated. Additional geochronology done on breccia pipe minerals includes Re-Os on fine-grained molybdenite and  $^{40}\text{Ar}/^{39}\text{Ar}$  on muscovite, biotite, and K-feldspar.

Ages ( $\pm 2$ -sigma errors) obtained by SHRIMP U-Pb analysis are as follows: (1) zircon from the two host rhyolite samples have ages of  $1473.6 \pm 8.0$  and  $1472.7 \pm 5.6$  Ma; most zircon in late felsic dikes is interpreted as xenocrystic (age range ca. 1522-1455 Ma); a population of rare spongy zircon is likely of igneous origin and yields an age of  $1441 \pm 9$  Ma; (2) pale yellow granular monazite— $1464.9 \pm 3.3$  Ma (no dated xenotime);

1  
2  
3  
4  
5  
6  
7  
8  
9  
10 (3) reddish matrix granular monazite— $1462.0 \pm 3.5$  Ma and associated xenotime— $1453$   
11  $\pm 11$  Ma; (4) coarse glassy yellow monazite— $1464.8 \pm 2.1$ ,  $1461.7 \pm 3.7$  Ma, with rims at  
12  $1447.2 \pm 4.7$  Ma; and (5) matrix monazite (*in situ*)— $1464.1 \pm 3.6$  and  $1454.6 \pm 9.6$  Ma,  
13 and matrix xenotime (*in situ*)— $1468.0 \pm 8.0$  Ma. Two slightly older ages of cores are  
14 about 1478 Ma. The young age of rims on the coarse glassy monazite coincides with a  
15 Re-Os age of  $1440.6 \pm 9.2$  Ma determined in this study for molybdenite intergrown with  
16 quartz and allanite, and with the age of monazite inclusions in apatite from the magnetite  
17 ore (Neymark et al., this volume). A  $^{40}\text{Ar}/^{39}\text{Ar}$  age of  $1473 \pm 1$  Ma was obtained for  
18 muscovite from a breccia pipe sample.  
19

20 Geochronology and trace element geochemical data suggest that the granular matrix  
21 monazite and xenotime (in polygonal texture), and cores of coarse glassy monazite  
22 precipitated from hydrothermal fluids during breccia pipes formation. The second  
23 episode of mineral growth at ca. 1443 Ma may be related to faulting and fluid flow that  
24 rebrecciated the pipes. The ca. 10 m.y. gap between the ages of host volcanic rocks and  
25 breccia pipe monazite and xenotime suggests that breccia pipe mineral formation cannot  
26 be related to the felsic magmatism represented by the rhyolitic volcanic rocks, and hence  
27 is linked to a different magmatic-hydrothermal system.  
28

## 29 INTRODUCTION

30 Mesoproterozoic rocks exposed in the St. Francois Mountains terrane of southeastern  
31 Missouri (USA) are in the eastern granite-rhyolite province of the Midcontinent region  
32 described by Van Schmus et al. (1996), Thomas et al. (2012), and Bickford et al. (2015).  
33 The crystalline basement of the St. Francois Mountains terrane is composed  
34 predominantly of felsic plutonic and volcanic rocks, having both A-type within-plate and  
35

1  
2  
3  
4  
5  
6  
7  
8  
9  
10  
11  
12  
13  
14  
15  
16  
17  
18  
19  
20  
21  
22  
23  
24  
25  
26  
27  
28  
29  
30  
31  
32  
33  
34  
35  
36  
37  
38  
39  
40  
41  
42  
43  
44  
45  
46  
47  
48  
49  
50  
51  
52  
53  
54  
55  
56  
57  
58  
59  
60  
61  
62  
63  
64  
65

I- and S-type volcanic arc compositions, with lesser amounts of mafic to intermediate-composition rocks (Day et al., this volume). Rhyolitic volcanic rocks host numerous iron oxide-apatite (IOA) deposits and at least one iron oxide-copper-gold (IOCG) deposit that together constitute the Missouri iron metallogenic province (Kisvarsanyi and Procter, 1967; Snyder, 1968; Nold et al., 2014). Although several of these deposits were mined until the late 20<sup>th</sup> century (i.e., Pea Ridge, Iron Mountain, lower Pilot Knob), all of the IOA mines are presently inactive; no IOCG deposits have been mined.

During the mining of magnetite ore at the Pea Ridge deposit, four breccia pipes were discovered (Husman, 1989; Seeger, 1992). These pipes have unusually elevated abundances of rare earth elements (REE), contain local gold concentrations (up to 10.8 oz/t; Husman, 1989), and have been considered attractive mining targets owing to anomalously high heavy REE (HREE) contents that reside mostly in xenotime (Nuelle et al., 1992). These breccia pipes contrast with better known, light REE (LREE)-rich deposits at Mountain Pass, California, and Bayan Obo, China (e.g., Wall, 2014). Global exploration for HREE-rich mineral deposits has increased recently owing to the critical importance of HREE in manufacturing modern technological products, including computers, cell phones, and rechargeable batteries.

In order to better understand the origin of the Pea Ridge REE-rich breccia pipes, the U.S. Geological Survey (USGS) initiated a project in 2012 to investigate the mineralogy, age, petrology, and origin of the Pea Ridge IOA deposit. Results described herein build on previous investigations by the USGS in the late 1980s and early 1990s as part of the Strategic and Critical Minerals Program in the Midcontinent region, and on topical and regional studies conducted in collaboration with the Missouri Geological Survey (e.g.,

1  
2  
3  
4  
5  
6  
7  
8  
9  
10  
11  
12  
13  
14  
15  
16  
17  
18  
19  
20  
21  
22  
23  
24  
25  
26  
27  
28  
29  
30  
31  
32  
33  
34  
35  
36  
37  
38  
39  
40  
41  
42  
43  
44  
45  
46  
47  
48  
49  
50  
51  
52  
53  
54  
55  
56  
57  
58  
59  
60  
61  
62  
63  
64  
65

Day et al., 1992; Nuelle et al., 1992; Sidder et al., 1993; Seeger et al., 2001). Although the Pea Ridge mine closed in 2001 and all underground workings became inaccessible, archived samples from earlier work, and drill core stored at the Pea Ridge mine and the Missouri Department of Natural Resources, were available for our new studies. In addition, recent advances in analytical techniques permit the acquisition of more accurate and precise geochronological data, resulting in improved interpretations of the geology and mineralization.

The specific purpose of this study is to establish a temporal framework for the Pea Ridge breccia pipes and associated igneous rocks, using (1) U-Pb ages of zircon from host rhyolites and from late cross-cutting felsic dikes; (2) U-Pb ages of monazite and xenotime, a Re-Os age molybdenite, and a  $^{40}\text{Ar}/^{39}\text{Ar}$  age of muscovite from the Pea Ridge breccia pipes; and (3) variations in trace element and REE abundances in monazite and xenotime as petrogenetic tracers. The ultimate goal is to constrain the timing of breccia pipe formation and, in concert with data obtained by other analytical methods, derive a genetic model for the origin of this potential REE resource. For information on related findings, the reader is referred to other papers in this special issue by Ayuso et al., Day et al., Johnson et al., Hofstra et al., Neymark et al., Harlov et al., and Starkey and Seeger.

**GEOLOGIC SETTING**

*Regional bedrock geology*

The St. Francois Mountains terrane is composed primarily of Mesoproterozoic (~1.48-1.32 Ga) plutonic and volcanic rocks that are unconformably overlain by early

1  
2  
3  
4  
5  
6  
7  
8  
9  
10  
11  
12  
13  
14  
15  
16  
17  
18  
19  
20  
21  
22  
23  
24  
25  
26  
27  
28  
29  
30  
31  
32  
33  
34  
35  
36  
37  
38  
39  
40  
41  
42  
43  
44  
45  
46  
47  
48  
49  
50  
51  
52  
53  
54  
55  
56  
57  
58  
59  
60  
61  
62  
63  
64  
65

Paleozoic (Cambrian to Ordovician) sedimentary rocks (Van Schmus et al., 1996). Very little Mesoproterozoic sedimentary material has been identified within the volcanic sequence (cf. Orndorff et al., 1999; McDowell and Harrison, 2000; Day et al., this volume). The distribution of Mesoproterozoic igneous rocks (Fig. 1) was compiled by Kisvarsanyi (1981) based on previous regional mapping (Tolman and Robertson, 1969; Pratt et al., 1979, Pratt et al., 1992), drill core from mining company exploration in the region, and data from regional airborne magnetic surveys. As reviewed by Day et al. (this volume), current interpretations suggest that the plutonic rocks comprise a series of subvolcanic massifs, ring intrusions, and plutons of metaluminous to peraluminous composition (Kisvarsanyi, 1980; Menuge et al., 2002; and references therein). The intrusive rocks are overlain by contemporaneous and comagmatic felsic volcanic rocks mostly of rhyolitic composition, which have been linked to sources in five ash-flow calderas (Fig. 1) (Pratt et al., 1979; Sides et al., 1981; Brown, 1989; Lowell, 1991). Gabbro forms small plutons and dikes (Van Schmus et al., 1996; Lowell and Young, 1999; Walker et al., 2002, and references therein); subvolcanic mafic to intermediate-composition rocks are relatively minor, although significant volumes of similar mafic rocks may be present at depth. Geochemical and radiogenic isotope (Sr, Nd, Pb) data suggest that the Mesoproterozoic basement rocks formed as juvenile magma, with minimal input from preexisting continental crust (Menuge et al., 2002; Walker et al., 2002; Ayuso et al., this volume; Day et al., this volume).

*Pea Ridge iron ore deposit*

1  
2  
3  
4  
5  
6  
7  
8  
9  
10  
11 Iron ore in the vicinity of Pea Ridge was discovered in 1950 during a regional  
12 airborne magnetic survey (Emery, 1968). After additional delineation by ground  
13 magnetic surveys, mining began in 1964 and continued until the mine closed in 2001;  
14 total ore production was 136 Mt (Seeger, 2003). The Pea Ridge iron ore deposit is a  
15 discordant tabular body hosted by Mesoproterozoic high-silica rhyolite tuff. The iron  
16 deposit consists of four main zones (Day et al., this volume) (Fig. 2). From oldest to  
17 youngest, these zones are (1) amphibole-quartz zone developed along the margins of the  
18 deposit; (2) core zone composed of massive magnetite and various iron oxide-cemented  
19 heterolithic breccias and pseudobreccias (wall rock partially replaced by iron ore along  
20 fractures); (3) specular hematite zone at the top and along the northwest margin of the  
21 deposit; and (4) silicified zone at the transition between the magnetite core and rhyolitic  
22 country rock. Four REE-rich breccia pipes cut the footwall rocks and contain xenoliths  
23 derived from each of the four mineralogic zones. Felsic and altered mafic dikes intrude  
24 each zone, except for the breccia pipes. Detailed geologic, mineralogic, and geochemical  
25 descriptions of the Pea Ridge iron ore deposit are presented by Emery (1968), Nuelle et  
26 al. (1992), Sidder et al. (1993), Seeger et al. (2001), and Kerr (1998). Nold et al. (2014)  
27 and Day et al. (this volume) provide information on the regional geologic setting and  
28 character of other iron deposits in the St. Francois Mountains terrane. Harlov et al. (this  
29 volume), Hofstra et al. (this volume), and Neymark et al. (this volume) studied the  
30 mineralogy and geochemistry of magnetite-hosted apatite (which typically contains  
31 abundant monazite inclusions) to discern the age and origin of the iron and REE  
32 mineralization.  
33  
34  
35  
36  
37  
38  
39  
40  
41  
42  
43  
44  
45  
46  
47  
48  
49  
50  
51  
52  
53  
54  
55  
56  
57  
58  
59  
60  
61  
62  
63  
64  
65

1  
2  
3  
4  
5  
6  
7  
8  
9  
10  
11  
12  
13  
14  
15  
16  
17  
18  
19  
20  
21  
22  
23  
24  
25  
26  
27  
28  
29  
30  
31  
32  
33  
34  
35  
36  
37  
38  
39  
40  
41  
42  
43  
44  
45  
46  
47  
48  
49  
50  
51  
52  
53  
54  
55  
56  
57  
58  
59  
60  
61  
62  
63  
64  
65

The origin of the Pea Ridge magnetite deposit is unresolved. Nold et al. (2014) suggested that the deposit crystallized from an iron oxide magma and was subsequently metasomatized by late, magmatically derived hydrothermal fluids. Preliminary fluid inclusion studies of interstitial gangue quartz from the magnetite ore zone, which therefore represents minimum ore-forming temperatures, are consistent with high temperatures (>450°C) and high salinities, in accord with models in which the primary ore-forming fluids have magmatic-hydrothermal origins (Day et al., 1992; Sidder et al., 1993). Paragenetically later REE-rich breccia pipes appear to have formed from fluids that were significantly cooler (about 300°C) during explosive emplacement (Sidder et al., 1993). Recent detailed work on fluid inclusion thermometry and geochemistry (Hofstra et al., this volume) provides critical and more refined information concerning the physiochemical conditions that prevailed during formation of the breccia pipes.

*Pea Ridge breccia pipes*

The four REE-rich breccia pipes were encountered at a depth of about 2275 ft (see schematic cross section, Fig. 2). The breccia pipes must be amongst the youngest rocks in the Pea Ridge deposit area because (1) they cut the rhyolite-hosted magnetite deposit, and (2) they contain clasts of nearly all local bedrock and mineralized lithologies (including hydrothermally altered rocks). However, age relations with numerous small felsic dikes (cf. Day et al., this volume) are indeterminate because contacts between these dikes and the breccia pipes are absent. The breccia pipes are relatively small, have maximum widths of about 15 m, maximum strike lengths of 60 m, and maximum vertical extents of 120 m (Husman, 1989; Nuelle et al., 1992; Sidder et al., 1993); the pipes may

1  
2  
3  
4  
5  
6  
7  
8  
9  
10 converge into a greater volume of REE-bearing rock at depth (Seeger, 1992). They are  
11 both matrix- and clast-supported. In mining nomenclature, three of the pipes are termed  
12 “soft” (i.e., friable), whereas the fourth pipe is termed “hard” (i.e., indurated). The  
13  
14 “soft” (i.e., friable), whereas the fourth pipe is termed “hard” (i.e., indurated). The  
15  
16 cause(s) for the “hard” vs. “soft” nature of the breccia pipes is unknown, but may reflect  
17  
18 the effects of late faulting and local deep weathering. On the basis of mineralogy,  
19  
20 Kerr (1998) defined two types of breccia pipes (I and II), both dominated by an  
21  
22 assemblage of monazite-xenotime-rutile-thorite-hematite-quartz. Type I also includes  
23  
24 late-stage allanite, apatite, and REE-fluorcarbonate minerals, whereas Type II contains  
25  
26 clasts of rock altered to K-feldspar and barite. Sidder et al. (1993) considered the breccia  
27  
28 pipes to have been deposited by late-stage fluids, emplaced explosively within magnetite  
29  
30 ore at about 300°C.

31  
32 The breccia pipes are important because they contain very high REE contents  
33  
34 (Husman, 1989); average total REE as RE<sub>2</sub>O<sub>3</sub> is ca. 20 wt % (Nuelle et al., 1992). The  
35  
36 most abundant REE-bearing mineral is monazite [(Ce,La,Nd,Th)PO<sub>4</sub>]; widespread, but  
37  
38 not ubiquitous, xenotime (YPO<sub>4</sub>) is also important because of its relative enrichment in  
39  
40 HREE. The potential economic significance of the Pea Ridge REE-rich breccia pipes is  
41  
42 indicated by HREE contents that rival those of the Dotson zone at Bokan Mountain,  
43  
44 Alaska, and that are significantly higher than those of other world-class REE deposits  
45  
46 such as Mountain Pass, California, and Bayan Obo, China (Fig. 3). Other less abundant,  
47  
48 REE-bearing minerals reported in the Pea Ridge breccia pipes include bastnaesite  
49  
50 [(Ce,La,Y)CO<sub>3</sub>F], britholite [(Ce,Ca,Th,La,Nd)<sub>5</sub>(SiO<sub>4</sub>,PO<sub>4</sub>)<sub>3</sub>(OH,F)], synchysite  
51  
52 [Ca(Ce,La)(CO<sub>3</sub>)<sub>2</sub>F], and allanite [Ce,Ca,Y,La)<sub>2</sub>(Al,Fe)<sub>3</sub>(SiO<sub>4</sub>)<sub>3</sub>(OH)] (Sidder et al.,  
53  
54 1993; Kerr, 1998; Ayuso et al., this volume; Harlov et al., this volume).  
55  
56  
57  
58  
59  
60  
61  
62  
63  
64  
65

1  
2  
3  
4  
5  
6  
7  
8  
9  
10  
11  
12 **PREVIOUS GEOCHRONOLOGY**  
13

14 Previous geochronological studies of igneous basement rocks of the St. Francois  
15 Mountains terrane involved dating multi-grain fractions of zircon by thermal ionization  
16 mass spectrometry (TIMS; cf. Bickford and Mose, 1975; Van Schmus et al., 1996).  
17  
18 These studies demonstrated that emplacement of the Mesoproterozoic igneous rocks  
19  
20 occurred during two episodes of magmatism: (1) in the early Mesoproterozoic at ~1.49-  
21  
22 1.44 Ga, and (2) in the middle Mesoproterozoic at ~1.39-1.34 Ga (Van Schmus et al.,  
23  
24 1996; Bickford et al., 2015), with an intervening hiatus of at least 50 m.y. Most of this  
25  
26 large data set is based on analysis of basement samples obtained from drill core; a few  
27  
28 outcrop samples were also dated. More recently, high-precision TIMS dating techniques  
29  
30 were applied to several additional basement samples, yielding similar, although more  
31  
32 precise and accurate ages (Harrison et al., 2000; Harrison et al., 2002; Thomas et al.,  
33  
34 2012). Two U-Pb dates determined by Van Schmus et al. (1996),  $1473 \pm 3$  Ma for the  
35  
36 host rhyolite at Pea Ridge and  $1466 \pm 4$  Ma for a crystal of xenotime collected from a  
37  
38 quartz vein adjacent to a breccia pipe underground in the mine, are directly applicable to  
39  
40 the present study.  
41

42 Whole-rock Rb-Sr analysis of igneous country rocks in early studies yielded ages that  
43  
44 are systematically younger than the zircon U-Pb ages, leading to the conclusion that the  
45  
46 Rb-Sr isotopic system was disturbed by the loss of radiogenic Sr (Bickford and Mose,  
47  
48 1975; Seeger, 2003). The cause(s) of this disturbance is unknown, but may be related to  
49  
50 K-metasomatism (Seeger, 2003) associated with younger Mesoproterozoic igneous  
51  
52  
53  
54  
55  
56  
57  
58  
59  
60  
61  
62  
63  
64  
65

1  
2  
3  
4  
5  
6  
7  
8  
9  
10 activity and/or to effects that accompanied late Paleozoic fluid flow during Mississippi  
11 Valley-type (MVT) ore deposition in the overlying Paleozoic sedimentary rocks.  
12  
13

14 Whole-rock Nd isotopic data for felsic volcanic rocks and granitic plutonic rocks  
15 yield  $\epsilon\text{Nd}_{(t)}$  values mostly in the range of 2 to 5 (Van Schmus et al., 1996; Menuge et al.,  
16 2002). These values correspond to model ages ( $T_{\text{DM}}$ ) of about 1.60-1.45 Ga. Using Nd  
17 isotopic systematics, Van Schmus et al. (1996) proposed a regional crustal boundary  
18 trending NE-SW across south-central Missouri. Rocks to the northwest of this boundary  
19 have  $T_{\text{DM}}$  ages  $>1.55$  Ga, whereas rocks to the southeast, including Mesoproterozoic  
20 crystalline rocks of the St. Francois Mountains terrane, have  $T_{\text{DM}}$  ages  $<1.55$  Ga  
21 suggesting derivation from juvenile sources. Ayuso et al. (this volume) present new Nd  
22 isotope data related to the Pea Ridge deposit and environs.  
23  
24  
25  
26  
27  
28  
29  
30  
31

### 32 33 **GEOCHRONOLOGY** 34

35 To understand the timing of emplacement and origin of the REE-rich breccia pipes at  
36 Pea Ridge, we pursued several related geochronologic investigations, including (1) U-Pb  
37 sensitive high resolution ion microprobe (SHRIMP) dating of zircon from rhyolite host  
38 rocks, (2) U-Pb SHRIMP dating of monazite and xenotime (in grain mounts of mineral  
39 separates and *in situ* using polished thin sections) from several breccia pipe samples (both  
40 “hard” and “soft” varieties), (3) TIMS Re-Os dating of molybdenite from the hard breccia  
41 pipe, and (4) Ar/Ar dating of muscovite, biotite, and K-feldspar from a breccia pipe  
42 sample. In addition, monazite and xenotime were analyzed by SHRIMP for trace  
43 element and REE abundances. Note that no zircon was recovered from any of the breccia  
44 pipe samples. Neymark et al. (this volume) report TIMS and laser ablation-inductively  
45  
46  
47  
48  
49  
50  
51  
52  
53  
54  
55  
56  
57  
58  
59  
60  
61  
62  
63  
64  
65

1  
2  
3  
4  
5  
6  
7  
8  
9  
10 coupled plasma mass spectrometry (LA-ICP-MS) ages of apatite from magnetite ore,  
11 SHRIMP and LA-ICP-MS dates for monazite inclusions within apatite from magnetite  
12 ore, and TIMS and LA-ICP-MS analyses of pyrite from magnetite ore to constrain the  
13  
14 initial Pb isotopic composition at the time of magnetite ore formation.  
15  
16  
17

18 Detailed descriptions of sample preparation procedures and analytical methods are  
19 provided in the Appendix. All weighted average ages reported here are cited with 2-  
20  
21 sigma uncertainties.  
22  
23  
24

## 25 **U-Pb RESULTS**

### 26 *Host rocks*

27  
28 To verify the previous multi-grain TIMS analysis of Pea Ridge host rhyolite (Van  
29 Schmus et al., 1996), two new samples of rhyolite, both from the 2275 ft level in the  
30  
31 mine, were dated by SHRIMP U-Pb geochronology. Sample PR-12, from a unit  
32  
33 originally defined by Husman (1989) as the “black rhyolite,” is a crystal-rich, quartz-  
34  
35 feldspar rhyolite tuff. Coarse-grained quartz and feldspar phenocrysts, which make up  
36  
37 25-30 vol % of the rock, are commonly fractured and broken, and set in a black, fine-  
38  
39 grained matrix. Pseudomorphs of primary mafic mineral clots are completely replaced by  
40  
41 fine-grained intergrowths of hornblende+biotite+magnetite+plagioclase. Primary  
42  
43 plagioclase phenocrysts are moderately altered to sericite.  
44  
45

46 The second dated host rhyolite sample (PR-91) is from the “2275 Porphyry.” It  
47  
48 contains coarse-grained phenocrysts of antiperthitic plagioclase having irregular  
49  
50 boundaries, and lesser amounts of euhedral quartz phenocrysts, set in a fine- to medium-  
51  
52 grained matrix composed of quartz and feldspar. The rock contains 12-15 vol %  
53  
54  
55  
56  
57  
58  
59  
60  
61  
62  
63  
64  
65

1  
2  
3  
4  
5  
6  
7  
8  
9  
10 phenocrysts. Fine-grained Fe-oxides (1-3 vol %) are disseminated uniformly throughout  
11 the sample. Quartz phenocrysts display undulatory extinction. For a detailed description  
12 of the distribution and geochemistry of the host rocks in the Pea Ridge mine, the reader is  
13 referred to Day et al. (this volume) and Day and Granitto (2014).  
14  
15

16  
17  
18 Zircon from both rhyolite samples is euhedral and blocky, having length-to-width  
19 (l/w) ratios of about 2-3. All grains display fine, concentric, growth (locally oscillatory)  
20 zoning in cathodoluminescence (CL) images (Fig. 4A, C). Twenty SHRIMP analyses of  
21 zircon grains from each sample yield concordant U-Pb isotopic data (Fig. 4B, D). Using  
22 the concordant data, the time of crystallization of zircon from each sample is calculated  
23 by determining (1) weighted averages of  $^{207}\text{Pb}/^{206}\text{Pb}$  ages (insets in Fig. 4B, D), and (2) a  
24 Concordia Age (Ludwig, 1980; 2003). The weighted average ages are  $1473.6 \pm 8.0$  Ma  
25 and  $1472.7 \pm 5.6$  Ma for samples PR-12 and PR-91, respectively; Concordia Ages are  
26  $1473.2 \pm 8.7$  Ma and  $1470.2 \pm 5.5$  Ma, respectively. These ages are identical, within  
27 uncertainty, to the  $1474 \pm 6$  Ma TIMS age determined by Van Schmus et al. (1996) for  
28 rhyolite from the Pea Ridge mine (their sample MOWA-PR2). The ages for the host  
29 rocks reported herein provide a maximum age for the emplacement of the Pea Ridge  
30 magnetite-apatite deposit and associated REE-rich breccia pipes.  
31  
32  
33  
34  
35  
36  
37  
38  
39  
40  
41  
42  
43

#### 44 *Late cross-cutting dikes*

45  
46 Two samples of felsic dikes (also termed alaskite or aplite; Day and Granitto,  
47 2014) were collected for SHRIMP analysis in order to determine minimum ages of the  
48 magnetite ore, and by inference the youngest igneous activity at Pea Ridge. These  
49 samples are medium-grained, hypidomorphic, nonfoliated leucogranite, and fine-grained  
50  
51  
52  
53  
54  
55  
56  
57  
58  
59  
60  
61  
62  
63  
64  
65

1  
2  
3  
4  
5  
6  
7  
8  
9  
10 pink aplite. Quartz phenocrysts are anhedral and have irregular patches that display  
11 undulatory extinction. Microcline contains small blebs of quartz and  
12 plagioclase. Sericite replaces primary plagioclase phenocrysts.  
13

14 Two morphologies of zircon occur in samples 966-5 (white leucogranite) and PR-  
15 25 (pink aplite): (1) euhedral, prismatic ( $l/w = 2-4$ ) grains composed primarily of fine  
16 concentric, growth-zoned cores overgrown by narrow, spongy, dark (in CL) rims (Fig.  
17 5A, E); and (2) subhedral, spongy, dark (in CL) grains that locally contain euhedral,  
18 poorly zoned cores (Fig 5C). Due to variable degrees of preservation, the most  
19 appropriate candidates for SHRIMP U-Pb analysis are grains of the type 1 morphology.  
20 Sample 966-5 yielded a significant quantity of zircon; numerous grains of each  
21 morphology were available for SHRIMP dating. In contrast, only a few grains were  
22 obtained from sample PR-25.  
23

24 Grains of type 1 morphology from both samples were dated. For sample 966-5,  
25 14 concordant analyses yield a range of  $^{207}\text{Pb}/^{206}\text{Pb}$  ages from  $1522 \pm 20$  to  $1455 \pm 15$   
26 Ma (1-sigma errors) (Table 1; Fig. 5B). For sample PR-25, 12 concordant analyses of  
27 cores define a range of  $^{207}\text{Pb}/^{206}\text{Pb}$  ages from  $1500 \pm 11$  to  $1459 \pm 15$  Ma (1-sigma errors)  
28 (Fig. 5F). These age ranges are similar to those obtained for zircon from the rhyolitic  
29 host rocks; the resulting weighted average ages for the dikes ( $1480 \pm 8$  Ma;  $1477 \pm 7$  Ma)  
30 are also similar to the calculated ages of the rhyolites. These data suggest that the  
31 relatively pristine, prismatic cores of zircon in the dikes are xenocrystic, and are not  
32 igneous grains that crystallized from magma that formed these late felsic dikes.  
33

34 Nineteen analyses of poorly zoned, dark zircon within subhedral spongy grains  
35 (type 2 morphology) from the 12 least-discordant analyses for sample 966-5 yield a  
36  
37  
38  
39  
40  
41  
42  
43  
44  
45  
46  
47  
48  
49  
50  
51

1  
2  
3  
4  
5  
6  
7  
8  
9  
10 weighted average of  $^{207}\text{Pb}/^{206}\text{Pb}$  ages of  $1441 \pm 9$  Ma (Table 1; Fig. 5D), interpreted as  
11 the crystallization age of this felsic dike. The discordant array trends toward a lower  
12 intercept of about 300 Ma (perhaps related to MVT fluid flow in nearby rocks). Due to  
13 the paucity of separated zircon, no type 2 grains from sample PR-25 were analyzed.  
14  
15  
16  
17  
18  
19

### 20 *Breccia pipes*

21 Both “soft” and “hard” breccia pipe types were sampled for SHRIMP U-Pb  
22 geochronology of monazite and xenotime. Four samples from the hard pipe were dated;  
23 these include mineral separates and grains analyzed *in situ* in polished thin sections in  
24 which textural relationships are preserved. Fine-grained monazite and xenotime grains,  
25 less than 25  $\mu\text{m}$  in diameter, are contained in the matrix that surrounds coarse breccia  
26 fragments; these minerals also form replacements of very coarse monazite (Fig. 6A).  
27 Textural relationships (i.e., similar grain size, polygonal grain boundaries) suggest that  
28 monazite and xenotime grains in the breccia matrix are coeval (Fig. 6B). Locally  
29 preserved in thin section are coarse, multigrain fragments of matrix material (Fig. 6C).  
30 Whether the granular (not granoblastic) nature of the matrix grains separated from whole-  
31 rock samples is probably the result of brecciation, likely not due to laboratory mineral  
32 separations.  
33  
34  
35  
36  
37  
38  
39  
40  
41  
42  
43

44 In sample PR95-30, monazite and xenotime occur as matrix material in the  
45 breccia pipes cementing clasts of the felsic volcanic host rocks, magnetite ore, and  
46 hematite ore (Fig. 7A). For both minerals in the matrix, grain sizes vary from about 10 to  
47 25  $\mu\text{m}$ . In addition, monazite also forms coarse individual grains as large as 100  $\mu\text{m}$  in  
48  
49  
50  
51  
52  
53  
54  
55  
56  
57  
58  
59  
60  
61  
62  
63  
64  
65

1  
2  
3  
4  
5  
6  
7  
8  
9  
10 diameter (Fig. 7B), and subhedral poikiloblastic grains up to nearly 3 cm in length  
11  
12 (Ayuso et al., this volume).  
13

14 Two populations of monazite can be distinguished based on Th/U. Ten analyses  
15 with Th/U of 1.9 to 3.4 yield a weighted average of  $^{207}\text{Pb}/^{206}\text{Pb}$  ages of  $1465.5 \pm 5.2$  Ma  
16  
17 (MSWD = 1.9); three analyses with Th/U of 15.0 to 16.7 have a weighted average of  
18  
19  $^{207}\text{Pb}/^{206}\text{Pb}$  ages of  $1454.6 \pm 9.6$  Ma (MSWD = 0.13) (Table 1; Fig. 7C). Although these  
20  
21 ages overlap within analytical uncertainty, differences in Th/U are significant, and  
22  
23 suggest that two growth episodes occurred.  
24

25 Isotopic data for xenotime in sample PR95-30 are slightly scattered (both  
26  
27 normally and reversely discordant). Excluding two analyses having somewhat higher  
28  
29 common Pb contents and lower  $^{207}\text{Pb}/^{206}\text{Pb}$  ages, 10 analyses yield a weighted average of  
30  
31  $^{207}\text{Pb}/^{206}\text{Pb}$  ages of  $1468.0 \pm 8.0$  Ma (MSWD = 1.75) (Fig. 7D), in agreement with the  
32  
33 monazite age. One statistically older analysis of about 1478 Ma was excluded from the  
34  
35 age calculation.  
36

37 Sample 2275-15, drill core from the hard pipe, was obtained on the 2275 ft level  
38  
39 of the mine. Granular aggregates composed of monazite and xenotime (plus minor  
40  
41 thorite) were extracted for SHRIMP U-Pb analysis (Fig. 8A, B). Seventeen (of 18)  
42  
43 SHRIMP U-Pb ages of matrix monazite yield concordant data with a weighted average of  
44  
45  $^{207}\text{Pb}/^{206}\text{Pb}$  ages of  $1462.0 \pm 3.5$  Ma (Table 1; Fig. 8C). One grain has a distinctly  
46  
47 younger  $^{207}\text{Pb}/^{206}\text{Pb}$  age of  $1448 \pm 7$  Ma. Five (of seven) xenotime analyses display a  
48  
49 weighted average of  $^{207}\text{Pb}/^{206}\text{Pb}$  ages of  $1453 \pm 11$  Ma (Fig. 8D). The relatively large  
50  
51 uncertainty associated with the xenotime age, a consequence of the small number of  
52  
53 analyses, precludes determining whether this weighted average age for xenotime is  
54  
55  
56  
57  
58  
59  
60  
61  
62  
63  
64  
65

1  
2  
3  
4  
5  
6  
7  
8  
9  
10 distinguishable from the monazite age. Two other xenotime analyses yield distinctly  
11 younger  $^{207}\text{Pb}/^{206}\text{Pb}$  ages of about 1405 Ma (Fig. 8D).  
12  
13

14 Sample PR-182 was a large rock sample (~5 kg) collected from the hard pipe  
15 exposed on the 2370 ft mine level. It is composed of coarse (up to 300  $\mu\text{m}$ ), broken  
16 crystals of barite, monazite, and K-feldspar in a clastic matrix of smaller (10-50  $\mu\text{m}$ )  
17 crystals of monazite, xenotime, quartz, and pyrite. The presence of small fragments of  
18 brecciated monazite and xenotime, partly cemented by pyrite (Fig. 9A), indicates that  
19 rebrecciation continued after deposition of these minerals. In addition to granular  
20 fragments of monazite and xenotime, many individual grains of relatively coarse (up to  
21 ca. 300  $\mu\text{m}$  diameter) monazite were obtained from this sample (Fig. 9A). These coarser  
22 grains are lemon yellow and glassy (Fig. 9B). In backscattered electron (BSE) images,  
23 many of the coarse glassy grains preserve faint zoning that delineates cores (slightly  
24 darker) and rims (slightly brighter) (Fig. 9C).  
25  
26  
27  
28  
29  
30  
31  
32  
33  
34

35 Granular monazite and xenotime from the matrix of sample PR-182 have very  
36 high proportions of common Pb, which results in age data with large uncertainties (3-  
37 28%); in contrast, 1-sigma errors for  $^{207}\text{Pb}/^{206}\text{Pb}$  data obtained from the other monazite  
38 samples range from about 0.3 to 1%). Isotopic data from coarse, glassy, yellow monazite  
39 are much more favorable for U-Pb geochronology owing to the very low contents of  
40 common Pb. Analyses of monazite cores in 39 grains yield concordant data with a  
41 weighted average of  $^{207}\text{Pb}/^{206}\text{Pb}$  ages of  $1464.8 \pm 2.1$  Ma (Table 1; Fig. 9D). Nine  
42 analyses of rims provide a weighted average of  $^{207}\text{Pb}/^{206}\text{Pb}$  ages of  $1447.2 \pm 4.7$  Ma (Fig.  
43  
44  
45  
46  
47  
48  
49  
50  
51  
52  
53  
54  
55  
56  
57  
58  
59  
60  
61  
62  
63  
64  
65

1  
2  
3  
4  
5  
6  
7  
8  
9  
10  
11       Sample 193488B is from a second large rock sample collected from the “hard”  
12 breccia pipe on the 2275 ft mine level. Like sample PR-182, it yielded two varieties of  
13 monazite (fine, granular, reddish grains, and coarse glassy yellow grains; Fig. 10A-C).  
14 Both of these varieties, plus granular xenotime, are intergrown with apatite (Fig. 10D).  
15 SEM-BSE imaging of the monazite reveals distinct cores and overgrowths (Fig. 10E).  
16 Neither granular mineral from 193488B was analyzed because of the poor U-Pb results  
17 obtained for granular monazite and xenotime in sample PR-182. Seventeen (of 18)  
18 analyses of cores of the coarse glassy monazite yield concordant data with a weighted  
19 average of  $^{207}\text{Pb}/^{206}\text{Pb}$  ages of  $1461.7 \pm 3.7$  Ma; six analyses of rims on the coarse grains  
20 yield a weighted average of  $^{207}\text{Pb}/^{206}\text{Pb}$  ages of  $1462.4 \pm 7.0$  Ma (Table 1; Fig. 10F).  
21 Unlike core and rim ages for coarse monazite from PR-182, which differ by about 20  
22 m.y., cores and rims in monazite from 193488B display obvious zoning differences, yet  
23 have statistically indistinguishable ages. One slightly older core yields a  $^{207}\text{Pb}/^{206}\text{Pb}$  age  
24 of  $1479 \pm 5$  Ma and was excluded from the age calculation.  
25  
26  
27  
28  
29  
30  
31  
32  
33  
34  
35  
36

37       The geochronology of one sample from a “soft” breccia pipe was also  
38 investigated. Sample PR-33C (about 0.25 kg) is from a pipe, exposed on the 2440 ft mine  
39 level, which contains large blocks (up to 50 cm diameter) of rhyolite host rock, plus  
40 magnetite and hematite ore. The matrix is composed of buff, non-indurated, friable  
41 material that includes rock flour, barite, monazite, quartz, light green mica, and  
42 clay. Mineral separates obtained from this sample are composite granular grains  
43 composed nearly entirely of pale yellow monazite (Fig. 11A, B); only a few tiny grains of  
44 xenotime were identified. The scarcity of xenotime is confirmed by low whole-rock  
45 HREE concentrations, which are atypical of the elevated HREE contents for the breccia  
46  
47  
48  
49  
50  
51  
52  
53  
54  
55  
56  
57  
58  
59  
60  
61  
62  
63  
64  
65

1  
2  
3  
4  
5  
6  
7  
8  
9  
10 pipe samples (Fig. 3). Twenty analyses of granular monazite from PR-33C yield  
11 concordant data with a weighted average of  $^{207}\text{Pb}/^{206}\text{Pb}$  ages of  $1464.9 \pm 3.3$  Ma (Table 1;  
12 Fig. 11C). One analysis of xenotime from PR-33C provides a  $^{207}\text{Pb}/^{206}\text{Pb}$  age of  $1469 \pm$   
13  
14  
15  
16 10 Ma.  
17  
18  
19

### 20 **Re-Os RESULTS**

21 Molybdenite was extracted from a quartz- and Mo-rich (700 ppm) 0.7 m interval of  
22 drill core DDH 2475-11. This sample, from the “hard” breccia pipe, is from the 2475 ft  
23 mine level. Molybdenite forms discrete, relatively large (~0.1-0.3 mm) grains  
24 disseminated in quartz, and also flakes ~10 to 100  $\mu\text{m}$  long intergrown with allanite,  
25 apatite, and xenotime (but not monazite), and as disseminated flakes in quartz (Fig. 12A,  
26 B). Re-Os analysis of this molybdenite reveals 4.78 ppm  $^{187}\text{Re}$  and 116.11 ppb  $^{187}\text{Os}$   
27  
28  
29  
30  
31  
32  
33 (Table 2), indicating an age of  $1440.6 \pm 9.2$  Ma (2-sigma uncertainty).  
34  
35  
36

### 37 $^{40}\text{Ar}/^{39}\text{Ar}$ RESULTS

38  
39  $^{40}\text{Ar}/^{39}\text{Ar}$  incremental heating data were acquired for muscovite, biotite, and K-  
40 feldspar from breccia pipe sample PR-182 on the 2370 ft mine level (Table 3; Fig. 13).  
41 Muscovite is a local constituent of the breccia pipe matrix (Day and Granitto, 2014);  
42 according to Kerr (1998), muscovite in this setting only occurs as an alteration product of  
43 K-feldspar. The petrologic significance of the analyzed muscovite is unclear, and its  
44 paragenetic position is indeterminate because it was not observed in thin section. The  
45 muscovite may be xenocrystic and may not have crystallized during emplacement of the  
46 breccia pipe, or it could reflect hydrothermal alteration of K-feldspar.  
47  
48  
49  
50  
51  
52  
53  
54  
55  
56

1  
2  
3  
4  
5  
6  
7  
8  
9  
10  
11 Three small grains of muscovite were incrementally heated with a CO<sub>2</sub> laser.  
12 These grains yield data that define a <sup>40</sup>Ar/<sup>39</sup>Ar plateau age (three or more consecutive  
13 heating steps with overlapping ages at the 95% confidence level and totaling >50% of the  
14 <sup>39</sup>Ar released) of 1473 ± 1 Ma, and an integrated age (roughly equivalent to a K-Ar age)  
15 of 1474 ± 2 Ma (Table 3; Fig. 13). A single grain of incrementally heated biotite from  
16 this sample did not produce a <sup>40</sup>Ar/<sup>39</sup>Ar plateau age, but did yield ages steadily rising  
17 from about 1440 Ma at the beginning of the step-heating experiment to about 1470 Ma  
18 during the intermediate and final incremental heating steps; the integrated <sup>40</sup>Ar/<sup>39</sup>Ar age  
19 of this biotite is 1462 ± 13 Ma. The K-feldspar produced variable <sup>40</sup>Ar/<sup>39</sup>Ar ages,  
20 consistent with the highly altered appearance of this mineral in thin section; early heating  
21 steps of ca. 400 Ma increased regularly to ca. 1200 Ma.  
22  
23  
24  
25  
26  
27  
28  
29  
30  
31  
32

### 33 *Summary*

34  
35 Results of previous zircon U-Pb geochronology in the St. Francois Mountains terrane  
36 (Van Schmus et al., 1996; Thomas et al., 2012) indicated two Mesoproterozoic episodes  
37 of igneous rock emplacement at ~1.49-1.44 Ga, and ~1.39-1.34 Ga (see also Bickford et  
38 al., 2015). Our new data (Table 4) for rocks at Pea Ridge constrain igneous activity  
39 associated with the older episode to between ca. 1475 Ma (time of extrusion of host  
40 volcanic rocks) and ca. 1440 Ma (age of late, cross-cutting felsic dikes). Additional new  
41 geochronological data (Neymark et al., this volume) on apatite from the magnetite ore  
42 suggest an age of ca. 1470 Ma for emplacement of the main IOA ore system. Most of the  
43 monazite, including fine grains occurring within granular fragments from both “hard” and  
44 “soft” breccia pipes, and coarse glassy individual grains from the “hard” breccia pipe,  
45  
46  
47  
48  
49  
50  
51  
52  
53  
54  
55  
56  
57  
58  
59  
60  
61  
62  
63  
64  
65

1  
2  
3  
4  
5  
6  
7  
8  
9  
10 formed at  $1464 \pm 4$  Ma, approximately 10 m.y. after local felsic volcanism. Fine-grained  
11 xenotime within granular fragments is about the same age as the fine-grained monazite,  
12 although its age is less well constrained. A few coarse monazite grains have slightly  
13 older ages of about 1475 Ma. This potentially older age is also preserved in muscovite  
14 ( $^{40}\text{Ar}/^{39}\text{Ar}$  age of  $1473 \pm 1$  Ma) from one sample of the “hard” pipe. A later event that  
15 post-dates iron ore deposition is recorded by igneous zircon in felsic dikes at  $1441 \pm 9$   
16 Ma, an age independently replicated by (1) molybdenite from a sample of “hard” breccia  
17 pipe that has a Re-Os age of  $1440.6 \pm 9.2$  Ma, and (2) rims on glassy monazite that yield  
18 an age of  $1447.2 \pm 4.7$  Ma.  $^{40}\text{Ar}/^{39}\text{Ar}$  data also suggest that biotite from the breccia pipe  
19 was thermally disturbed at this time.  
20  
21  
22  
23  
24  
25  
26  
27  
28  
29  
30

### 31 REE GEOCHEMISTRY

32 REE abundances of minerals contained in several Pea Ridge breccia pipe samples  
33 were determined by SHRIMP-RG analysis. These include granular and coarse glassy  
34 monazite from “hard” pipe sample PR-182, granular monazite and xenotime from “hard”  
35 pipe sample 2275-15, and granular monazite from “soft” pipe sample PR-33C (Table 5).  
36 Bulk rock geochemistry for samples from all mineralized zones of the Pea Ridge deposit,  
37 including the breccia pipes, is given in Day and Granitto (2014) and Day et al. (this  
38 volume). The petrologic conditions responsible for breccia pipe formation are  
39 constrained by comparison of REE data for monazite grains from within single samples  
40 and among different samples.  
41  
42  
43  
44  
45  
46  
47  
48  
49

50 Monazite from Pea Ridge breccia pipe samples is relatively LREE rich and HREE  
51 depleted. REE patterns for coarse glassy monazite ( $n = 10$ ) in sample PR-182 are  
52  
53  
54  
55  
56  
57  
58  
59  
60  
61  
62  
63  
64  
65

1  
2  
3  
4  
5  
6  
7  
8  
9  
10 consistent and include modest negative Eu anomalies (Eu/Eu\* values) of 0.42-0.46 (Fig.  
11 14A, Table 5); in contrast, granular monazite ( $n = 9$ ) has much larger negative Eu/Eu\*  
12 values (0.02-0.21), and lower and somewhat variable normalized HREE abundances (Fig.  
13 14B). Granular monazite from 2275-15 ( $n = 15$ ) and PR-33C ( $n = 10$ ) has modest  
14 negative Eu/Eu\* values (0.34-0.48; 0.42-0.45, respectively; Figs. 14C, D). Xenotime  
15 from sample 2275-15 is by comparison HREE-enriched, and has relatively small Eu  
16 anomalies (0.49-0.54; Fig. 14E, Table 5).

17  
18 Because petrographic and geochronologic evidence suggests that the granular matrix  
19 monazite and xenotime in sample 2275-15 are in textural equilibrium, we applied the  
20 geothermometer that utilizes Gd partitioning between coeval monazite and xenotime  
21 (Gratz and Heinrich, 1998). Criteria for application of this geothermometer include (1)  
22 grains of monazite and xenotime must be in contact, (2) monazite must contain <10 ppm  
23 Lu (i.e., minimal xenotime contamination), and (3) xenotime must contain <10 ppm La  
24 (i.e., minimal monazite contamination). Criteria 2 and 3 are critical because at least half  
25 of all REE analyses of both monazite and xenotime have elevated concentrations of Lu or  
26 La, respectively, suggesting that those REE analyses record mixtures of the two minerals,  
27 possibly as micro-inclusions of one mineral within the other (Fig. 14B, E). Although  
28 analyses indicative of mixtures involving monazite and xenotime were excluded from the  
29 geothermometric calculations, these analyses are valuable in providing additional  
30 evidence for co-genetic formation of monazite and xenotime in the breccia matrix.

31  
32 Gd abundances determined for eight monazite-xenotime pairs from sample 2275-15  
33 were deemed suitable for temperature calculation (Table 6). Among these, two pairs  
34 yield extremely high temperatures of about 1170 and 1280°C. Xenotime in one of these  
35  
36  
37  
38  
39  
40  
41  
42  
43  
44  
45  
46  
47

1  
2  
3  
4  
5  
6  
7  
8  
9  
10 samples has an atypically (compared to other data pairs) low Gd content; monazite in the  
11 other pair has an atypically high Gd content. The other six analyses yield lower  
12 calculated temperatures of about 770 to 950°C.  
13  
14  
15  
16  
17

## 18 **DISCUSSION**

19  
20 Complementary geochronologic and geochemical data sets for several samples of  
21 monazite (and for less abundant xenotime) robustly characterize the complex mineralogy  
22 and petrogenesis of the Pea Ridge breccia pipes. SHRIMP U-Pb data define at least two  
23 episodes of monazite crystallization. Coarse glassy monazite and granular matrix  
24 monazite (analyzed both in separated grains and *in situ*) formed at ca. 1464 Ma; rims on  
25 coarse glassy monazite formed during another growth episode at ca. 1450-1440 Ma.  
26  
27 Additional evidence for the younger event includes a Re-Os age of  $1440.6 \pm 9.2$  Ma on  
28 molybdenite from the “hard” pipe, a SHRIMP U-Pb age of  $1441.8 \pm 3.4$  Ma for monazite  
29 inclusions within apatite from the magnetite ore (Neymark et al., this volume), and a U-  
30 Pb age of  $1441 \pm 9.0$  Ma on zircon from a late felsic dike.  
31  
32  
33  
34  
35  
36  
37  
38

39 REE abundances in monazite from several samples provide additional  
40 geochemical constraints on the origin of the breccia pipes. Sample PR-182 from the  
41 “hard” pipe contains both coarse glassy monazite and fine granular monazite that have  
42 different REE patterns (Fig. 14A, B). These two morphologies also show distinctly  
43 different Th/U (Fig. 15A) and chondrite-normalized La/Lu (Fig. 15B). Large negative  
44 Eu anomalies can result from co-precipitation with plagioclase (see red curves in Fig.  
45 14D) under reduced magmatic conditions that produce  $\text{Eu}^{2+}$ . However, the presence of  
46 primary (specular) hematite in the breccia pipes (Nuelle et al., 1992; Kerr, 1998; Ayuso  
47  
48  
49  
50  
51  
52  
53  
54  
55  
56  
57  
58  
59  
60  
61  
62  
63  
64  
65

1  
2  
3  
4  
5  
6  
7  
8  
9  
10 et al., this volume) suggests oxidizing conditions, at least locally, which would produce  
11  
12  $\text{Eu}^{3+}$  that is easily accommodated in monazite and xenotime crystal structures. Thus, the  
13  
14 low chondrite-normalized abundances of Eu in the whole-rock REE patterns (Fig. 3), and  
15  
16 in matrix xenotime and both morphologies of monazite (Fig. 14A, C, D), must reflect the  
17  
18 composition of the fluid from which these minerals crystallized (Kerr, 1998). Additional  
19  
20 Eu depletion shown by very large negative Eu anomalies (Fig. 14B) in matrix monazite  
21  
22 from sample PR-182 perhaps represents a local reducing environment whereby  $\text{Eu}^{2+}$  was  
23  
24 fractionated into coeval barite (Fig. 9A) (cf. Guichard et al., 1979; Morgan and Wandless,  
25  
26 1980). The unique composition of PR-182 matrix monazite is also highlighted by  
27  
28 distinctive Th/U and La/Lu, both of which are much higher than in other Pea Ridge  
29  
30 samples of matrix monazite and in glassy monazite from sample PR-182.

31  
32 Matrix monazite from samples 2275-15 (“hard” pipe) and PR-33C (“soft” pipe)  
33  
34 could have formed by (1) *in situ* crystallization of breccia infill from hydrothermal fluids,  
35  
36 or (2) comminution/recrystallization of preexisting coarse glassy monazite. In BSE  
37  
38 images, matrix monazite displays polygonal textures and minimal preferred orientation of  
39  
40 composite grains (cf. Fig. 4B, 9A), both of which are consistent with precipitation from a  
41  
42 fluid. Given that these samples of matrix monazite and coarse glassy monazite (PR-182)  
43  
44 have similar REE abundances, the fine-grained matrix material could record milling of  
45  
46 coarse-grained glassy monazite. However, such a process would result in shattered or  
47  
48 splintered grains, which are rarely observed (e.g., small monazite and xenotime grains  
49  
50 immediately left of large barite crystal in Fig. 9A). Thus, textural and geochemical  
51  
52 evidence suggests that most of the matrix monazite crystallized from hydrothermal fluids  
53  
54 of probable magmatic origin. Because monazite and xenotime can form at a wide range  
55  
56

1  
2  
3  
4  
5  
6  
7  
8  
9  
10 of temperatures (from below 400°C; Muhling et al., 2012, and references therein) to  
11 magmatic temperatures, the specific conditions of hydrothermal deposition of monazite  
12 and xenotime within breccia pipes at Pea Ridge remain unclear (see Harlov et al., this  
13 volume; Hofstra et al., this volume; Johnson et al., this volume).

14  
15  
16  
17  
18 REE patterns for xenotime from sample 2275-15 are somewhat distinct relative to  
19 those for xenotime from other localities and various origins (Fig. 15C). Igneous  
20 xenotime characteristically shows a distinctive negative Eu anomaly (commonly due to  
21 co-precipitation of plagioclase) and elevated HREE abundances. In contrast, xenotime of  
22 metamorphic or hydrothermal origin tends to be middle REE (MREE)-enriched and  
23 HREE-depleted (due to co-precipitation of garnet or some other unknown mineral;  
24 Kositsin et al., 2003; Aleinikoff et al., 2015). Pea Ridge matrix xenotime has Eu/Eu\*  
25 values similar to those of hydrothermal xenotime from other localities, but lower Gd/Lu  
26 (Fig. 15D). LREE and MREE abundances in Pea Ridge xenotime are somewhat lower  
27 than those of other hydrothermal xenotime, perhaps due to co-precipitation of LREE-rich  
28 monazite and apatite. The presence of elevated HREE abundances of Pea Ridge  
29 xenotime, coupled with modest negative Eu anomalies, suggests a hybrid history  
30 involving crystallization from a magmatically derived hydrothermal fluid (cf. Harlov et  
31 al., 2005; 2011).

32  
33  
34  
35  
36  
37  
38  
39  
40  
41  
42  
43  
44 If matrix monazite (and xenotime) were derived from coarse glassy monazite by  
45 milling (apparently at temperatures of 400°C or less), then the geochemical and  
46 geochronological information preserved therein would be inherited from coarse glassy  
47 grains. As such, ages determined for matrix grains would record the time of growth of  
48 the coarse glassy grains, not the time of brecciation. If the matrix grains formed by the  
49  
50  
51  
52  
53  
54  
55  
56  
57  
58  
59  
60  
61  
62  
63  
64  
65

1  
2  
3  
4  
5  
6  
7  
8  
9  
10 dissolution of coarse glassy monazite followed by reprecipitation during emplacement of  
11 the breccia pipes, the second episode of monazite growth must have transpired shortly  
12 after formation of the hydrothermal coarse monazite, because the two types of monazite  
13 have identical ages (within SHRIMP U-Pb geochronologic analytical uncertainty).  
14  
15

16  
17  
18 Gd partitioning between adjacent grains of matrix monazite and xenotime in  
19 sample 2275-15 suggests crystallization at magmatic temperatures of >700°C (Table 6).  
20  
21 However, small Eu anomalies present in both of these minerals are atypical of an igneous  
22 parentage, and hence suggest a hydrothermal origin. Other geothermometric methods  
23 suggest lower temperatures of ~300 to 450°C for breccia pipe emplacement (Sidder et al.,  
24 1993; Johnson et al., this volume); moreover, the  $1473 \pm 1$  Ma  $^{40}\text{Ar}/^{39}\text{Ar}$  age determined  
25 for muscovite (closure temperature of ca. 400°C; Kirschner et al., 1996) was not reset to  
26 the younger ca. 1464 Ma age. Consequently, >700°C temperatures calculated from Gd  
27 partitioning between coeval matrix monazite and xenotime are unreasonably high for the  
28 Pea Ridge breccia pipes. Factors that may have adversely influenced these calculated  
29 temperatures include (1) the experimentally derived Gd geothermometer (Gratz and  
30 Heinrich, 1998) was calibrated at 2 kbar, whereas the Pea Ridge breccia pipes formed at  
31 less than 1 kbar (or possibly <0.5 kbar; Kerr, 1998); (2) the lowest experimental  
32 temperature determined for the calculated distribution coefficient is about 550°C, which  
33 is higher than the maximum estimated temperatures of formation for the Pea Ridge  
34 breccia pipes, as determined by other methods; (3) the bulk composition used in the Gd  
35 partitioning experiments may have been significantly different from those typical of Pea  
36 Ridge rocks; (4) the monazite and xenotime in the analyzed samples might not have been  
37 a cogenetic, equilibrium assemblage; and (5) the small grain sizes of the monazite and  
38  
39  
40  
41  
42  
43  
44  
45  
46  
47  
48  
49  
50  
51  
52  
53  
54  
55  
56  
57  
58  
59  
60  
61  
62  
63  
64  
65

1  
2  
3  
4  
5  
6  
7  
8  
9  
10 xenotime suggest rapid crystallization during which equilibrium may not have been  
11 attained. Similarly, Kerr (1998) was unsuccessful in determining reasonable  
12 geothermometry of the Pea Ridge breccia pipes using the distribution of Y in coexisting  
13 monazite and xenotime (as proposed by Gratz and Heinrich, 1997). Geological evidence  
14 of brittle fracturing during breccia pipe formation also argues against magmatic  
15 temperatures.  
16  
17  
18  
19  
20

21 U-Pb ages of coarse glassy monazite and matrix monazite and xenotime suggest  
22 that the Pea Ridge breccia pipes formed at ca. 1464 Ma. Growth of coarse monazite  
23 could have started earlier and continued longer than for the finer-grained matrix  
24 monazite; alternatively, formation of these two morphologies may represent two closely  
25 spaced crystallization episodes (unresolvable using current dating technology). A  
26 second, but volumetrically minor, episode of REE enrichment via hydrothermal activity  
27 is recorded by ages of rims on the coarse glassy monazite cores, on monazite inclusions  
28 in apatite (Neymark et al., this volume), and on molybdenite intergrown with apatite and  
29 allanite in the “hard” pipe. In terms of REE, it is important to note that this second  
30 hydrothermal event was not limited to recrystallization of preexisting monazite and  
31 xenotime, but instead involved the hydrothermal introduction of new REE as documented  
32 by the presence of xenotime and allanite intergrown with the dated molybdenite (Fig.  
33 12B). Very limited data on monazite suggest the possibility of an earlier thermal event at  
34 ca. 1475 Ma and a later minor event at ca. 1405 Ma.  
35  
36  
37  
38  
39  
40  
41  
42  
43  
44  
45  
46  
47

48 Because our large U-Pb data set suggests that the Pea Ridge breccia pipes formed  
49 at about 1464 Ma, the  $1473 \pm 1$  Ma  $^{40}\text{Ar}/^{39}\text{Ar}$  age on muscovite does not appear related to  
50 breccia pipe formation. We propose that this muscovite is xenocrystic and derived from  
51  
52  
53  
54  
55  
56  
57  
58  
59  
60  
61  
62  
63  
64  
65

1  
2  
3  
4  
5  
6  
7  
8  
9  
10 a breccia fragment. The 1473 Ma  $^{40}\text{Ar}/^{39}\text{Ar}$  age is consistent with a few older monazite  
11 ages and with the crystallization age of the host volcanic rocks. Although the origin of  
12 the muscovite is uncertain, preservation of the  $1473 \pm 1$  Ma age (i.e., not reset to ca. 1464  
13 Ma) is significant. Consequently, the “hard” breccia pipe must have formed at relatively  
14 low temperature, below the ca. 400°C closure temperature of muscovite. This  
15 interpretation supports other calculated temperature results (Sidder et al., 1993; Johnson  
16 et al., this volume; Harlov et al., this volume), and further discredits the application of the  
17 Gd-in-coexisting-monazite-and-xenotime geothermometer to this hydrothermal system.  
18 It is unlikely that the temperature information was inherited, because the monazite and  
19 xenotime grains are phases that crystallized from a hydrothermal fluid, and are not  
20 xenocrysts.

21  
22  
23  
24  
25  
26  
27  
28  
29  
30  
31 The source of REE in the Pea Ridge breccia pipes has not been resolved  
32 definitively. Kerr (1998) proposed a magmatic source, involving either (1) late-stage,  
33 residual fluids from a differentiating magma at depth; or (2) fluids derived from a  
34 younger pluton. Although geologic evidence indicates that the breccia pipes are younger  
35 than the magnetite ore, the lack of sufficient precision in the age data precludes definition  
36 of a precise timescale for the Pea Ridge events. Harlov et al. (this volume) suggest that  
37 the REE were scavenged by hypersaline fluids derived from the parent magma  
38 responsible for forming the original magnetite-apatite deposit. Day et al. (this volume)  
39 propose that the REE breccia pipes formed from residual fluids related to the magnetite  
40 ore-forming event, the source of which was magmatic-hydrothermal in origin and  
41 genetically related to the high-iron, mafic to intermediate-composition volcanic rock  
42 suite. Alternatively, Hofstra et al. (this volume) and Harlov et al. (this volume) suggest

1  
2  
3  
4  
5  
6  
7  
8  
9  
10 that the REE were derived from REE-rich apatite that occurs throughout much of the  
11 magnetite ore. This source requires the dissolution of apatite, fluid transport of REE, and  
12 reprecipitation of fine-grained matrix monazite and xenotime during explosive  
13  
14 emplacement of the breccia pipes. Although feasible, this model would involve the  
15  
16 dissolution of an enormous mass of apatite (LREE-enriched, HREE-depleted) in order to  
17  
18 produce the relatively high abundances of HREE observed in the breccia pipes (expressed  
19  
20 by the presence of xenotime) (Fig. 3).  
21  
22

## 23 24 25 **CONCLUSIONS**

26  
27 The Pea Ridge iron oxide deposit, in the St. Francois Mountains of southeast  
28 Missouri, hosts four REE-rich breccia pipes (“hard” and “soft” varieties). REE are  
29 primarily contained in monazite and xenotime. In contrast to the more common LREE-  
30 rich deposits, significant concentrations of HREE-rich xenotime render this deposit of  
31 economic interest. Geochronologic and geochemical data obtained for samples of both  
32  
33 types of breccia pipes and associated rocks reveal the following:  
34  
35  
36  
37

- 38 (1) SHRIMP U-Pb dating of host volcanic rocks and late cross-cutting felsic dikes  
39  
40 constrain the timing of explosive breccia pipe formation at Pea Ridge. Euhedral  
41  
42 prismatic zircon from two samples of host rhyolite is dated at  $1473.6 \pm 8.0$  and  
43  
44  $1472.7 \pm 5.6$  Ma. Felsic dikes contain abundant zircon interpreted as xenocrystic  
45  
46 (age range ca. 1455-1522 Ma), plus unusual spongy zircon, considered to be of  
47  
48 igneous origin, dated at  $1441 \pm 9$  Ma.  
49  
50  
51  
52  
53  
54  
55  
56  
57  
58  
59  
60  
61  
62  
63  
64  
65

- 1  
2  
3  
4  
5  
6  
7  
8  
9  
10  
11 (2) The breccia pipes contain two types of monazite: (a) coarse (up to ca. 300  $\mu\text{m}$   
12 diameter) glassy grains, and (b) fine (<50  $\mu\text{m}$  diameter) grains in a granular  
13 matrix that includes variable proportions of xenotime.  
14  
15  
16 (3) SHRIMP U-Pb geochronologic data for cores of both types of monazite and  
17 xenotime yield ages of ca. 1464 Ma. One exception is a sample of granular  
18 monazite that contains very high proportions of common Pb, which consequently  
19 precludes a precise age determination. In addition, this sample has an unusual  
20 geochemical signature (large negative Eu anomaly, high Th/U) that is distinct  
21 from all other samples of matrix monazite.  
22  
23  
24 (4) Polygonal textures and chondrite-normalized REE patterns suggest that the matrix  
25 monazite and xenotime were deposited contemporaneously by a magmatic-  
26 hydrothermal fluid. A  $^{40}\text{Ar}/^{39}\text{Ar}$  plateau age of  $1473 \pm 1$  Ma determined on  
27 muscovite from the matrix of a “hard” breccia pipe was not reset by the associated  
28 hydrothermal activity at about 1464 Ma, suggesting that temperatures  
29 accompanying brecciation did not exceed ca. 400°C.  
30  
31  
32 (5) Pea Ridge was affected by an additional episode of hydrothermal activity about  
33 20 m.y. later, as indicated by an age of  $1447.2 \pm 4.7$  Ma determined for rims on  
34 glassy monazite. This age is in agreement with a Re-Os age of  $1440.6 \pm 9.2$  Ma  
35 for REE-related molybdenite, a U-Pb zircon age for the late cross-cutting felsic  
36 dike, and U-Pb ages of monazite inclusions within apatite (Neymark et al., this  
37 volume) from the magnetite deposit.  
38  
39  
40  
41  
42  
43  
44  
45  
46  
47  
48  
49  
50  
51

## 52 ACKNOWLEDGMENTS

53  
54  
55  
56  
57  
58  
59  
60  
61  
62  
63  
64  
65

1  
2  
3  
4  
5  
6  
7  
8  
9  
10  
11  
12  
13  
14  
15  
16  
17  
18  
19  
20  
21  
22  
23  
24  
25  
26  
27  
28  
29  
30  
31  
32  
33  
34  
35  
36  
37  
38  
39  
40  
41  
42  
43  
44  
45  
46  
47  
48  
49  
50  
51  
52  
53  
54  
55  
56  
57  
58  
59  
60  
61  
62  
63  
64  
65

This study was made possible by access provided to underground workings at Pea Ridge in the early 1990s by the former Meramec Mining Company, and recently (2012-2014) to drill core maintained at the mine site by Pea Ridge Resources Inc. and at the Missouri Department of Natural Resources (MDNR) in Rolla. We thank Patrick Scheel and Molly Starkey (both MDNR) for help in obtaining excellent core samples. Discussions with Craig Johnson, Albert Hofstra, Robert Ayuso, and Robert Wintsch are appreciated. We thank Jorge Vazquez (USGS) for help in collecting trace element data on the USGS/Stanford SHRIMP-RG. Earlier versions of this manuscript were substantially improved by the reviews of Sophie Decrée, Ed duBray, John Hanchar, Chris McFarlane, and guest editor Louise Corriveau. Any use of trade, product, or firm names is for descriptive purposes only and does not imply endorsement by the U.S. Government.

**APPENDIX**

**METHODS**

*Sample preparation*

Zircon, monazite, xenotime, molybdenite, K-feldspar, muscovite, and biotite were obtained from archival samples that were collected underground in the early 1990s while the Pea Ridge iron deposit was being actively mined. Sample sizes vary from fist-size pieces to 50 x 30 x 10 cm rock slabs. Zircon from felsic host rocks, and monazite, xenotime, K-feldspar, muscovite, and biotite from breccia pipe samples were extracted using crushing, pulverizing, rinsing (to remove clay-size particles), and processing through a Frantz Isodynamic Magnetic Separator. For breccia pipe samples, biotite was concentrated using settings that varied from about 0.2 to 0.4 amps (15° side tilt), monazite

1  
2  
3  
4  
5  
6  
7  
8  
9  
10 and xenotime were concentrated using settings that varied from 0.6 to 0.8 amps, and  
11 muscovite and K-feldspar were concentrated as non-magnetic separates at about 1.8  
12 amps. For igneous host rock samples, the non-magnetic fraction containing zircon was  
13  
14  
15  
16 further concentrated by sinking in methylene iodide (density 3.3 grams/cc). Molybdenite  
17  
18 was isolated from the host silicate matrix (quartz) using room temperature HF (Lawley  
19  
20 and Selby, 2012). Further purification of molybdenite was done using standard  
21  
22 separation techniques, including heavy liquids and water flotation (Selby and Creaser,  
23  
24 2004), and handpicking.

25  
26 Prior to SHRIMP U-Pb analysis, two sample preparation strategies were employed  
27  
28 (1) individual grains of zircon, monazite, and xenotime were handpicked; and (2)  
29  
30 polished thin sections were analyzed by scanning electron microscope (SEM) imaging to  
31  
32 identify monazite and xenotime. Handpicked grains were placed onto double-sided tape  
33  
34 under a binocular microscope, mounted in epoxy, ground to about half thickness using  
35  
36 2500-grit wet-dry sandpaper, and polished sequentially using 6 and 1  $\mu\text{m}$  diamond  
37  
38 suspensions. All grains were imaged in reflected and transmitted light on a petrographic  
39  
40 microscope. Using the U.S. Geological Survey (USGS) JEOL 5800LV SEM, zircon was  
41  
42 imaged in cathodoluminescence (CL); monazite and xenotime were imaged using  
43  
44 backscattered electron microscopy (BSE).

#### 45 46 *SHRIMP U-Pb analysis*

47  
48 Zircon from Pea Ridge was analyzed using the USGS/Stanford SHRIMP-RG,  
49  
50 Stanford, California. For all analyses, analysis spot was about 20-25  $\mu\text{m}$  in diameter.  
51  
52 The magnet was cycled through the appropriate mass stations five times. Measured  
53  
54  
55  
56  
57  
58  
59  
60  
61  
62  
63  
64  
65

1  
2  
3  
4  
5  
6  
7  
8  
9  
10  $^{206}\text{Pb}/^{238}\text{U}$  for zircon was normalized to values for standard R33 (419 Ma; Black et al.,  
11 2004). Zircon standard FC-1 (1099 Ma; Paces and Miller, 1993) was run as a secondary  
12 standard to verify accuracy of  $^{207}\text{Pb}/^{206}\text{Pb}$  ages, providing confidence in the analytical  
13 procedure.  
14  
15  
16  
17

18 Monazite and xenotime were analyzed on SHRIMP II at the Research School of Earth  
19 Sciences (RSES), Australian National University, using a 15 to 25  $\mu\text{m}$  spot size,  
20 following the methods of Williams (1998). Energy filtering was utilized to eliminate an  
21 isobaric interference at mass 204 (suspected to be a  $\text{NdThO}^{++}$  molecule; Ireland et al.,  
22 1999) during monazite analysis. By closing the energy filter slits ca. 50-65%, the UO  
23 peak (mass 254) was decreased by about half, most or all of the counts at mass 204 could  
24 be attributed to  $^{204}\text{Pb}$ , and these counts could then be used to reliably correct for the  
25 presence of common Pb when calculating a  $^{207}\text{Pb}/^{206}\text{Pb}$  or  $^{206}\text{Pb}/^{238}\text{U}$  age. Measured  
26  $^{206}\text{Pb}/^{238}\text{U}$  for monazite was normalized to the value for standard 44069 (424 Ma;  
27 Aleinikoff et al., 2006). We did not use a secondary monazite or xenotime standard, but  
28 accurate  $^{207}\text{Pb}/^{206}\text{Pb}$  ages were routinely obtained during SHRIMP U-Pb analysis of  
29 zircon, indicating proper instrument operation.  
30  
31  
32  
33  
34  
35  
36  
37  
38  
39  
40

41 Data for several samples of monazite are slightly (~1-10%) reversely discordant, i.e.,  
42 plot above the Concordia curve, such that  $^{206}\text{Pb}/^{238}\text{U}$  ages are older than  $^{207}\text{Pb}/^{206}\text{Pb}$  ages.  
43 This effect is occasionally observed in young (i.e., Tertiary) igneous monazite (Schärer et  
44 al., 1986; Caddick et al., 2007) and has been attributed to incorporation of  $^{230}\text{Th}$  (an  
45 intermediate daughter product of  $^{238}\text{U}$  decay) during monazite crystallization (e.g.,  
46 Schärer, 1984; Parrish, 1990); this results in excess  $^{206}\text{Pb}$  that causes  $^{206}\text{Pb}/^{238}\text{U}$  ages to be  
47 too old and  $^{207}\text{Pb}/^{206}\text{Pb}$  ages to be too young. For igneous monazite, the effect of excess  
48  
49  
50  
51  
52  
53  
54  
55  
56  
57  
58  
59  
60  
61  
62  
63  
64  
65

1  
2  
3  
4  
5  
6  
7  
8  
9  
10  $^{206}\text{Pb}$  can be calculated using the assumed Th/U of the parent magma (Schärer, 1984). In  
11 hydrothermal monazite samples from the Pea Ridge breccia pipes, Th/U for the source  
12 fluid is unknown. By assuming an average crustal value for Th/U of 4, we determine that  
13 the impact of possible excess  $^{206}\text{Pb}$  is small (<1 m.y.) and close to the calculated  
14 weighted average age uncertainty. Another, possibly more likely, cause for the reverse  
15 discordance relates to matrix effects associated with a compositional mismatch between  
16 standard and unknowns (Fletcher et al., 2010). Due to the presence of the reverse  
17 discordance, we use only  $^{207}\text{Pb}/^{206}\text{Pb}$  data to calculate weighted average ages.

18  
19  
20  
21  
22  
23  
24  
25  
26  
27  
28  
29  
30  
31  
32  
33  
34  
35  
36  
37  
38  
39  
40  
41  
42  
43  
44  
45  
46  
47  
48  
49  
50  
51  
52  
53  
54  
55  
56  
57  
58  
59  
60  
61  
62  
63  
64  
65  
Xenotime standard MG-1 (490 Ma, Fletcher et al., 2004) was used to calibrate  
SHRIMP  $^{206}\text{Pb}/^{238}\text{U}$  ages of Pea Ridge xenotime grains. However, owing to  
compositional variability (particularly REE, Th, and U concentrations),  $^{206}\text{Pb}/^{238}\text{U}$  ages of  
xenotime are likely impacted by matrix effects associated with compositional mismatches  
between standard and unknowns (Fletcher et al., 2004). Thus, arrays of U-Pb data shown  
on a Concordia plot may reflect both geologic (e.g., Pb-loss) and analytical  
complications. Because the xenotime grains are Mesoproterozoic, the use of  $^{207}\text{Pb}/^{206}\text{Pb}$   
data (which are not affected by matrix bias) is appropriate for determining ages of the Pea  
Ridge xenotime. No energy filtering was used during xenotime analysis.

SHRIMP U-Pb data were reduced using Squid 2 (Ludwig, 2009) and plotted using  
Isoplot 3 (Ludwig, 2003). Ages of Mesoproterozoic zircon, monazite, and xenotime are  
calculated using the weighted average of selected  $^{207}\text{Pb}/^{206}\text{Pb}$  ages, as explained below.

REE data for monazite and xenotime were collected using the USGS/Stanford  
SHRIMP-RG (Mazdab and Wooden, 2006). A primary ion beam was operated at about  
0.5-1 nA with a spot size of ca. 10-15  $\mu\text{m}$  in diameter. Mass resolution was set to about

1  
2  
3  
4  
5  
6  
7  
8  
9  
10 11,000 in order to separate all HREE from middle REE (MREE) oxides. Monazite  
11 standard NAM and xenotime standard BS-1 (Aleinikoff et al., 2012) were used to  
12 calibrate REE concentrations, normalized to the chondritic values of McDonough and  
13 Sun (1995). Trace element concentrations are believed to be reproducible to about 2-5%.  
14  
15  
16  
17  
18  
19

20 *TIMS Re-Os analysis*

21 Re-Os data were acquired at the University of Durham, Durham, UK. Re and Os  
22 analysis of molybdenite was achieved by an acid (3:1 mix [9mL] of HNO<sub>3</sub>:HCl)  
23 digestion and equilibration with a tracer solution (<sup>185</sup>Re + normal Os) in a Carius tube at  
24 220°C for 24 hrs. Os was isolated using CHCl<sub>3</sub> solvent extraction and micro-distillation.  
25 Purification of Re was achieved using NaOH-acetone solvent extraction and anion  
26 chromatography (Selby and Creaser, 2004; Cumming et al., 2013). Isotope compositions  
27 of the isolated Re and Os fractions were determined by negative-ion TIMS using a  
28 Thermo-Scientific TRITON mass spectrometer. Although insignificant, the Re (1.4 pg/g)  
29 and Os (0.2 pg/g, with <sup>187</sup>Os/<sup>188</sup>Os = ~0.28) data are blank-corrected using the average  
30 Re-Os blank values at the time of analysis. The Re-Os data are presented with a total of  
31 three different uncertainties (at 2-sigma level): (1) error that includes mass spectrometry  
32 uncertainties only; (2) error that includes all sources of analytical uncertainty (Re and Os  
33 mass spectrometer measurements, blank abundances and isotopic compositions, spike  
34 calibrations and reproducibility of standard Re and Os isotopic values); and (3) error that  
35 includes all sources of analytical uncertainty (#2 above), plus uncertainty in the decay  
36 constant (0.35%; Smoliar et al., 1996; Selby et al., 2007; Table 2).  
37  
38  
39  
40  
41  
42  
43  
44  
45  
46  
47  
48  
49  
50  
51  
52  
53  
54  
55  
56  
57  
58  
59  
60  
61  
62  
63  
64  
65

1  
2  
3  
4  
5  
6  
7  
8  
9  
10 *Ar/Ar analysis*  
11

12 <sup>40</sup>Ar/<sup>39</sup>Ar data were acquired at the USGS in Denver, CO. Mineral grains were  
13 selected under a binocular microscope from sieved and washed fractions of crushed rock.  
14 Handpicked grains, generally between 0.2 and 0.1 mm in diameter, were loaded into  
15 aluminum disks, together with mineral standards for monitoring the neutron flux and  
16 zero-aged K-glass, and CaF<sub>2</sub> for determining the production ratios of nucleogenic argon  
17 produced during sample irradiation. The aluminum disks were stacked and wrapped in  
18 aluminum foil and vacuum-encapsulated in a quartz vial, which was then sealed into an  
19 aluminum irradiation can and positioned in the central thimble position of the USGS  
20 TRIGA reactor, where it was rotated at 1 rpm for 80 MW hours. Two neutron flux  
21 standards were employed, Fish Canyon Tuff (FCT) sanidine and GA1550 biotite. An age  
22 of 28.201 Ma (Kuiper et al., 2008) was applied to the FCT sanidine and an age of 99.44  
23 Ma was applied to biotite GA1550. Although the biotite Ar/Ar age is slightly older than  
24 the 98.5 Ma age reported by McDougall and Wellman (2011), this recalculated age is  
25 self-consistent with both the 28.201 Ma age of FCT sanidine and the decay constants  
26 used in this study (Min et al., 2000). The irradiated mineral grains were loaded into a  
27 stainless steel planchette and positioned into a laser chamber with a ZnSe window. The  
28 laser chamber and entire stainless steel extraction system were evacuated to pressures of  
29 <1 x 10<sup>-9</sup> Torr. Samples were incrementally heated using a 50 W CO<sub>2</sub> laser. Argon was  
30 isolated from other reactive gases by exposure to a cryogenic trap maintained at -130°C  
31 and a hot SAES GP50 getter. The purified sample gas was introduced and expanded into  
32 a Thermo Scientific ARGUS-VI mass spectrometer. Argon isotopes were measured  
33 simultaneously during 300 sec of data collection using a combination of Faraday  
34  
35  
36  
37  
38  
39  
40  
41  
42  
43  
44  
45  
46  
47  
48  
49  
50  
51  
52  
53  
54  
55  
56  
57  
58  
59  
60  
61  
62  
63  
64  
65

1  
2  
3  
4  
5  
6  
7  
8  
9  
10  
11  
12  
13  
14  
15  
16  
17  
18  
19  
20  
21  
22  
23  
24  
25  
26  
27  
28  
29  
30  
31  
32  
33  
34  
35  
36  
37  
38  
39  
40  
41  
42  
43  
44  
45  
46  
47  
48  
49  
50  
51  
52  
53  
54  
55  
56  
57  
58  
59  
60  
61  
62  
63  
64  
65

detectors for masses 40, 39, 38, 37 and ion counting for mass 36. Argon isotopic ratios were calculated from time-zero isotopic values determined by linear and parabolic regressions of the data. Detector inter-calibration was accomplished using gas from the standards and atmospheric argon. Ages were calculated after correction for blanks, detector intercalibration (<0.1%), radioactive decay subsequent to irradiation, and interfering nucleogenic reactions. Calculated ages include 2-sigma uncertainties.

1  
2  
3  
4  
5  
6  
7  
8  
9  
10  
11 **REFERENCES**

- 12 Aleinikoff, J.N., Grauch, R.I., Mazdab, F.K., Fanning, C.M., and Kamo, S., 2012,  
13 SHRIMP U-Pb and trace element evidence from an unusual monazite-xenotime  
14 gneiss for multiple thermal events in the Hudson Highlands, NY: American Journal of  
15 Science, v. 312, p. 723–765.
- 16  
17 Aleinikoff, J.N., Lund, K., and Fanning, C.M., 2015, SHRIMP U-Pb and REE data  
18 pertaining to the origins of xenotime in Belt Supergroup rocks: Evidence for ages of  
19 deposition, hydrothermal alteration, and metamorphism: Canadian Journal of Earth  
20 Sciences, v. 2, p. 722–745.
- 21  
22 Aleinikoff, J.N., Schenck, W.S., Plank, M.O., Srogi, L., Fanning, C.M., Kamo, S.L., and  
23 Bosbyshell, H., 2006, Deciphering igneous and metamorphic events in high grade  
24 rocks of the Wilmington Complex, Delaware: Morphology, CL and BSE zoning, and  
25 SHRIMP U-Pb geochronology of zircon and monazite: Geological Society of  
26 America Bulletin, v. 118, p. 39–64.
- 27  
28 Ayuso, R.A., Slack, J.F., Day, W.C., and McCafferty, A.E., this volume, Nd-Pb isotope  
29 geochemistry of the iron-oxide apatite Pea Ridge deposit, St. Francois Mountains,  
30 Missouri: Role of the subcontinental lithosphere and regional comparisons: Economic  
31 Geology.
- 32  
33 Bickford, M.E., and Mose, D.G., 1975, Geochronology of Precambrian rocks in the St.  
34 Francois Mountains, southeastern Missouri: Geological Society of America Special  
35 Paper 165, 48 p.
- 36  
37 Bickford, M.E., Van Schmus, W.R., Karlstrom, K.E., Mueller, P.A., and Kamenov, G.D.,  
38 2015, Mesoproterozoic-trans-Laurentian magmatism: A synthesis of continent-wide  
39 age distributions, new SIMS U–Pb ages, zircon saturation temperatures, and Hf and  
40 Nd isotopic compositions: Precambrian Research, v. 265, p. 286–312.
- 41  
42 Black, L.P., Kamo, S.L., Allen, C.M., Davis, D.W., Aleinikoff, J.N., Valley, J.W.,  
43 Mundil, R., Campbell, I.H., Korsuch, R.J., Williams, I.S., and Foudoulis, C., 2004,  
44 Improved  $^{206}\text{Pb}/^{238}\text{U}$  microprobe geochronology by the monitoring of a trace-element-  
45 related matrix effect; SHRIMP, ID–TIMS, ELA–ICP–MS and oxygen isotope  
46 documentation for a series of zircon standards: Chemical Geology, v. 205, p. 115–  
47 140.
- 48  
49 Brown, M.V., 1989, Volcanics of the southern St. Francois Mountains, Missouri, *in*  
50 Brown, M.V., Kisvarsanyi, E.B., and Hagni, R.D., eds., “Olympic Dam-type”  
51 deposits and geology of middle Proterozoic rocks in the St. Francois Mountains  
52 terrane, Missouri: Society of Economic Geologists Guidebook Series, v. 4, p. 110–  
53 132.
- 54  
55  
56  
57  
58  
59  
60  
61  
62  
63  
64  
65

Commented [JLS1]: Not checked.

But I did notice one reference that is out of alphabetical order.

- 1  
2  
3  
4  
5  
6  
7  
8  
9  
10 Caddick, M.J., Bickle, M.J., Harris, N.B.W., Holland, T.J.B., Horstwood, M.S.A.,  
11 Parrish, R.R., and Ahmad, T., 2007, Burial and exhumation history of a Lesser  
12 Himalayan schist: Recording the formation of an inverted metamorphic sequence in  
13 NW India: *Earth and Planetary Science Letters*, v. 264, p. 375–390.  
14
- 15 Castor, S.B., and Hedrick, L.B., 2006, Rare earth elements, *in* Kogel, J.E, Trivedi, N.C.,  
16 Barker, J.M., and Krukowski, S.T., eds., *Industrial minerals volume*, 7th edition:  
17 Littleton, Colorado, Society for Mining, Metallurgy, and Exploration, p. 769–792.  
18
- 19 Cumming, V.M., Poulton, S.W., Rooney, AD., and Selby, D., 2013, Anoxia in the  
20 terrestrial environment during the late Mesoproterozoic: *Geology*, v. 41, p. 583–586.  
21
- 22 Day, W.C., and Granitto, M., 2014, Geologic field notes and geochemical analyses of  
23 outcrop and drill core from Mesoproterozoic rocks and iron-oxide deposits and  
24 prospects of southeast Missouri: U.S. Geological Survey Open-File Report 2014–  
25 1053.  
26
- 27 Day, W.C., Sidder, G.B., Rye, R.O., Nuelle, L.M., and Kisvarsanyi, E.B., 1992, The  
28 middle Proterozoic rhyolite-hosted Pea Ridge iron and rare-earth-element deposit—A  
29 magmatic source for Olympic Dam-type deposits in the Midcontinent region of the  
30 U.S.A., *in* Brown, P.E., and Chappell, B.W., eds., *Second Hutton symposium on the*  
31 *origin of granites and related rocks [abs.]*: *Transactions of the Royal Society of*  
32 *Edinburgh, Earth Sciences*, v. 83, pt. 2, p. 489.
- 33 Day, W.C., Slack, J.F., Ayuso, R.A., and Seeger, C.M., this volume, Regional geologic  
34 and petrologic framework of iron oxide ± apatite± rare earth element (IOA ± REE)  
35 and iron oxide-copper-gold (IOCG) deposits of the Mesoproterozoic St. Francois  
36 Mountains terrane, southeast Missouri: *Economic Geology*.  
37
- 38 Dostal, J., Kontak, D.J., and Karl, S.M., 2014, The Early Jurassic Bokan Mountain  
39 peralkaline granitic complex (southeastern Alaska): *Geochemistry, petrogenesis and*  
40 *rare-metal mineralization: Lithos*, v. 202-203, p. 395–412.  
41
- 42 Emery, J.A., 1968, Geology of the Pea Ridge iron ore body, *in* Ridge, J.D., ed., *Ore*  
43 *deposits of the United States, 1933-1967, The Graton-Sales volume*: New York,  
44 American Institute of Mining, Metallurgical, and Petroleum Engineers, v. I, p. 359–  
45 369.
- 46 Fletcher, I.R., McNaughton, N.J., Aleinikoff, J.N., Rasmussen, B., and Kamo, S.L., 2004,  
47 Improved calibration procedures and new standards for U-Pb and Th-Pb dating of  
48 Phanerozoic xenotime by ion microprobe: *Chemical Geology*, v. 209, p. 295–314.  
49
- 50 Fletcher, I.R., McNaughton, N.J., Davis, W.J., and Rasmussen, B., 2010, Matrix effects  
51 and calibration limitations in ion probe U–Pb and Th–Pb dating of monazite:  
52 *Chemical Geology*, v. 270, p. 31–44.  
53  
54  
55  
56  
57  
58  
59  
60  
61  
62  
63  
64  
65

- 1  
2  
3  
4  
5  
6  
7  
8  
9  
10 Gratz, R., and Heinrich, W., 1997, Monazite-xenotime thermobarometry: Experimental  
11 calibration of the miscibility gap in the binary system  $CePO_4$ - $YPO_4$ : American  
12 Mineralogist, v. 82, p. 772–780.  
13
- 14 Gratz, R., and Heinrich, W., 1998, Monazite-xenotime thermometry. III. Experimental  
15 calibration of the partitioning of gadolinium between monazite and xenotime:  
16 European Journal of Mineralogy, v. 10, p. 579–588.  
17
- 18 Guichard, F., Church, T.M., Treuil, M., and Jaffrezic, H., 1979, Rare earths in barites:  
19 Distribution and effects on aqueous partitioning: *Geochimica et Cosmochimica Acta*,  
20 v. 43, p. 983–997.  
21
- 22 Harlov, D.E., Meighn, C., Kerr, I., and Samson, I.D., this volume, Mineralogy, chemistry,  
23 and hydrothermal evolution of the Pea Ridge Fe-oxide-REE deposit, southeast  
24 Missouri, USA: *Economic Geology*.
- 25 Harlov, D.E., Wirth, R., and Förster, H.-J., 2005, An experimental study of dissolution-  
26 reprecipitation in fluorapatite: fluid infiltration and the formation of monazite :  
27 *Contributions to Mineralogy and Petrology*, v. 150, p. 268–286.  
28
- 29 Harlov, D.E., Wirth, R., and Hetherington, C.J., 2011, Fluid-mediated partial alteration of  
30 monazite: the role of coupled dissolution–reprecipitation in element redistribution and  
31 mass transfer : *Contributions to Mineralogy and Petrology*, v. 162, p. 329–348.  
32
- 33 Harrison, R.W., Lowell, G.R., and Unruh, D.M., 2000, Geology, geochemistry, and age  
34 of Mesoproterozoic igneous rocks in the Eminence-Van Buren area: A major  
35 structural outlier of the St. Francois terrane, south-central Missouri [abs.]: *Geological*  
36 *Society of America Abstracts with Programs*, v. 32, no. 3, p. A-14.  
37
- 38 Harrison, R.W., Orndorff, R.C., and Weary, D.J., 2002, Geology of the Stegall Mountain  
39 7.5-minute quadrangle, Shannon and Carter Counties, south-central Missouri: U.S.  
40 Geological Survey Geologic Investigations Series Map I-2767, scale 1:24,000.  
41
- 42 Hofstra, A.H., Meighan, C.J., Song, X., and Samson, I., this volume, Mineral  
43 thermometry and fluid inclusion studies of the Pea Ridge iron oxide-apatite-rare earth  
44 element deposit, Mesoproterozoic St. Francois Mountains terrane, southeast Missouri,  
45 USA: *Economic Geology*.
- 46 Husman, J.R., 1989, Gold, rare earth element, and other potential by-products of the Pea  
47 Ridge iron ore mine: Missouri Department of Natural Resources, Division of Geology  
48 and Land Survey Contribution to Precambrian Geology no. 21, OFR-89-78-MR, 18 p.  
49
- 50 Ireland, T.R., Wooden, J.L., Persing, H.M., and Ito, B., 1999, Geological applications and  
51 analytical development of the SHRIMP-RG [abs.]: *Eos, Transactions of the American*  
52 *Geophysical Union*, v. 80, no. 46, Supplement, p. F1117.  
53  
54  
55  
56  
57  
58  
59  
60  
61  
62  
63  
64  
65

- 1  
2  
3  
4  
5  
6  
7  
8  
9  
10 Johnson, C.A., Day, W.C, and Rye, R.O., this volume, Oxygen, hydrogen, sulfur and  
11 carbon isotopes in the Pea Ridge magnetite-apatite deposit, southeast Missouri, and  
12 sulfur isotope comparisons to other iron deposits in the region: *Economic Geology*.  
13  
14 Kerr, I.D., 1998, Mineralogy, chemistry, and hydrothermal evolution of the Pea Ridge  
15 Fe-oxide-REE deposit, Missouri, USA: Unpublished M.S thesis, University of  
16 Windsor, Windsor, Ontario, Canada, 113 p.  
17  
18 Kirschner, D.L., Cosca, M.A., Masson, H., and Hunziker, J.C., 1996, Staircase  $^{40}\text{Ar}/^{39}\text{Ar}$   
19 spectra of fine-grained white mica: Timing and duration of deformation and empirical  
20 constraints on argon diffusion: *Geology*, v. 24, p. 747–750.  
21  
22 Kisvarsanyi, E.B., 1980, Granitic ring complexes and hotspot activity in the St. Francois  
23 terrane, Midcontinent region, United States: *Geology*, v. 8, p. 43–47.  
24  
25 Kisvarsanyi, E.B., 1981, Geology of the Precambrian St. Francois terrane southeastern  
26 Missouri: Missouri Department of Natural Resources, Division of Geology and Land  
27 Survey, Report of Investigations 64, 58 p.  
28  
29 Kisvarsanyi, G., and Procter, P.D., 1967, Trace element content of magnetites and  
30 hematites, southeast Missouri iron metallogenic province, U.S.A.: *Economic*  
31 *Geology*, v. 62, p. 449–471.  
32  
33 Korotev R.L., 1996, On the relationship between the Apollo 16 ancient regolith breccias  
34 and feldspathic fragmental breccias, and the composition of the prebasin crust in the  
35 Central Highlands of the Moon: *Meteoritics & Planetary Science*, v. 31, p. 403–412.  
36  
37 Kositcin, N., McNaughton, N.J., Griffin, B.J., Fletcher, I.R., Groves, D.I., and  
38 Rasmussen, B., 2003, Textural and geochemical discrimination between xenotime of  
39 different origins in the Archaean Witwatersrand basin, South Africa: *Geochimica et*  
40 *Cosmochimica Acta*, v. 67, p. 709–731.  
41  
42 Kuiper, K.F., Deino, A., Hilgen, F.J., Krijgsman, W., Renne, P.R., and Wijbrans, J.R.,  
43 2008, Synchronizing rock clocks of Earth history: *Science*, v. 320, p. 500-504. doi:  
44 10.1126/science.1154339.  
45  
46 Lawley, C.J.M., and Selby, D., 2012, Re-Os geochronology of quartz-enclosed ultra-fine  
47 molybdenite: Implications for ore geochronology: *Economic Geology*, v. 107, p.  
48 1499–1506.  
49  
50 Lee, J.-Y., Marti, K., Yoo, H.-S., Severinghaus, J.P., Lee, J.B., Kawamura, K., and Kim,  
51 J.S., 2006, A redetermination of the isotopic abundances of atmospheric Ar:  
52 *Geochimica et Cosmochimica Acta* v. 70, p. 4507–4512.  
53  
54 Lowell, G.R., 1991, The Butler Hill caldera: A mid-Proterozoic ignimbrite-granite  
55 complex: *Precambrian Research*, v. 51, p. 245–263.  
56  
57  
58  
59  
60  
61  
62  
63  
64  
65

- 1  
2  
3  
4  
5  
6  
7  
8  
9  
10  
11 Lowell, G.R., and Young, G.J., 1999, Interaction between coeval mafic and felsic melts  
12 in the St. Francois terrane of Missouri, USA: *Precambrian Research*, v. 95, p. 66–  
13 88.  
14  
15 Ludwig, K.R., 1980, Calculation of uncertainties of U-Pb isotope data: *Earth and*  
16 *Planetary Science Letters*, v. 46, p. 212–220.  
17  
18 Ludwig, K.R., 2003, Isoplot/Ex version 3.00, A geochronological toolkit for Microsoft  
19 Excel: Berkeley, California, Berkeley Geochronology Center Special Publication  
20 No. 4, 73 p.  
21  
22 Ludwig, K.R., 2009, Squid 2, version 2.50, A user's manual: Berkeley, California,  
23 Berkeley Geochronology Center, Special Publication No. 5, 110 p.  
24  
25 Mazdab, F.K., and Wooden, J.L., 2006, Trace element analysis of accessory and rock-  
26 forming minerals by ion microprobe (SHRIMP-RG) [abs.]: *Eos, Transactions of*  
27 *the American Geophysical Union*, v. 87, Fall Meeting Supplement, Abstract  
28 V33A-0630.  
29  
30 McDonough, W.F., and Sun, S.-S., 1995, The composition of the Earth: *Chemical*  
31 *Geology*, v. 120, p. 223–253.  
32  
33 McDougall, I., and Wellman, P., 2011, Calibration of GA1550 biotite standard for K/Ar  
34 and  $^{40}\text{Ar}/^{39}\text{Ar}$  dating: *Chemical Geology*, v. 280, p. 19–25.  
35  
36 McDowell, R.C., and Harrison, R.W., 2000, Geologic map of the Powder Mill Ferry  
37 quadrangle, Shannon and Reynolds Counties, Missouri: U.S. Geological Survey  
38 Geologic Investigations Series, Map I-2722, scale 1:24,000.  
39  
40 Menuge, J.F., Brewer, T.S., and Seeger, C.M., 2002, Petrogenesis of metaluminous A-  
41 type rhyolites from the St Francois Mountains, Missouri and the Mesoproterozoic  
42 evolution of the southern Laurentian margin: *Precambrian Research*, v. 113, p.  
43 269–291.  
44  
45 Min, K., Mundil, R., Renne, P.R., and Ludwig, K.R., 2000, A test for systematic errors in  
46 Ar/Ar geochronology through U–Pb analysis of 1.1 Ga rhyolite: *Geochimica et*  
47 *Cosmochimica Acta*, v. 64, p. 73–98.  
48  
49 Morgan, J.W., and Wandless, G.A., 1980, Rare earth element distribution in some  
50 hydrothermal minerals: Evidence for crystallographic control: *Geochimica et*  
51 *Cosmochimica Acta*, v. 44, p. 973-980.  
52  
53 Muhling, J.R., Fletcher, I.R., and Rasmussen, B., 2012, Dating fluid flow and Mississippi  
54 Valley type base-metal mineralization in the Paleoproterozoic Earaheedy Basin,  
55 Western Australia: *Precambrian Research*, v. 212–213, p. 75–90.  
56  
57  
58  
59  
60  
61  
62  
63  
64  
65

- 1  
2  
3  
4  
5  
6  
7  
8  
9  
10 Neymark, L.A., Holm-Denoma, C.S., Pietruszka, A.J., Aleinikoff, J.N., Fanning, C.M.,  
11 Pillers, R.M., and Moscati, R.J., this volume, High spatial resolution U-Pb  
12 geochronology and Pb-isotope geochemistry of magnetite-apatite ore from the Pea  
13 Ridge iron oxide-apatite (IOA) deposit, Saint Francois Mountains, SE Missouri,  
14 USA: *Economic Geology*.
- 15  
16 Nold, J.L., Dudley, M.A., and Davidson, P., 2014, The southeast Missouri (USA)  
17 Proterozoic iron metallogenic province—Types of deposits and genetic relationships  
18 to magnetite-apatite and iron oxide-copper-gold deposits: *Ore Geology Reviews*, v.  
19 57, p. 154–171.
- 20  
21 Nuelle, L.M., Day, W.C., Sidder, G.B., and Seeger, C.M., 1992, Geology and mineral  
22 paragenesis of the Pea Ridge iron ore mine, Washington County, Missouri—  
23 Origin of the rare-earth-element- and gold-bearing breccia pipes: *U.S. Geological  
24 Survey Bulletin 1989-A*, 11 p.
- 25  
26 Orndorff, R.C., Harrison, R.W., and Weary, D.J., 1999, Geologic map of the Eminence  
27 quadrangle, Shannon County, Missouri: U.S. Geological Survey Geologic  
28 Investigations Series Map I-2653, scale 1:24,000.
- 29  
30 Parrish, R.R., 1990, U–Pb dating of monazite and its application to geological problems:  
31 *Canadian Journal of Earth Science*, v. 27, p. 1431–1450.
- 32  
33 Pratt, W.P., Anderson, R.E., Berry, A.W., Jr., Bickford, M.E., Kisvarsanyi, E.B., and  
34 Sides, J.R., 1979, Geologic map of exposed Precambrian rocks, Rolla 1° x 2°  
35 quadrangle, Missouri: U. S. Geological Survey Miscellaneous Investigations  
36 Series Map I-1161, scale 1:250,000.
- 37  
38 Pratt, W.P., Middendorf, M.A., Satterfield, I.R., and Gerdemann, P.E., 1992, Geologic  
39 map of the Rolla 1° x 2° quadrangle, Missouri: U. S. Geological Survey,  
40 Miscellaneous Investigations Series Map I-1998, scale 1:250,000.
- 41  
42 Robinson, R.J., Power, M.A., and Barker, J.C., 2011, Technical report on the exploration  
43 program and mineral resource estimate for the Bokan Mountain property, Prince  
44 of Wales Island, Alaska: Ucore Rare Metals, Inc., NI 43-101, 190 p. Available at:  
45 <http://ucore.com/projects/bokan-mountain-alaska/43-101>
- 46  
47 Schärer, U., 1984, The effect of initial <sup>230</sup>Th disequilibrium on young U-Pb ages: The  
48 Makalu case, Himalaya: *Earth and Planetary Science Letters*, v. 77, p. 35–48.
- 49  
50 Schärer, U., Xu, R.H., and Allègre, C.J., 1986, U-(Th)-Pb systematics and ages of  
51 Himalayan leucogranites, South Tibet: *Earth and Planetary Science Letters*, v. 77,  
52 p. 35–48.
- 53  
54 Seeger, C.M., 1992, Three-dimensional modeling of rare earth element-bearing breccia  
55 pipes at the Pea Ridge mine, southeast Missouri: What can it tell us? [abs.]:  
56 *Geological Society of America Abstracts with Programs*, v. 24, no. 4, p. 63–64.

1  
2  
3  
4  
5  
6  
7  
8  
9  
10  
11  
12  
13  
14  
15  
16  
17  
18  
19  
20  
21  
22  
23  
24  
25  
26  
27  
28  
29  
30  
31  
32  
33  
34  
35  
36  
37  
38  
39  
40  
41  
42  
43  
44  
45  
46  
47  
48  
49  
50  
51  
52  
53  
54  
55  
56  
57  
58  
59  
60  
61  
62  
63  
64  
65

Seeger, C.M., 2003, Lithology and alteration assemblages of the Boss iron-copper deposit, Iron and Dent Counties, southeast Missouri: Unpublished Ph.D. Thesis, University of Missouri–Rolla, Rolla, Missouri, 138 p.

Seeger, C.M., Nuelle, L.M., Day, W.C., Sidder, G.B., Marikos, M.A., and Smith, D.C., 2001, Geologic maps and cross sections of mine levels at the Pea Ridge iron mine, Washington County, Missouri U.S. Geological Survey Miscellaneous Field Studies Map MF-2353, 6 p., 5 sheets, scale 1:2400.

Selby, D., and Creaser, R.A., 2004, Macroscale NTIMS and microscale LA-MC-ICP-MS Re-Os isotopic analysis of molybdenite: Testing spatial restrictions for reliable Re-Os age determinations, and implications for the decoupling of Re and Os within molybdenite: *Geochimica et Cosmochimica Acta*, v. 68, p. 3897–3908.

Selby, D., Creaser, R.A., Stein, H.J., Markey, R.J., and Hannah, J.L., 2007, Assessment of the  $^{187}\text{Re}$  decay constant accuracy and precision: Cross calibration of the  $^{187}\text{Re}$ - $^{187}\text{Os}$  molybdenite and U-Pb zircon chronometers: *Geochimica et Cosmochimica Acta*, v. 71, p. 1999–2013.

Sidder, G.B., Day, W.C., Nuelle, L.M., Seeger, C.M., and Kisvarsanyi, E.B., 1993, Mineralogic and fluid-inclusion studies of the Pea Ridge iron–rare-earth-element deposit, southeast Missouri: *U.S. Geological Survey Bulletin* 2039, p. 205–216.

Sides, J.R., Bickford, M.E., Shuster, R.D., and Nusbaum, R.L., 1981, Calderas in the Precambrian terrane of the St. Francois Mountains, southeastern Missouri: *Journal of Geophysical Research*, v. 86, no. B11, p. 10,349–10,364.

Smoliar, M.I., Walker, R.J., and Morgan, J.W., 1996, Re-Os ages of Group IIA, IIIA, IVA, and IVB iron meteorites: *Science*, v. 271, p. 1099–1102.

Snyder, F.G., 1968, Geology and mineral deposits, Midcontinent United States, *in* Ridge, J.D., ed., *Ore deposits of the United States, 1933-1967, The Graton-Sales volume*: New York, American Institute of Mining, Metallurgical, and Petroleum Engineers, v. I, p. 258–286.

Stacey, J.S., and Kramers, J.D., 1975, Approximation of terrestrial Pb isotope composition by a two-stage model: *Earth and Planetary Science Letters*, v. 26, p. 207–222.

Starkey, M.A., and Seeger, C.M., this volume, Mining and exploration history of the southeast Missouri iron metallogenic province, United States: *Economic Geology*.

Steiger, R.H., and Jäger, E., 1977, Subcommittee on geochronology: Convention on the use of decay constants in geo- and cosmochronology: *Earth and Planetary Science Letters*, v. 36, p. 359–362.

1  
2  
3  
4  
5  
6  
7  
8  
9  
10  
11  
12  
13  
14  
15  
16  
17  
18  
19  
20  
21  
22  
23  
24  
25  
26  
27  
28  
29  
30  
31  
32  
33  
34  
35  
36  
37  
38  
39  
40  
41  
42  
43  
44  
45  
46  
47  
48  
49  
50  
51  
52  
53  
54  
55  
56  
57  
58  
59  
60  
61  
62  
63  
64  
65

Thomas, W.A, Tucker, R.D., Astini, R.A., and Denison, R.E., 2012, Ages of pre-rift basement and synrift rocks along the conjugate rift and transform margins of the Argentine Precordillera and Laurentia: *Geosphere*, v. 8, p. 1–18.

Tolman, C., and Robertson, F., 1969, Exposed Precambrian rocks in southeast Missouri: Missouri Geological Survey and Water Resources, Contribution to Precambrian Geology 1, Report of Investigations 44, 68 p.

Van Schmus, W.R., Bickford, M.E., and Turek, A., 1996, Proterozoic geology of the east-central Midcontinent basement, *in* van der Pluijm, B., and Catacosinos, P., eds., *Basement and basins of eastern North America: Geological Society of America Special Paper 308*, p. 7–31.

Walker, J.A., Pippin, C.G., Cameron, B.I., and Patino, L., 2002, Tectonic insights provided by Mesoproterozoic mafic rocks of the St. Francois Mountains, southeastern Missouri: *Precambrian Research*, v. 117, p. 251–268.

Wall, F., 2014, Rare earth elements, *in* Gunn, G., ed., *Critical metals handbook*: Oxford, U.K., John Wiley & Sons, doi: 10.1002/9781118755341.ch13.

Williams, I.S., 1998, U-Th-Pb geochronology by ion microprobe: *Reviews in Economic Geology*, v. 7, p. 1–35.

Yang, X.-Y., Sun, W.-D., Zhang, Y.-X., and Zheng, Y.-F., 2009, Geochemical constraints on the genesis of the Bayan Obo Fe-Nb-REE deposit in Inner Mongolia, China: *Geochimica et Cosmochimica Acta*, v. 73, p. 1417–1435.

1  
2  
3  
4  
5  
6  
7  
8  
9  
10 **Figure Captions**  
11

12 Figure 1. Regional basement geologic map of St. Francois Mountains terrane,  
13 southeastern Missouri (modified from Kisvarsanyi, 1981). Locations of caldera  
14 structures from Pratt et al. (1979) and Brown (1989). Pea Ridge deposit is at  
15 northwestern end of the belt of Mesoproterozoic rocks.  
16

17 Figure 2. Schematic cross section of Pea Ridge deposit (modified from Seeger et al.,  
18 2001). Note that breccia pipe (only one of four is shown) and felsic dike are not in  
19 contact.  
20

21 Figure 3. Comparative plot of chondrite-normalized whole-rock REE data from REE-rich  
22 deposits. Sources of data: Bayan Obo (Yang et al., 2009), Mountain Pass (Castor and  
23 Hedrick, 2006), Bokan Mountain (Robinson et al., 2011), Pea Ridge (Nuelle et al.,  
24 1992; Ayuso et al., this volume). Dashed line shows bulk REE analysis of sample PR-  
25 33C (xenotime-depleted soft breccia pipe; Nuelle et al., 1992). Dotted line shows  
26 bulk REE analysis of sample 2475-11-169.0 (molybdenite-bearing hard breccia pipe).  
27 Chondrite values from McDonough and Sun (1995).  
28

29 Figure 4. SEM images of representative zircon and U-Pb isotopic data from host  
30 rhyolitic rocks, Pea Ridge deposit. A, B, CL and transmitted light image pairs, and  
31 Concordia plot with inset showing weighted average of  $^{207}\text{Pb}/^{206}\text{Pb}$  ages for sample  
32 PR-12 (black rhyolite). C, D, CL and transmitted light image pairs, and Concordia  
33 plot with inset showing weighted average of  $^{207}\text{Pb}/^{206}\text{Pb}$  ages for sample PR-91 (pink  
34 rhyolite).  
35

36 Figure 5. SEM images of representative zircon and U-Pb isotopic data from late felsic  
37 dikes, Pea Ridge deposit. A, B, CL and transmitted light image pairs, and Concordia  
38 plot for xenocrystic grains from sample 966-5. C, D, CL and transmitted light image  
39 pairs, and Concordia plot with inset showing weighted average of  $^{207}\text{Pb}/^{206}\text{Pb}$  ages for  
40 spongy igneous grains from sample 966-5. E, F, CL and transmitted light image  
41 pairs, and Concordia plot for xenocrystic grains from sample PR-25. Note in A, C,  
42 and E irregular spongy overgrowths surrounding xenocrystic cores.  
43

44 Figure 6. SEM images showing textural relationships of monazite and xenotime from  
45 breccia pipe samples. A, Fractured angular fragment composed of small grains of  
46 monazite, xenotime, and thorite. Square indicates location of image B. B, High-  
47 magnification image showing granular textures. Minerals present are monazite  
48 (medium gray), xenotime (dark gray), thorite (light gray), and galena (white). C,  
49 Fractured granular matrix of mostly monazite and xenotime. Abbreviations: Ap,  
apatite; Chl, chlorite; Gn, galena; Mnz, monazite; Thr, thorite; Xtm, xenotime.  
50

51 Figure 7. Microscope and SEM images and U-Pb isotopic data for sample PR95-30  
52 (“hard” pipe). A, Low-magnification microscope image of polished thin section  
53 under crossed nicols. Note fine-grained matrix (composed of monazite and xenotime)  
54 surrounding most coarse breccia clasts. B, High-magnification BSE image of  
55  
56  
57  
58  
59  
60  
61  
62  
63  
64  
65

1  
2  
3  
4  
5  
6  
7  
8  
9  
10 granular matrix monazite and xenotime. Note polygonal texture of fine  
11 monazite+xenotime grains. C, Concordia plot with inset showing weighted average  
12 of  $^{207}\text{Pb}/^{206}\text{Pb}$  ages for monazite. Data for older grain shown by blue error ellipse and  
13 blue error bar excluded from age calculation. D, Concordia plot with inset showing  
14 weighted average of  $^{207}\text{Pb}/^{206}\text{Pb}$  ages for xenotime. Abbreviations: Mnz, monazite;  
15 Xnt, xenotime.  
16

17 Figure 8. SEM images and U-Pb isotopic data for sample 2275-15 (“hard” pipe). A,  
18 BSE image of unpolished granular fragment composed mostly of monazite (medium  
19 gray), xenotime (dark gray), and thorite (light gray). B, BSE image of polished  
20 granular fragment showing polygonal texture of intergrown monazite and xenotime.  
21 C, Concordia plot with inset showing weighted average of  $^{207}\text{Pb}/^{206}\text{Pb}$  ages for  
22 monazite. Data for slightly younger grain shown by blue error ellipse and blue error  
23 bar excluded from age calculation. D, Concordia plot with inset showing weighted  
24 average of  $^{207}\text{Pb}/^{206}\text{Pb}$  ages for xenotime. Data for slightly younger grains shown by  
25 blue error ellipses and error bars excluded from age calculation. Abbreviations: Mnz,  
26 monazite; Xnt, xenotime.  
27

28 Figure 9. SEM and microscope images, and U-Pb isotopic data for sample PR-182  
29 (“hard” pipe). A, BSE image showing granular matrix of monazite and xenotime  
30 between two large grains of barite. A narrow zone (width marked by red line) within  
31 the area of granular grains is composed of slivers of monazite and xenotime, some of  
32 which are cemented by apatite. B, Binocular microscope image showing granular and  
33 glassy monazite morphologies. C, BSE image of coarse glassy monazite. Note  
34 slightly brighter rims on both grains. D, Concordia plot with insets showing weighted  
35 average of  $^{207}\text{Pb}/^{206}\text{Pb}$  ages for cores (red error ellipses and error bars) and rims (blue  
36 error ellipses and error bars) of monazite. Abbreviations: Bar, barite; Mnz, monazite;  
37 Pyr, pyrite; Xnt, xenotime.  
38

39 Figure 10. SEM and microscope images, and U-Pb isotopic data for sample 193488B  
40 (“hard” pipe). A, BSE image showing granular matrix composed of monazite (lighter  
41 gray) and xenotime (darker gray). B, BSE image of two grains of glassy monazite. C,  
42 Binocular microscope image of glassy monazite. D, BSE image of granular monazite  
43 and xenotime cemented by apatite (dark gray). E, BSE image of polished grains of  
44 monazite, showing darker cores and brighter rims. F, Concordia plot with insets  
45 showing weighted average of  $^{207}\text{Pb}/^{206}\text{Pb}$  ages for cores (red error ellipses and error  
46 bars) and rims (blue error ellipses and error bars) of monazite. Data for older grains  
47 shown by green error ellipse and error bar excluded from age calculation.  
48

49 Figure 11. Microscope and SEM images, and U-Pb isotopic data for sample PR-33C  
50 (“soft” pipe). A, Binocular microscope image of granular monazite. B, BSE image  
51 of polished granular matrix monazite. C, Concordia plot with inset showing weighted  
52 average of  $^{207}\text{Pb}/^{206}\text{Pb}$  ages for granular monazite.  
53

54 Figure 12. Images of molybdenite in “hard” pipe sample DDH 2475-1. A, Binocular  
55 microscope image of core surface showing relatively coarse molybdenite and pyrite.  
56  
57  
58  
59  
60  
61  
62  
63  
64  
65

1  
2  
3  
4  
5  
6  
7  
8  
9  
10 B, BSE image showing fine flakes of molybdenite intergrown with quartz and  
11 allanite. Abbreviations: Aln, allanite; Ap, apatite; Mlb, molybdenite; Qtz, quartz;  
12 Xnt, xenotime.  
13

14 Figure 13. Results of  $^{40}\text{Ar}/^{39}\text{Ar}$  heating experiments for minerals from sample PR-182.  
15 A, Data for muscovite (red) and biotite (black). B, Data for K-feldspar.  
16

17 Figure 14. Chondrite-normalized REE plots for monazite and xenotime from Pea Ridge  
18 breccia pipes. A, Coarse glassy monazite from PR-182. B-D, Granular matrix  
19 monazite from samples PR-182, 2275-15, and PR-33C, respectively. Red curves  
20 shown in D pertain to igneous monazite (Aleinikoff et al., 2012). E, Granular matrix  
21 xenotime from 2275-15. REE data from *in situ* analysis by SHRIMP-RG. Dashed  
22 gray line segments in B and E suggest mixed data resulting from minor overlap of  
23 SHRIMP spot on adjacent grain.  
24

25 Figure 15. Comparative trace element and REE plots for monazite and xenotime. A-B,  
26 Th/U and La/Lu vs. chondrite-normalized Eu/Eu\*, highlighting compositional  
27 difference between matrix monazite from sample PR-182 and other samples of matrix  
28 monazite and coarse glassy monazite in PR-182. Gray fields show SHRIMP-RG  
29 trace element data for igneous monazite from three samples of granite based on 29  
30 SHRIMP-RG trace element analyses (Aleinikoff et al., 2012). C-D, REE abundances  
31 in matrix xenotime from sample 2275 compared to those characteristic of xenotime  
32 generated by igneous, metamorphic, and hydrothermal processes (see Aleinikoff et  
33 al., 2015, for additional explanation).  
34  
35  
36

### 37 Tables

38  
39 Table 1. SHRIMP U-Pb data for zircon, monazite, and xenotime from Pea Ridge REE-  
40 rich breccia pipes and related rocks.

41  
42 Table 2. Re-Os data for molybdenite from Pea Ridge breccia pipe sample DDH 2475-1.

43  
44 Table 3.  $^{40}\text{Ar}/^{39}\text{Ar}$  data for muscovite, biotite, and K-feldspar from Pea Ridge breccia  
45 pipe sample PR-182.

46  
47 Table 4. Summary of geochronological data.

48  
49 Table 5. Trace element data for monazite and xenotime from breccia pipes, plus one  
50 whole-rock sample, Pea Ridge, St. Francois Mountains, Missouri.

51  
52 Table 6. Calculation of temperatures of crystallization of monazite and xenotime in  
53 sample 2275-15.  
54  
55

Figure 1

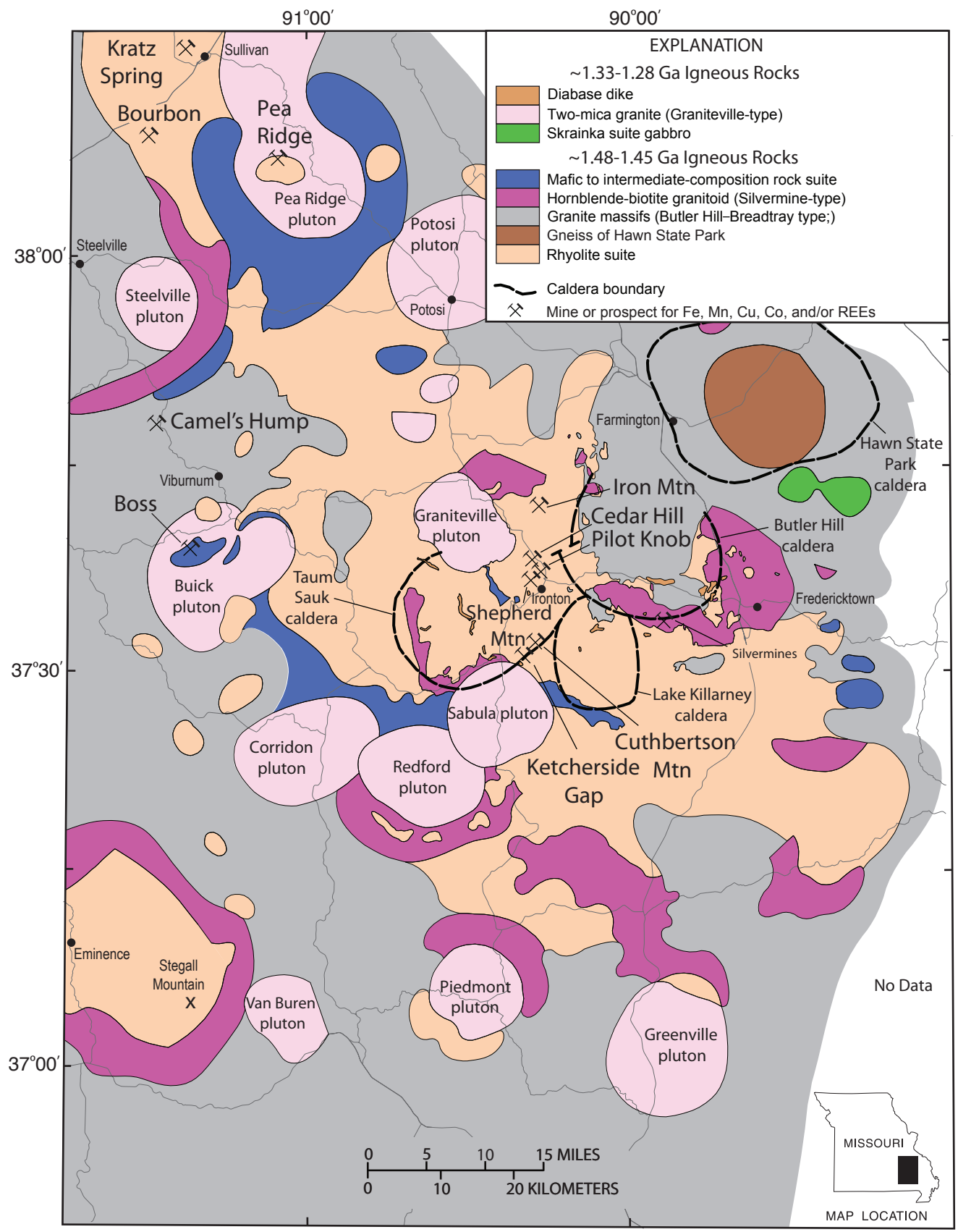


Figure 1

Figure 2

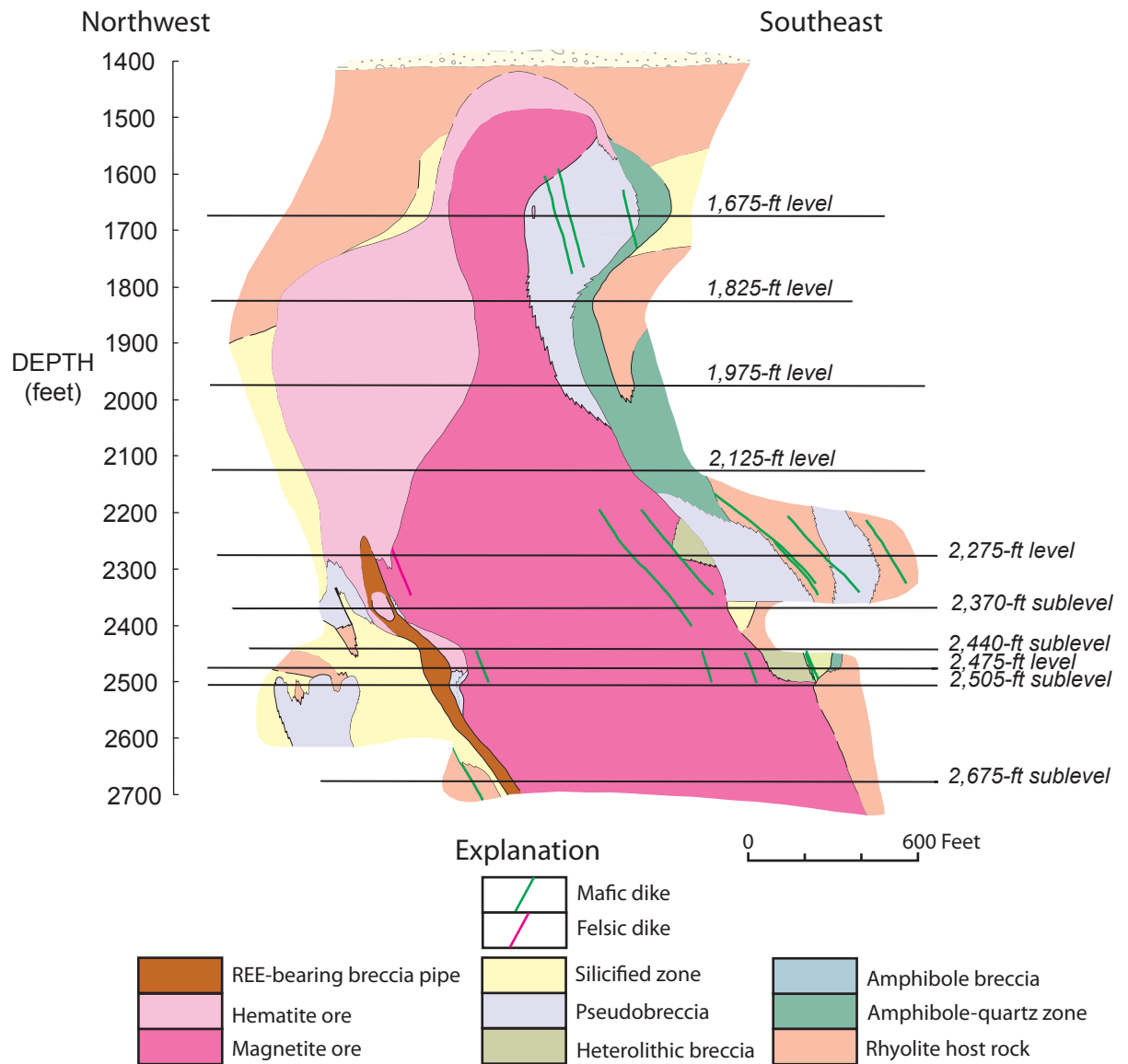


Figure 2

Figure 3

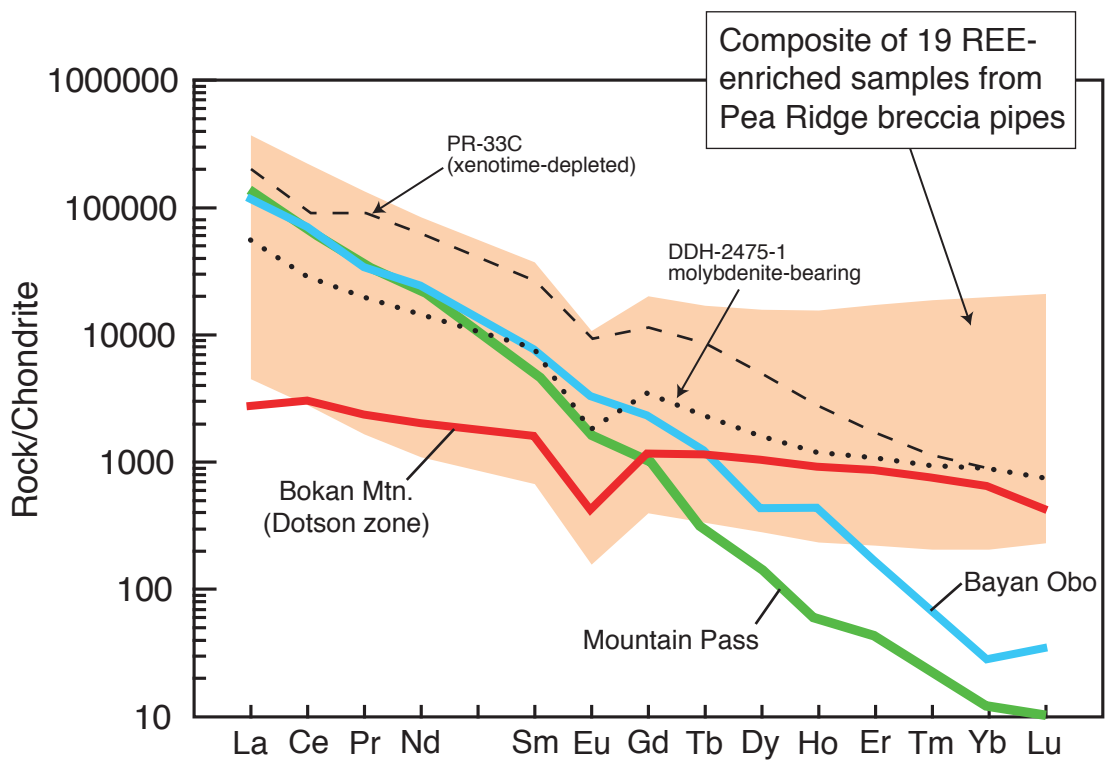


Figure 3

Figure 4

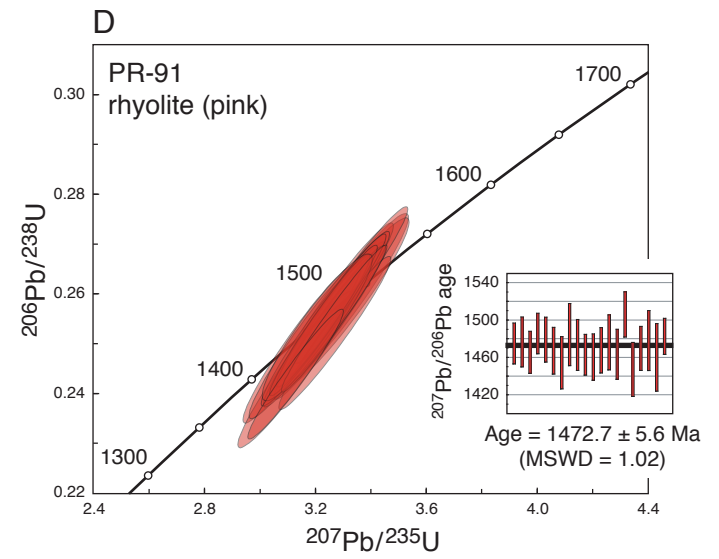
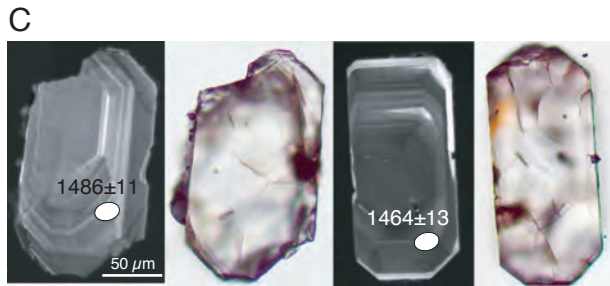
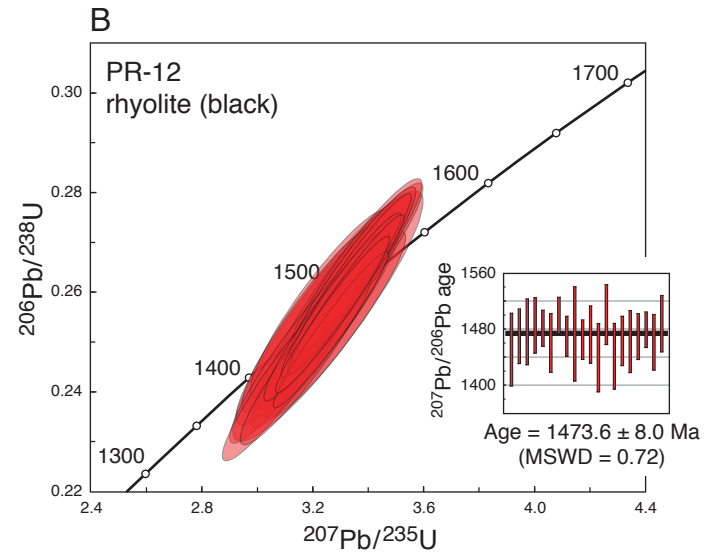
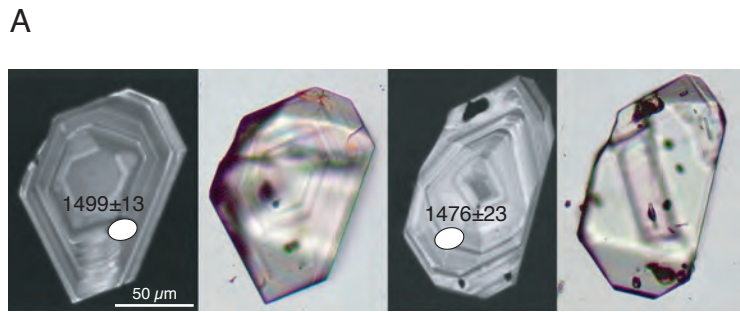


Figure 4

Figure 5

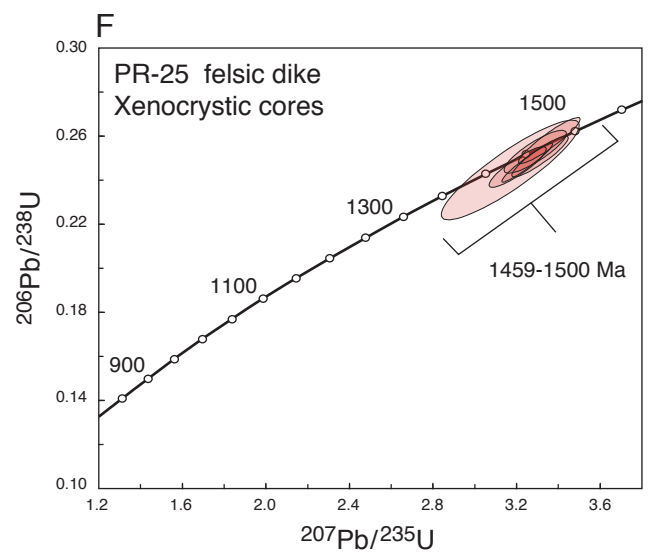
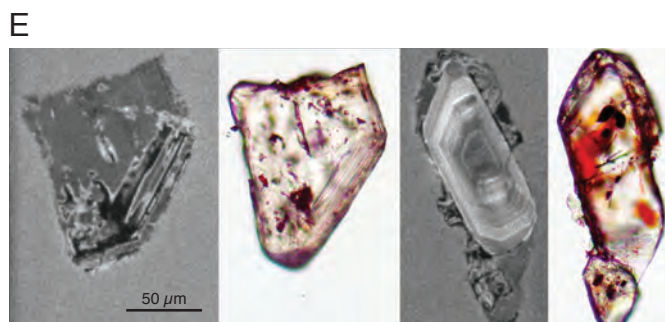
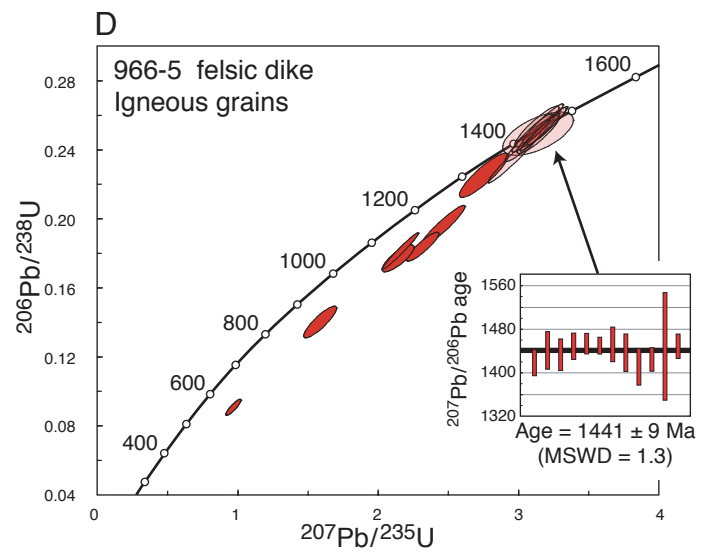
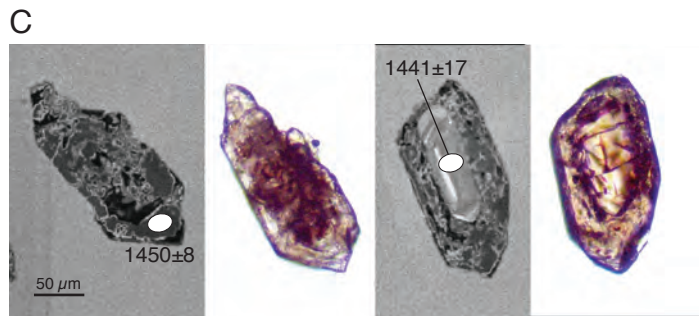
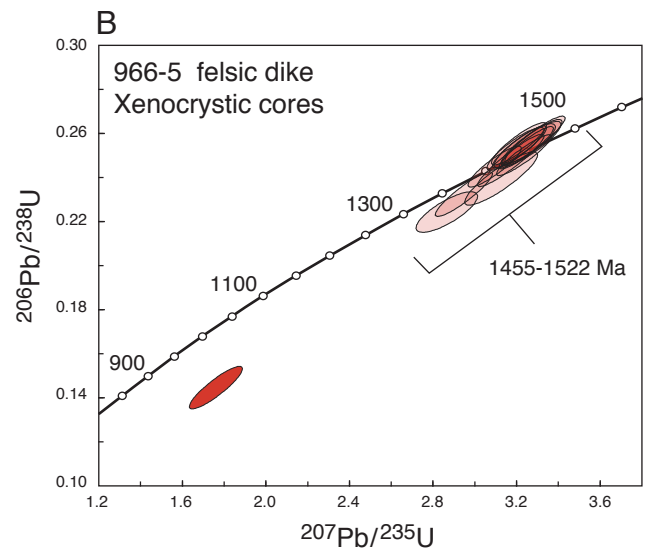
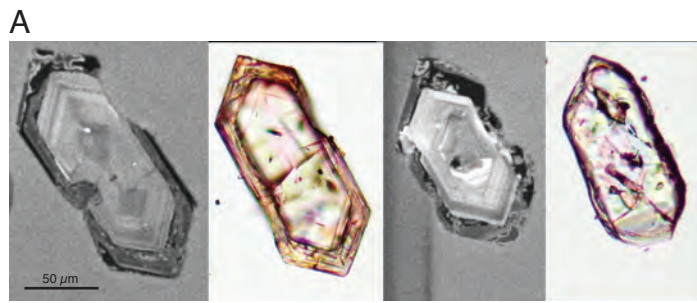


Figure 5

Figure 6

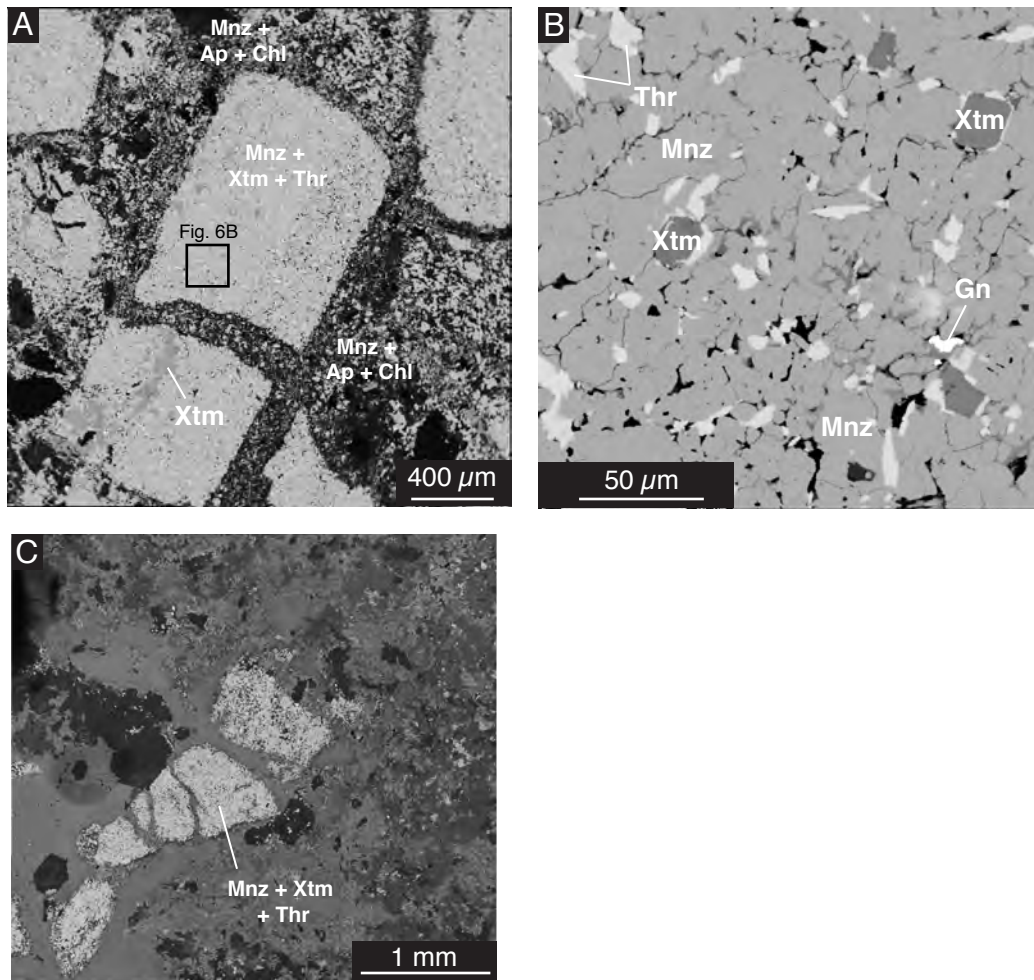


Figure 6

Figure 7

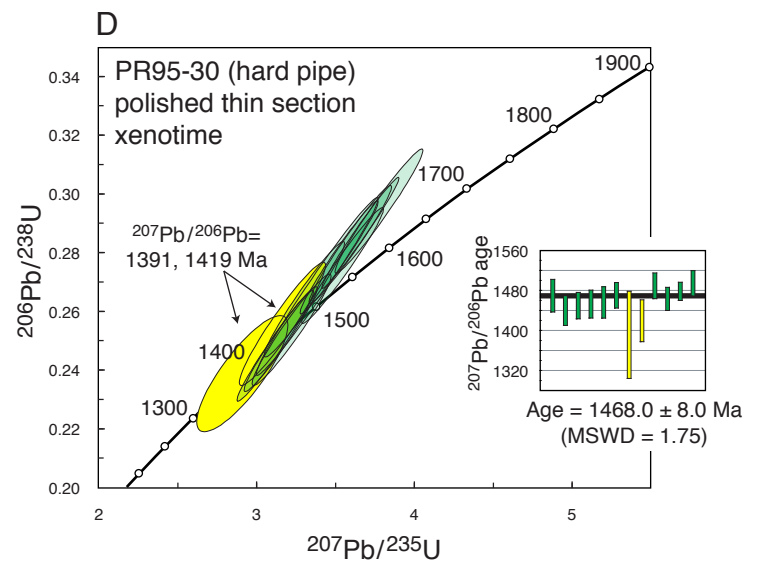
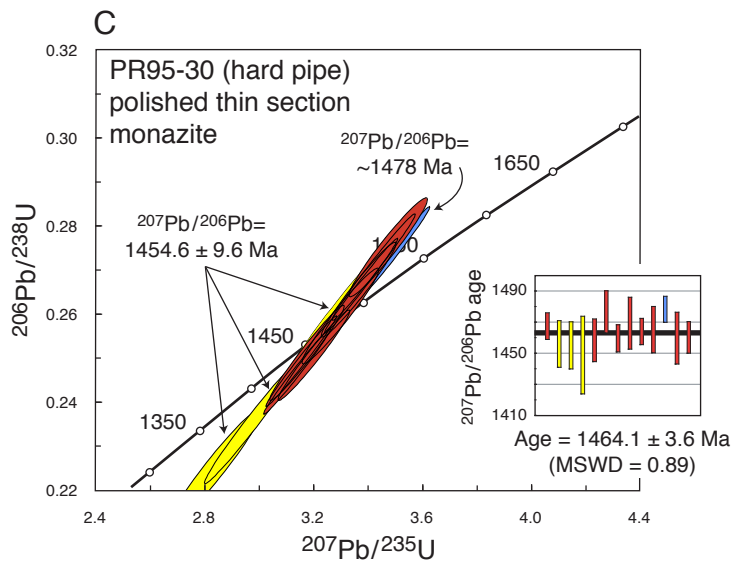
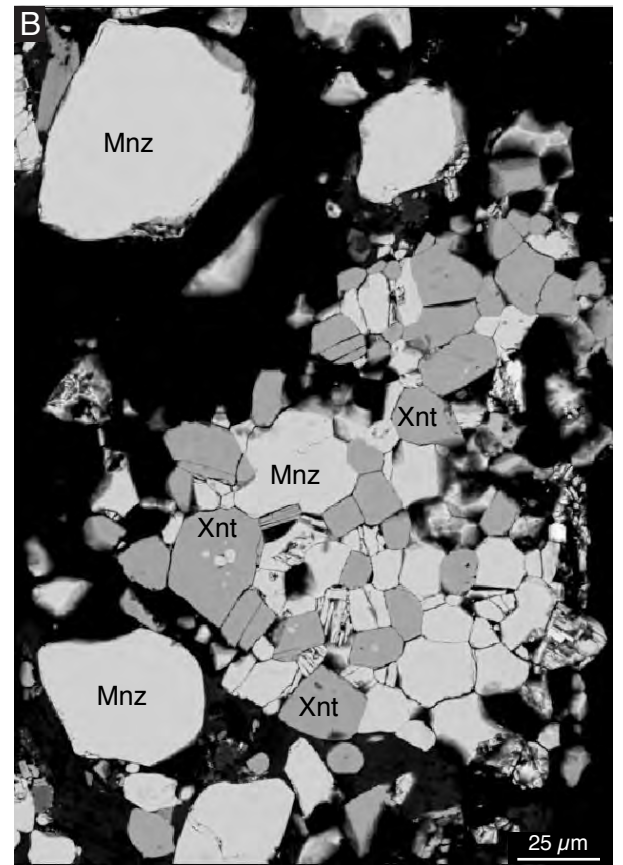
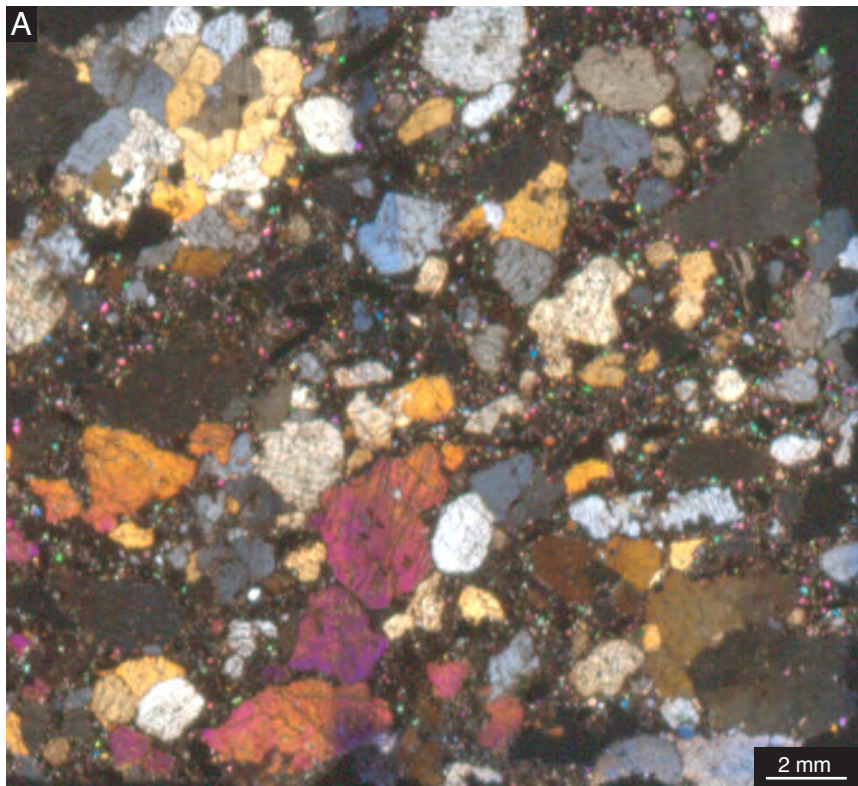


Figure 7

Figure 8

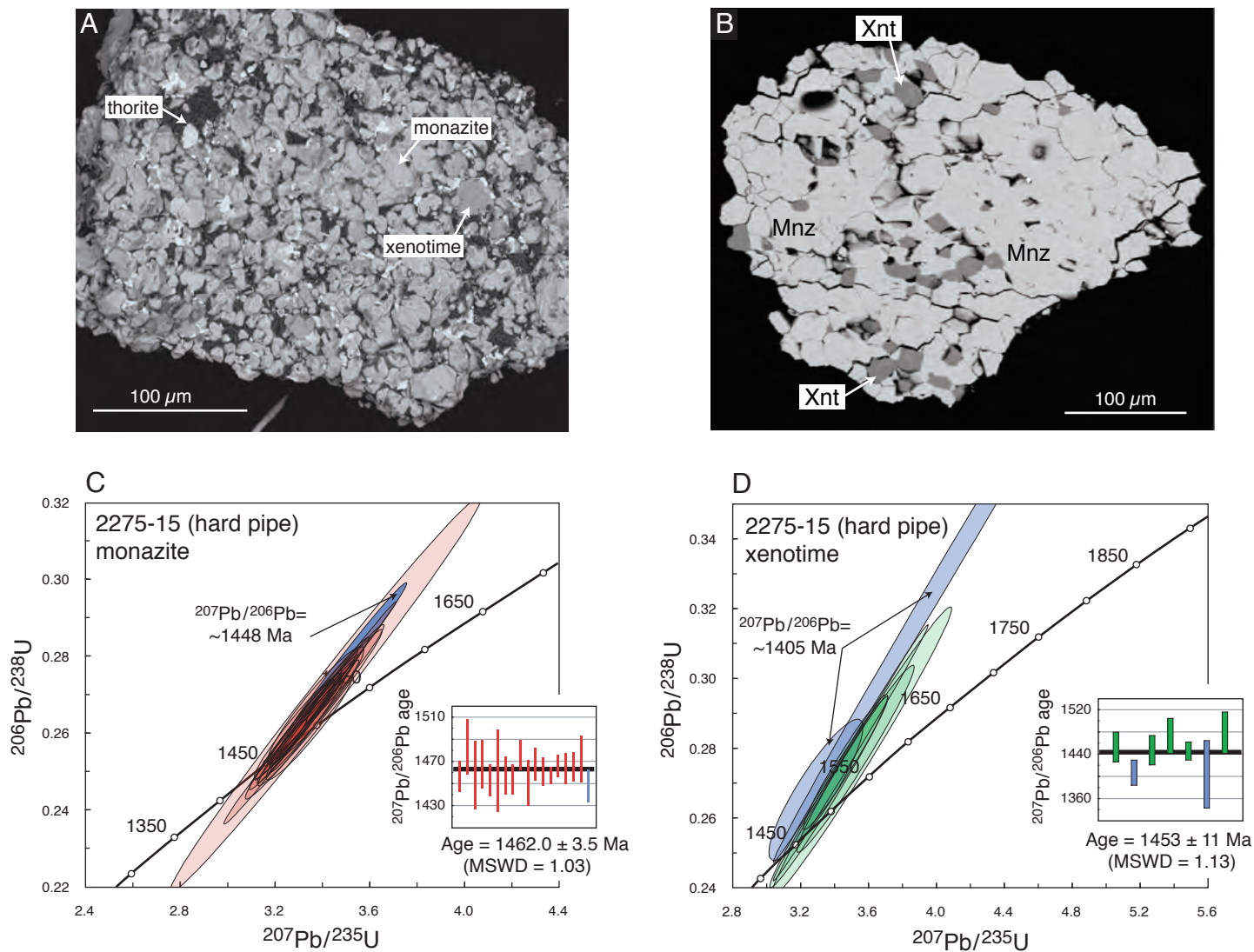


Figure 8

Figure 9

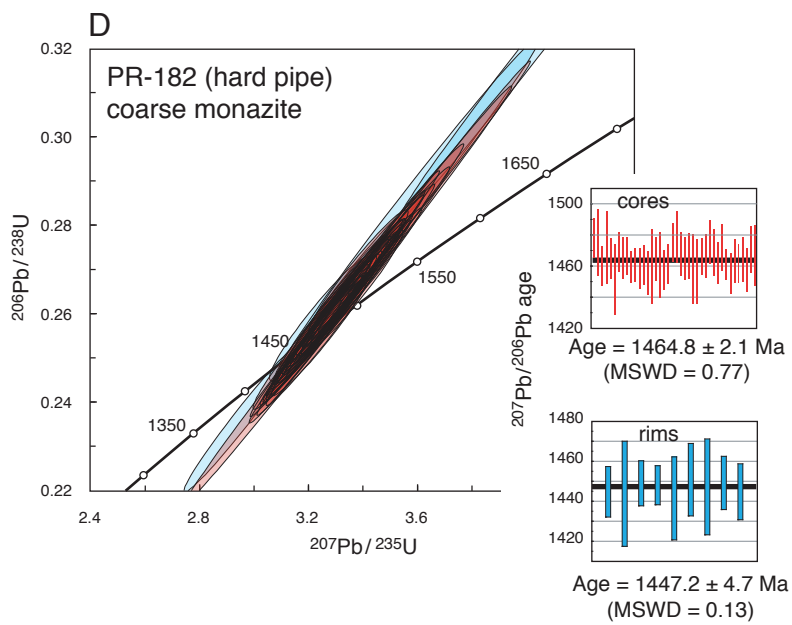
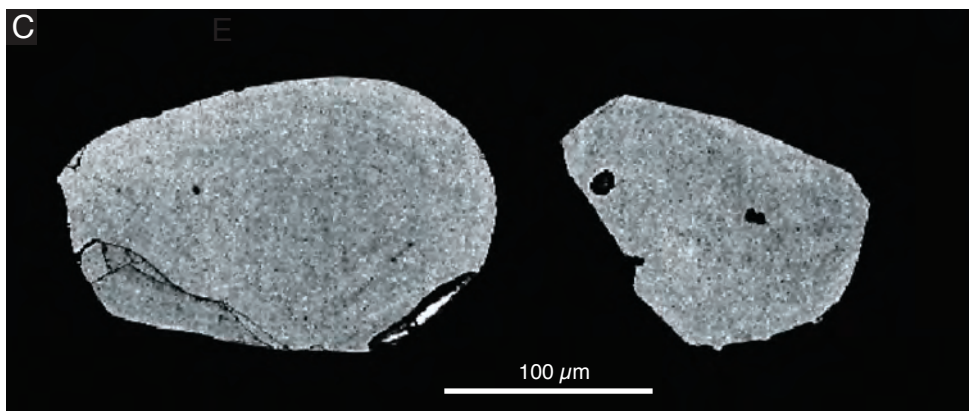
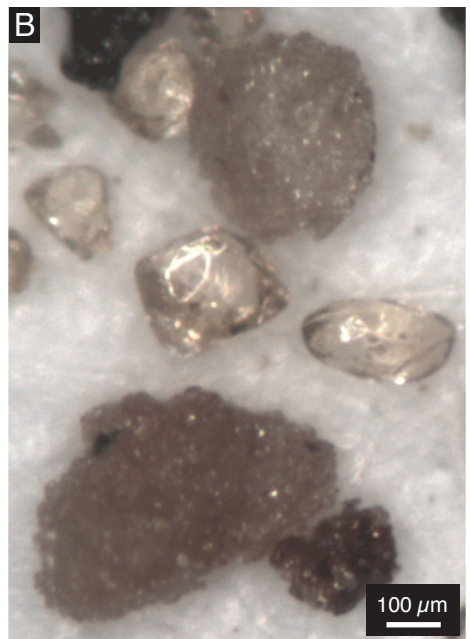
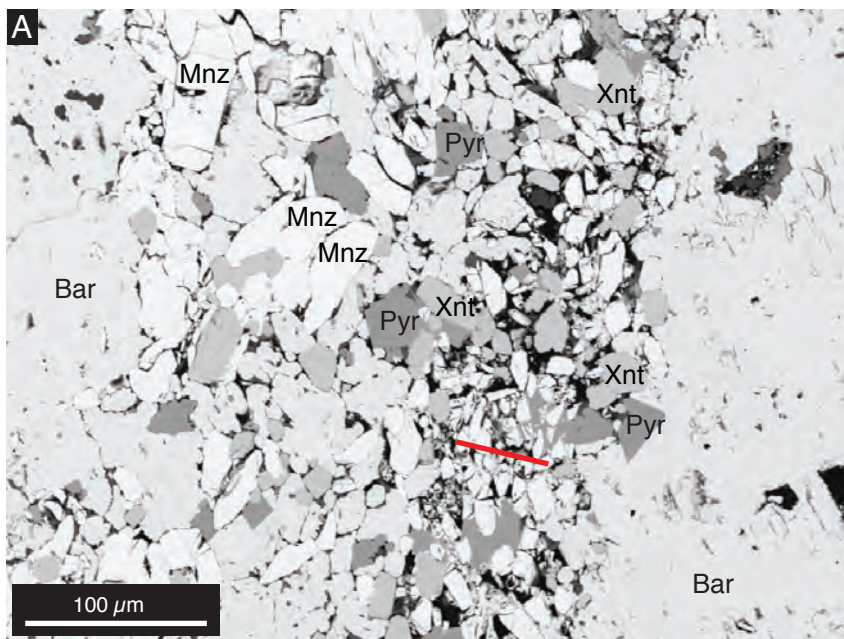


Figure 9

Figure 10

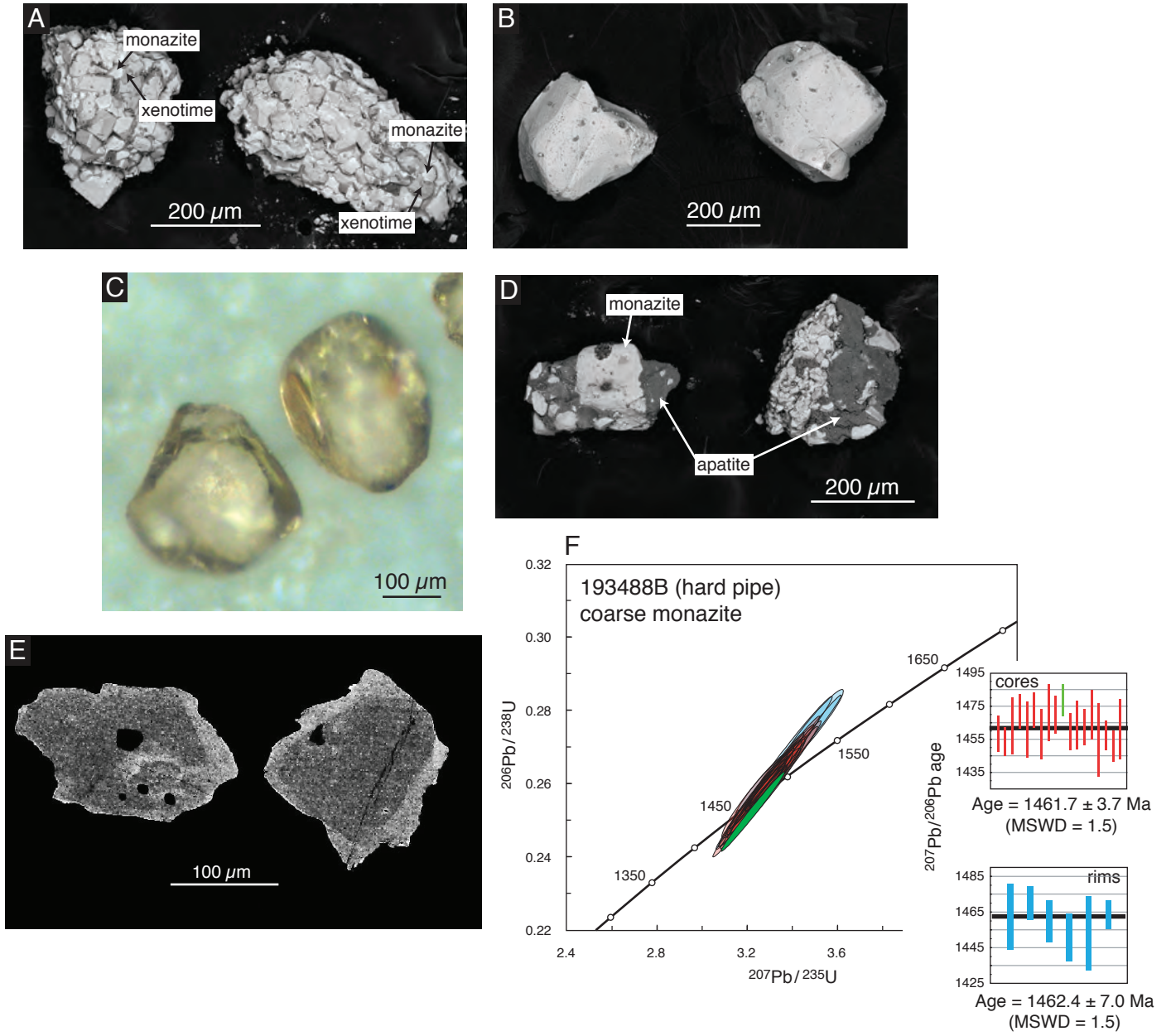


Figure 10

Figure 11

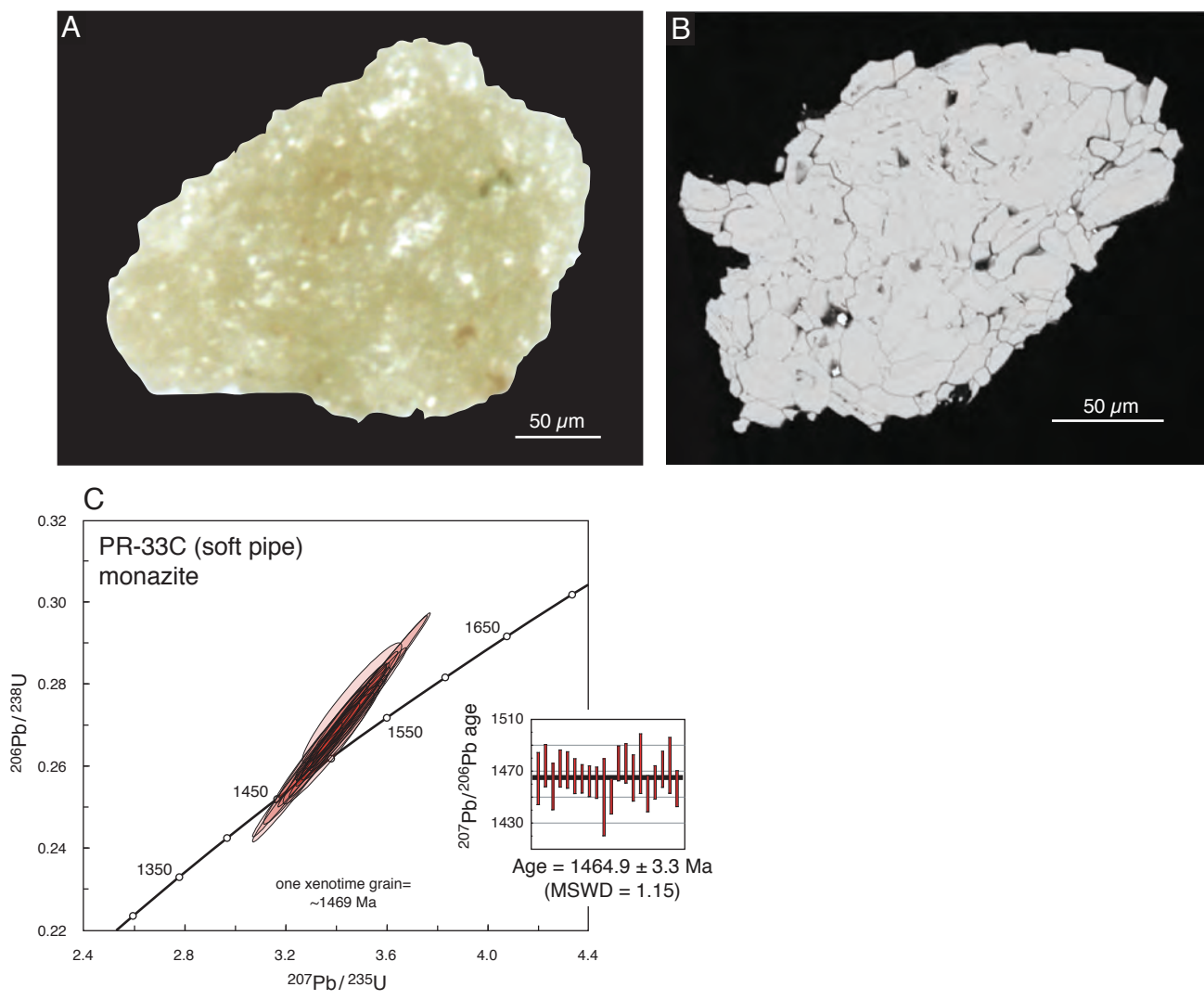


Figure 11

Figure 12

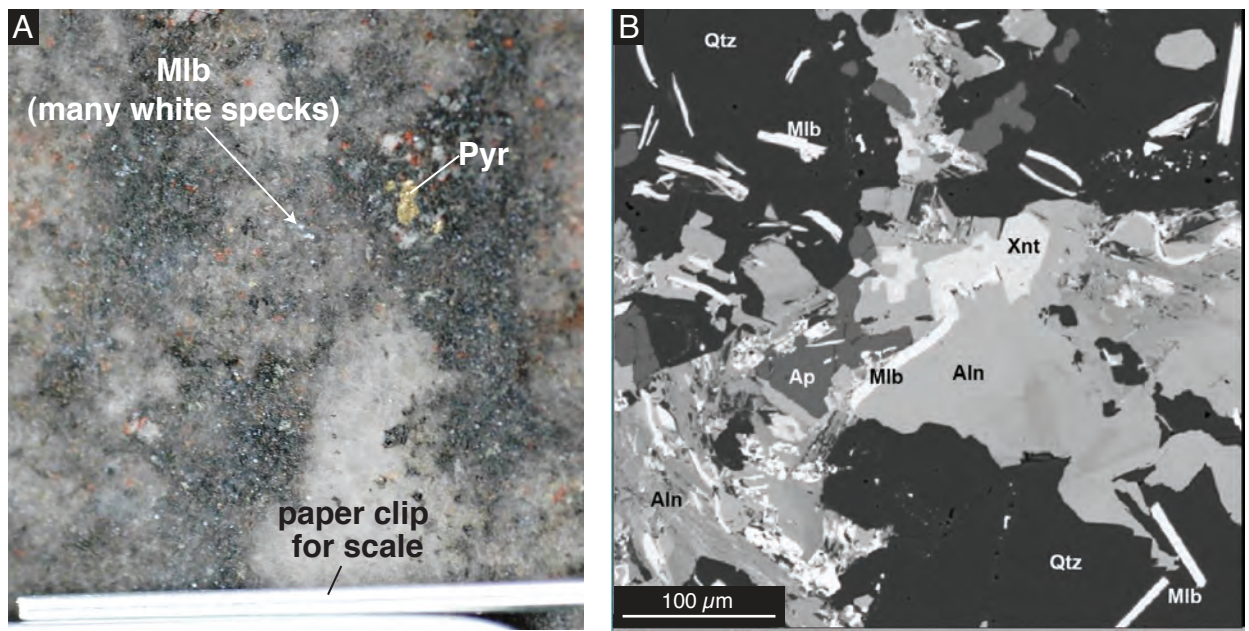


Figure 12

Figure 13

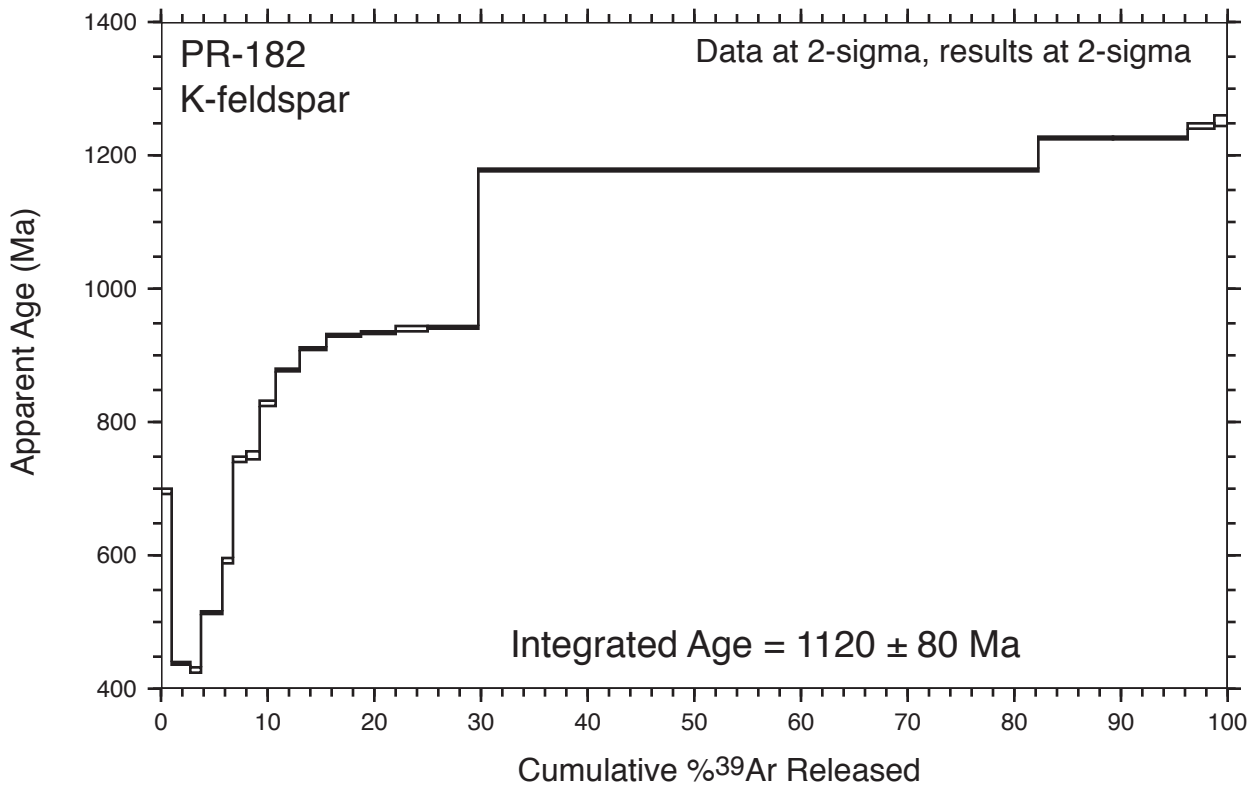
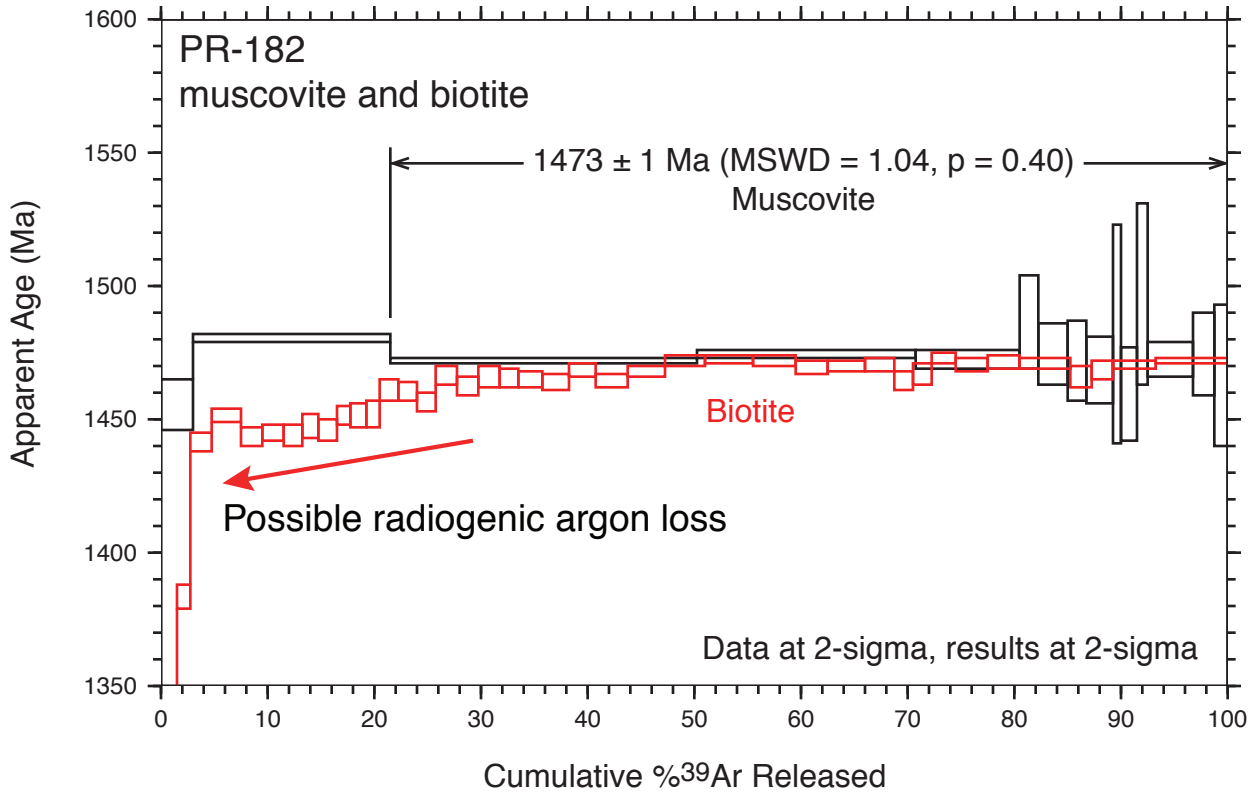


Figure 13

Figure 14

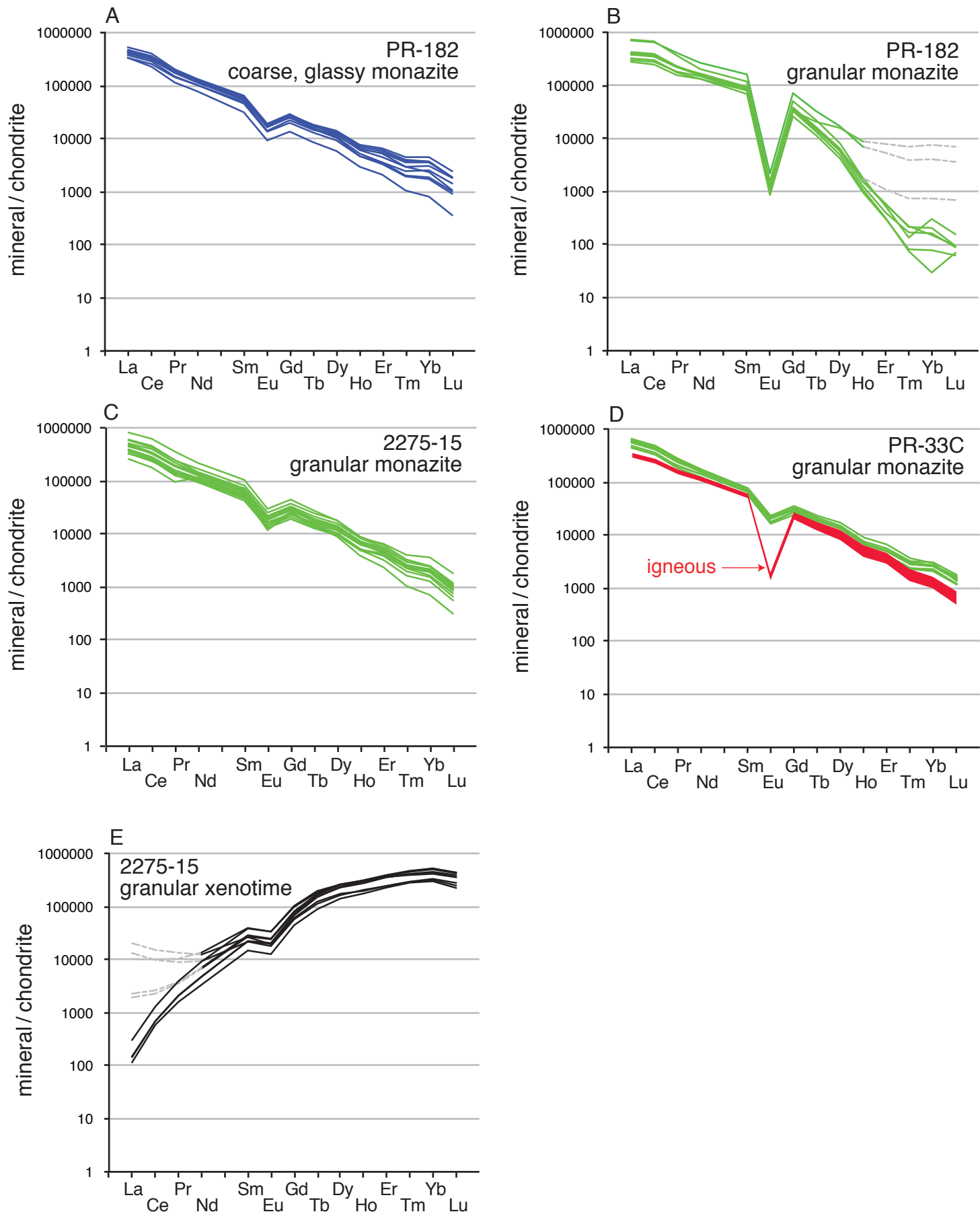


Figure 14

Figure 15

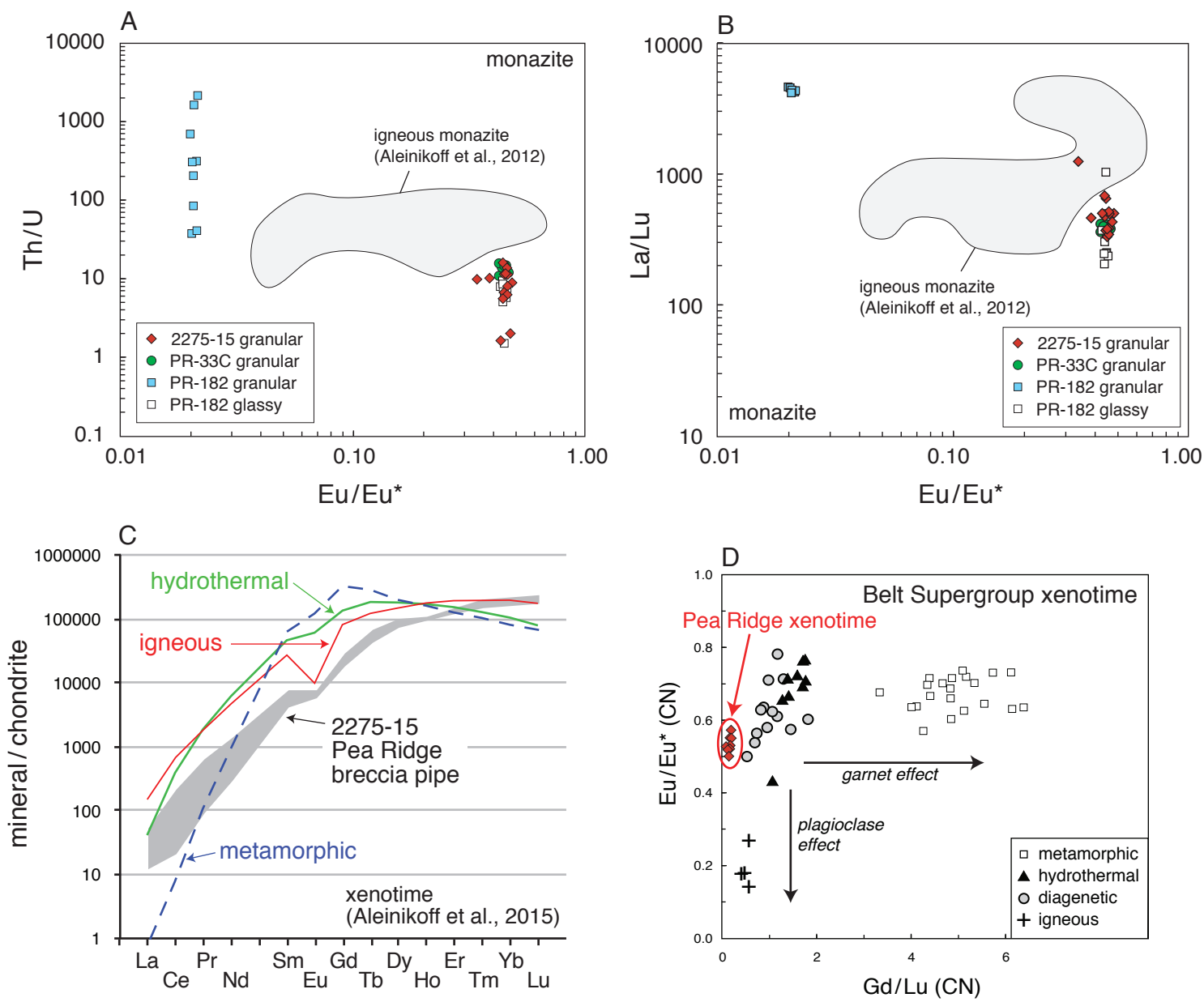


Figure 15

Table 1. SHRIMP U-Th-Pb data for zircon, monazite, and xenotime from Mesoproterozoic rocks of Pea Ridge, St. Francois Mountains, Missouri.

sample <sup>1</sup>	measured $\frac{^{204}\text{Pb}}{^{206}\text{Pb}}$	measured $\frac{^{207}\text{Pb}}{^{206}\text{Pb}}$	% common $^{206}\text{Pb}$	U (ppm)	Th/U	in Ma				$\frac{^{207}\text{Pb}^4}{^{235}\text{U}}$	err <sup>3</sup> (%)	$\frac{^{206}\text{Pb}^4}{^{238}\text{U}}$	err <sup>3</sup> (%)	□ ho
						$\frac{^{206}\text{Pb}^2}{^{238}\text{U}}$	err <sup>3</sup>	$\frac{^{207}\text{Pb}^2}{^{206}\text{Pb}}$	err <sup>3</sup>					
PR-12 (rhyolite)														
zPR-12-2.1	0.000045	0.0927	0.072	132	0.425	1509	38	1470	19	3.351	3.0	0.2638	2.8	0.940
zPR-12-3.1	0.000077	0.0935	0.125	95	0.551	1463	40	1476	23	3.246	3.3	0.2547	3.0	0.928
zPR-12-4.1	0.000000	0.0929	0.000	107	0.513	1447	39	1485	20	3.223	3.2	0.2517	3.0	0.945
zPR-12-5.1	0.000028	0.0930	0.045	263	0.387	1468	33	1481	13	3.267	2.6	0.2557	2.5	0.965
zPR-12-6.1	0.000051	0.0924	0.082	102	0.454	1430	38	1460	21	3.139	3.2	0.2484	3.0	0.938
zPR-12-7.1	0.000008	0.0937	0.012	227	0.562	1453	33	1499	13	3.261	2.6	0.2528	2.5	0.966
zPR-12-8.1	0.000033	0.0926	0.054	214	0.474	1488	34	1470	14	3.297	2.7	0.2596	2.6	0.960
zPR-12-9.1	-0.000047	0.0916	-0.076	119	0.410	1467	52	1473	33	3.251	4.3	0.2555	4.0	0.914
zPR-12-10.1	0.000025	0.0922	0.040	227	0.395	1507	34	1465	14	3.336	2.7	0.2633	2.5	0.961
zPR-12-11.1	0.000018	0.0925	0.029	102	0.430	1411	38	1472	20	3.112	3.2	0.2447	3.0	0.942
zPR-12-12.1	0.000135	0.0925	0.220	108	0.469	1480	39	1439	24	3.225	3.2	0.2580	3.0	0.919
zPR-12-13.1	0.000053	0.0944	0.086	111	0.519	1458	39	1500	21	3.275	3.2	0.2537	3.0	0.936
zPR-12-14.1	0.000117	0.0924	0.190	107	0.451	1464	39	1441	23	3.191	3.2	0.2550	3.0	0.925
zPR-12-15.1	0.000085	0.0930	0.137	183	0.244	1510	36	1463	17	3.340	2.8	0.2639	2.7	0.945
zPR-12-16.1	0.000097	0.0931	0.157	120	0.462	1494	39	1462	22	3.300	3.1	0.2609	2.9	0.929
zPR-12-17.1	-0.000033	0.0916	-0.054	164	0.458	1467	36	1469	16	3.245	2.8	0.2555	2.7	0.954
zPR-12-18.1	0.000014	0.0928	0.023	277	0.422	1489	33	1479	13	3.315	2.6	0.2598	2.5	0.966
zPR-12-19.1	0.000070	0.0927	0.114	136	0.669	1513	38	1461	20	3.345	3.0	0.2646	2.8	0.938
zPR-12-20.1	0.000073	0.0940	0.118	136	0.674	1424	37	1488	20	3.170	3.1	0.2472	2.9	0.938
PR-91 (rhyolite)														
zPR-91-1.1	0.000016	0.0926	0.025	348	0.493	1427	31	1475	11	3.155	2.5	0.2477	2.4	0.973
zPR-91-2.1	0.000008	0.0926	0.013	237	0.381	1443	33	1477	13	3.198	2.6	0.2509	2.5	0.964
zPR-91-3.1	0.000011	0.0921	0.018	334	0.469	1474	32	1466	11	3.255	2.5	0.2568	2.4	0.972
zPR-91-4.1	0.000034	0.0934	0.055	399	0.451	1408	27	1486	11	3.127	2.2	0.2441	2.2	0.967
zPR-91-5.1	0.000007	0.0927	0.011	281	0.442	1462	32	1479	12	3.248	2.5	0.2545	2.5	0.969
zPR-91-6.1	0.000026	0.0924	0.042	282	0.499	1475	33	1467	12	3.261	2.6	0.2571	2.5	0.967
zPR-91-7.1	0.000039	0.0919	0.063	240	0.498	1443	33	1455	14	3.161	2.6	0.2509	2.5	0.961
zPR-91-8.1	0.000053	0.0936	0.086	186	0.672	1482	35	1484	17	3.309	2.8	0.2585	2.6	0.950
zPR-91-9.1	0.000030	0.0927	0.049	247	0.460	1463	33	1473	13	3.242	2.6	0.2547	2.5	0.963
zPR-91-10.1	0.000005	0.0919	0.009	346	0.453	1464	32	1463	11	3.225	2.5	0.2549	2.4	0.973
zPR-91-11.1	0.000018	0.0919	0.029	321	0.469	1454	32	1461	12	3.197	2.5	0.2529	2.4	0.967
zPR-91-12.1	0.000030	0.0924	0.049	298	0.481	1453	32	1468	12	3.208	2.5	0.2529	2.5	0.968
zPR-91-13.1	0.000035	0.0929	0.057	211	0.568	1413	33	1476	15	3.123	2.7	0.2450	2.6	0.959

zPR-91-14.1	0.000048	0.0925	0.077	282	0.488	1482	33	1464	13	3.273	2.6	0.2585	2.5	0.962
zPR-91-15.1	0.000019	0.0942	0.031	316	0.533	1451	32	1506	12	3.267	2.5	0.2524	2.5	0.968
zPR-91-16.1	0.000026	0.0914	0.042	218	0.442	1440	33	1447	14	3.142	2.7	0.2503	2.6	0.960
zPR-91-17.1	0.000018	0.0924	0.029	317	0.472	1499	33	1470	12	3.326	2.5	0.2619	2.4	0.970
zPR-91-18.1	0.000000	0.0925	0.000	190	0.677	1486	35	1478	16	3.307	2.8	0.2593	2.7	0.954
zPR-91-19.1	0.000013	0.0918	0.021	457	0.518	1456	31	1460	18	3.203	2.5	0.2535	2.4	0.928
zPR-91-20.1	-0.000004	0.0927	-0.007	473	0.575	1465	31	1483	10	3.263	2.4	0.2552	2.4	0.977

966-5 (felsic dike)

Session 1

z966-5-1.1	0.000048	0.0924	0.077	222	0.412	1441	34	1462	16	3.169	2.7	0.2506	2.6	0.954
z966-5-2.1	0.000027	0.0929	0.044	147	0.606	1399	36	1479	18	3.092	3.0	0.2424	2.8	0.948
z966-5-3.1	0.000061	0.0914	0.099	211	0.429	1491	35	1438	17	3.249	2.8	0.2601	2.6	0.949
z966-5-4.1	0.000419	0.0927	0.687	274	0.473	944	21	1357	26	1.888	2.8	0.1577	2.4	0.879
z966-5-5.1	0.000064	0.0929	0.104	294	0.492	1458	32	1467	13	3.218	2.6	0.2537	2.5	0.963
z966-5-6.1	0.000000	0.0930	0.000	266	0.514	1444	33	1488	13	3.220	2.6	0.2511	2.5	0.967
z966-5-7.1	-0.000017	0.0926	-0.028	217	0.581	1492	35	1485	14	3.333	2.7	0.2603	2.6	0.962
z966-5-8.1	0.000072	0.0927	0.117	272	0.562	1400	32	1461	14	3.067	2.6	0.2426	2.5	0.959
z966-5-9.1	-0.000009	0.0929	-0.014	219	0.668	1444	43	1489	14	3.223	3.4	0.2511	3.3	0.977
z966-5-10.1	0.000201	0.0952	0.326	151	0.523	1282	27	1475	25	2.802	2.7	0.2200	2.3	0.875
z966-5-11.1	0.000076	0.0925	0.123	268	0.486	1449	33	1455	15	3.176	2.6	0.2520	2.5	0.956
z966-5-12.1	0.000050	0.0954	0.080	133	0.478	1366	28	1522	20	3.084	2.5	0.2361	2.3	0.905
z966-5-13.1	0.000007	0.0940	0.012	273	0.614	1423	32	1506	12	3.196	2.6	0.2469	2.5	0.968
z966-5-14.1	0.000027	0.0933	0.044	215	0.567	1473	34	1487	15	3.289	2.7	0.2567	2.6	0.959
z966-5-15.1	0.000034	0.0923	0.056	243	0.579	1317	43	1463	15	2.868	3.7	0.2267	3.6	0.978
z966-5-16.1	0.000012	0.0932	0.020	164	0.526	1423	35	1488	17	3.168	2.9	0.2470	2.8	0.953

Session 2

z966-5-1.1	0.000019	0.0900	0.031	684	0.21	1438	25	1419	12	3.09	1.9	0.250	1.8	0.946
z966-5-2.1	0.000158	0.0879	0.261	1641	0.58	1065	24	1330	10	2.15	2.4	0.182	2.3	0.978
z966-5-3.1	0.000011	0.0909	0.017	391	0.37	1072	19	1441	17	2.31	2.0	0.184	1.8	0.898
z966-5-4.1	0.000503	0.0823	0.853	4356	1.18	559	11	1072	21	0.96	2.3	0.092	2.0	0.887
z966-5-5.1	0.000007	0.0905	0.012	420	0.70	1413	27	1433	14	3.06	2.1	0.245	2.0	0.936
z966-5-6.1	0.000030	0.0915	0.048	685	0.82	1455	25	1449	12	3.18	1.9	0.253	1.8	0.944
z966-5-7.1	0.000025	0.0917	0.040	1070	0.63	1458	25	1454	9	3.20	1.8	0.254	1.8	0.963
z966-5-8.1	0.000004	0.0912	0.006	1721	0.40	1438	24	1450	8	3.14	1.8	0.250	1.8	0.975
z966-5-9.1	0.000486	0.0879	0.811	2072	0.14	838	21	1220	29	1.58	3.0	0.141	2.6	0.870
z966-5-10.1	0.000017	0.0915	0.027	1128	0.74	1430	25	1452	16	3.13	2.0	0.249	1.8	0.906
z966-5-11.1	0.000025	0.0887	0.042	624	0.25	1305	29	1388	23	2.74	2.6	0.225	2.3	0.884
z966-5-12.1	0.000338	0.0918	0.556	1070	0.51	1040	18	1360	24	2.13	2.2	0.178	1.8	0.814
z966-5-13.1	0.000047	0.0912	0.077	397	0.48	1139	27	1437	17	2.45	2.7	0.196	2.5	0.941
z966-5-14.1	0.000010	0.0895	0.016	336	0.53	1459	27	1411	17	3.12	2.1	0.253	1.9	0.907
z966-5-15.1	0.000030	0.0904	0.050	754	0.13	1467	25	1425	11	3.16	1.9	0.255	1.8	0.955
z966-5-16.1	0.000024	0.0915	0.040	126	0.51	1433	29	1448	49	3.13	3.3	0.249	2.0	0.620
z966-5-17.1	0.000030	0.0916	0.049	748	0.67	1357	33	1449	11	2.96	2.6	0.236	2.5	0.974

## PR-25 (felsic dike)

zPR-25-1.1	0.000016	0.0926	0.026	423	0.659	1480	32	1475	11	3.287	2.5	0.2580	2.4	0.972
zPR-25-2.1	0.000080	0.0931	0.129	185	0.564	1429	29	1467	18	3.149	2.4	0.2483	2.2	0.921
zPR-25-3.1	0.000002	0.0926	0.004	785	1.092	1452	29	1478	7	3.224	2.3	0.2527	2.2	0.987
zPR-25-4.1	0.000489	0.0985	0.793	586	0.311	1384	28	1461	35	3.029	2.9	0.2396	2.2	0.768
zPR-25-5.1	0.000004	0.0918	0.006	578	0.688	1434	30	1462	9	3.151	2.4	0.2492	2.3	0.980
zPR-25-6.1	0.000000	0.0936	0.000	324	0.555	1473	32	1500	11	3.313	2.5	0.2568	2.4	0.972
zPR-25-7.1	0.000056	0.0923	0.090	253	0.546	1444	33	1459	15	3.171	2.7	0.2511	2.6	0.958
zPR-25-8.1	-0.000015	0.0932	-0.024	276	0.519	1399	32	1496	13	3.121	2.6	0.2424	2.5	0.965
zPR-25-9.1	-0.000007	0.0930	-0.011	284	0.497	1451	32	1490	19	3.240	2.7	0.2524	2.5	0.926
zPR-25-10.1	0.000045	0.0928	0.073	260	0.533	1398	32	1470	15	3.077	2.7	0.2422	2.6	0.955
zPR-25-11.1	0.000010	0.0928	0.016	623	0.661	1391	29	1482	9	3.080	2.3	0.2409	2.3	0.981
zPR-25-12.1	0.000033	0.0925	0.053	327	0.526	1491	33	1467	13	3.302	2.6	0.2603	2.5	0.966

## PR95-30 matrix monazite and xenotime (in thin section) from hard breccia pipe

mPR95-1.1	0.000004	0.0921	0.007	1563	2.8	1427	20	1468	4	3.144	1.6	0.2478	1.6	0.990
mPR95-2.1	0.000040	0.0920	0.065	520	16.7	1494	30	1456	8	3.289	2.3	0.2609	2.2	0.985
mPR95-4.1	0.000043	0.0920	0.070	536	15.7	1368	29	1455	8	2.980	2.4	0.2364	2.3	0.986
mPR95-5.1	0.000030	0.0915	0.049	640	15.0	1317	27	1449	13	2.847	2.4	0.2266	2.3	0.962
mPR95-6.1	0.000011	0.0917	0.018	1143	2.6	1448	22	1458	7	3.180	1.8	0.2519	1.7	0.978
mPR95-7.1	-0.000002	0.0924	-0.003	1471	2.9	1446	21	1477	7	3.205	1.7	0.2514	1.6	0.977
mPR95-8.1	0.000004	0.0917	0.006	1445	3.4	1439	21	1460	4	3.159	1.7	0.2501	1.6	0.990
mPR95-9.1	0.000016	0.0923	0.025	1362	3.4	1490	22	1469	8	3.302	1.7	0.2600	1.7	0.967
mPR95-11.1	0.000012	0.0920	0.019	1359	3.0	1524	22	1464	4	3.378	1.6	0.2668	1.6	0.991
mPR95-12.1	0.000007	0.0920	0.011	1487	2.3	1520	22	1465	7	3.370	1.7	0.2660	1.6	0.972
mPR95-13.1	0.000010	0.0927	0.016	1448	2.6	1561	22	1478	4	3.496	1.6	0.2740	1.6	0.990
mPR95-14.1	0.000002	0.0917	0.004	1424	1.9	1568	23	1460	8	3.478	1.7	0.2753	1.6	0.966
mPR95-15.1	0.000014	0.0918	0.022	912	2.8	1546	25	1460	5	3.425	1.8	0.2710	1.8	0.989
xPR95-1.1	-0.000055	0.0913	-0.089	1176	8.3	1457	40	1469	16	3.22	3.2	0.254	3.0	0.963
xPR95-2.1	0.000039	0.0912	0.064	1051	0.1	1511	41	1439	15	3.30	3.1	0.264	3.0	0.969
xPR95-3.1	0.000000	0.0911	0.000	1075	2.4	1429	40	1449	13	3.12	3.2	0.248	3.1	0.976
xPR95-4.1	0.000114	0.0929	0.185	1293	0.5	1441	38	1452	14	3.15	3.0	0.251	2.9	0.970
xPR95-5.1	0.000024	0.0917	0.038	789	7.0	1533	63	1455	16	3.38	4.7	0.268	4.6	0.984
xPR95-6.1	0.000037	0.0926	0.060	527	0.2	1605	41	1470	13	3.59	3.0	0.283	2.9	0.974
xPR95-7.1	0.000288	0.0924	0.471	394	0.6	1380	42	1391	43	2.91	4.1	0.239	3.4	0.831
xPR95-8.1	0.000207	0.0926	0.337	406	11.2	1468	44	1419	21	3.16	3.5	0.256	3.3	0.951
xPR95-9.1	0.000045	0.0937	0.072	778	9.8	1662	43	1489	13	3.77	3.0	0.294	2.9	0.974
xPR95-10.1	0.000046	0.0924	0.075	870	1.2	1583	40	1462	12	3.52	2.9	0.278	2.8	0.978
xPR95-11.1	-0.000012	0.0923	-0.020	1160	0.3	1625	39	1478	9	3.66	2.7	0.287	2.7	0.985
xPR95-12.1	-0.000088	0.0921	-0.143	712	3.6	1569	41	1494	13	3.54	3.0	0.276	2.9	0.975

## 2275-15 matrix monazite and xenotime (hand-picked grains) from hard breccia pipe

m2275--1.1	0.000026	0.09	0.041	801	12.5	1542	31	1457	7	3.408	2.3	0.2702	2.3	0.987
m2275--2.1	0.000012	0.09	0.019	1742	5.2	1497	28	1484	13	3.345	2.2	0.2615	2.1	0.954

m2275--3.1	0.000035	0.09	0.056	730	6.8	1527	32	1458	15	3.374	2.5	0.2674	2.3	0.944
m2275--4.1	0.000145	0.09	0.235	710	17.6	1487	34	1467	11	3.291	2.7	0.2594	2.6	0.977
m2275--5.1	0.000013	0.09	0.022	725	7.4	1525	31	1453	7	3.362	2.3	0.2670	2.3	0.987
m2275--6.1	0.000020	0.09	0.032	906	13.9	1542	107	1462	18	3.418	7.8	0.2703	7.8	0.992
m2275--7.1	0.000074	0.09	0.120	556	16.5	1492	32	1458	9	3.287	2.4	0.2605	2.4	0.983
m2275--8.1	0.000022	0.09	0.035	807	9.7	1501	30	1454	7	3.301	2.3	0.2621	2.2	0.988
m2275--9.1	0.000015	0.09	0.024	674	7.4	1513	30	1476	7	3.371	2.3	0.2645	2.2	0.987
m2275--10.1	0.000013	0.09	0.021	1336	5.5	1496	27	1451	10	3.284	2.1	0.2612	2.0	0.966
m2275--11.1	0.000006	0.09	0.010	535	12.6	1570	26	1468	7	3.498	1.9	0.2757	1.9	0.979
m2275--12.1	0.000004	0.09	0.007	842	1.6	1438	29	1461	6	3.161	2.2	0.2500	2.2	0.989
m2275--13.1	0.000002	0.09	0.003	2060	3.1	1584	32	1457	4	3.515	2.3	0.2785	2.3	0.996
m2275--14.1	0.000015	0.09	0.024	1321	4.0	1522	27	1466	5	3.374	2.0	0.2662	2.0	0.992
m2275--15.1	-0.000013	0.09	-0.020	521	6.5	1520	30	1464	7	3.366	2.3	0.2658	2.2	0.987
m2275--16.1	0.000031	0.09	0.050	730	13.1	1494	29	1465	7	3.304	2.2	0.2608	2.2	0.987
m2275--17.1	-0.000008	0.09	-0.013	1477	2.0	1524	42	1473	10	3.392	3.2	0.2667	3.1	0.985
m2275--18.1	0.000038	0.09	0.061	890	12.1	1587	41	1448	7	3.507	2.9	0.2792	2.9	0.991
x2275-15-1.1	0.000066	0.09	0.11	1279	14.4	1531	56	1453	13	3.37	4.2	0.268	4.1	0.986
x2275-15-2.1	0.000015	0.09	0.02	1167	2.7	1891	182	1407	11	4.19	11.1	0.341	11.1	0.999
x2275-15-2.2	0.000009	0.09	0.01	575	3.8	1575	39	1447	13	3.47	2.9	0.277	2.8	0.972
x2275-15-3.1	-0.000071	0.09	-0.12	845	17.2	1579	54	1473	16	3.53	4.0	0.278	3.9	0.978
x2275-15-4.1	0.000022	0.09	0.04	1236	1.9	1588	74	1446	8	3.50	5.3	0.279	5.3	0.997
x2275-15-5.1	0.000215	0.09	0.35	475	11.3	1535	41	1404	30	3.30	3.4	0.269	3.0	0.888
x2275-15-6.1	0.000046	0.09	0.07	2477	0.5	1589	84	1478	18	3.57	6.1	0.280	6.0	0.987

PR-182 coarse glassy monazite (hand-picked grains) from hard pipe

Session 1

mPR182-1.1*	0.000030	0.0913	0.048	681	8.7	1511	29	1445	6	3.311	2.2	0.2641	2.1	0.988
mPR182-2.1	0.000019	0.0928	0.031	918	9.2	1542	28	1478	6	3.448	2.1	0.2702	2.1	0.987
mPR182-3.1	0.000000	0.0924	0.000	817	9.5	1464	28	1476	11	3.248	2.2	0.2549	2.1	0.968
mPR182-4.1*	0.000020	0.0911	0.032	1023	5.9	1485	29	1444	13	3.246	2.3	0.2591	2.2	0.954
mPR182-5.1	0.000022	0.0920	0.036	760	7.9	1506	29	1460	6	3.327	2.2	0.2632	2.1	0.989
mPR182-6.1	0.000013	0.0924	0.020	708	6.1	1515	30	1472	11	3.368	2.3	0.2649	2.2	0.964
mPR182-7.1	0.000010	0.0920	0.017	774	7.1	1523	29	1465	6	3.376	2.1	0.2665	2.1	0.987
mPR182-8.1	0.000019	0.0914	0.031	1060	8.8	1498	28	1449	6	3.286	2.1	0.2616	2.1	0.990
mPR182-8.2*	0.000006	0.0912	0.010	1236	7.4	1502	27	1448	5	3.295	2.0	0.2624	2.0	0.992
mPR182-13.1	0.000002	0.0913	0.003	730	8.3	1538	29	1452	11	3.391	2.2	0.2695	2.1	0.964
mPR182-13.2	-0.000002	0.0921	-0.004	887	9.1	1530	31	1470	6	3.402	2.3	0.2679	2.2	0.989
mPR182-19.1	0.000024	0.0922	0.039	698	8.2	1463	29	1466	6	3.230	2.2	0.2548	2.2	0.988
mPR182-19.2	0.000011	0.0921	0.018	940	6.9	1513	28	1467	6	3.355	2.1	0.2645	2.1	0.989
mPR182-22.1	0.000009	0.0918	0.014	1196	4.6	1486	27	1460	5	3.275	2.0	0.2592	2.0	0.991
mPR182-22.2	0.000016	0.0919	0.026	1696	5.1	1460	27	1461	5	3.215	2.1	0.2542	2.0	0.991
mPR182-26.1	0.000014	0.0918	0.023	803	8.2	1483	29	1459	6	3.266	2.2	0.2586	2.2	0.989
mPR182-26.2	0.000022	0.0920	0.036	825	7.9	1505	29	1462	6	3.327	2.2	0.2630	2.2	0.989
mPR182-27.1	0.000017	0.0917	0.027	610	10.8	1482	30	1456	7	3.260	2.3	0.2585	2.3	0.988

mPR182-27.2*	0.000010	0.0909	0.016	492	10.1	1369	36	1442	10	2.961	2.9	0.2366	2.9	0.983
mPR182-28.1	0.000021	0.0920	0.034	1207	11.6	1478	28	1461	12	3.256	2.2	0.2576	2.1	0.961
mPR182-28.2	0.000024	0.0922	0.039	855	11.3	1454	29	1465	7	3.204	2.2	0.2530	2.2	0.987
mPR182-29.1	0.000009	0.0918	0.014	836	10.9	1502	40	1461	10	3.317	3.0	0.2624	3.0	0.984
mPR182-29.2	0.000018	0.0918	0.030	820	9.9	1525	30	1458	6	3.369	2.2	0.2669	2.2	0.989
mPR182-30.1	0.000027	0.0921	0.045	947	7.9	1438	28	1462	6	3.161	2.2	0.2500	2.1	0.988
mPR182-30.2	0.000012	0.0925	0.019	1132	9.3	1442	28	1475	6	3.193	2.2	0.2506	2.2	0.989
mPR182-9.1	0.000023	0.0929	0.037	580	9.3	1462	32	1479	8	3.250	2.5	0.2546	2.5	0.985
mPR182-10.1	0.000007	0.0922	0.012	694	8.4	1464	30	1468	7	3.236	2.3	0.2550	2.3	0.988
mPR182-11.1	0.000016	0.0921	0.025	1180	8.6	1491	29	1465	7	3.298	2.2	0.2603	2.2	0.987
mPR182-12.1	0.000011	0.0921	0.018	1033	8.2	1461	30	1467	7	3.226	2.3	0.2544	2.3	0.987
mPR182-21.1	0.000013	0.0918	0.021	708	7.9	1504	31	1459	11	3.319	2.4	0.2628	2.3	0.970
mPR182-21.2	0.000013	0.0917	0.022	1259	6.7	1449	29	1458	10	3.181	2.3	0.2521	2.2	0.971

Session 2

mPR182-1.1	0.000006	0.0920	0.009	847	6.9	1648	53	1467	6	3.695	3.6	0.2914	3.6	0.996
mPR182-2.1*	0.000035	0.0917	0.057	676	12.7	1798	81	1451	9	4.044	5.2	0.3216	5.1	0.996
mPR182-3.1	0.000005	0.0921	0.008	521	7.4	1540	40	1467	7	3.424	3.0	0.2699	2.9	0.993
mPR182-4.1	0.000010	0.0925	0.016	789	7.4	1507	37	1476	7	3.355	2.8	0.2633	2.8	0.992
mPR182-5.1	-0.000011	0.0919	-0.018	541	9.7	1564	39	1469	7	3.486	2.8	0.2745	2.8	0.990
mPR182-6.1	0.000023	0.0921	0.037	801	7.8	1604	33	1463	7	3.573	2.3	0.2824	2.3	0.989
mPR182-7.1	0.000003	0.0923	0.005	407	9.5	1519	26	1473	7	3.379	1.9	0.2657	1.9	0.980
mPR182-8.1	-0.000001	0.0917	-0.002	1060	3.1	1530	28	1461	5	3.388	2.1	0.2679	2.1	0.993
mPR182-9.1	0.000016	0.0917	0.027	778	5.6	1544	45	1456	6	3.413	3.3	0.2707	3.3	0.995
mPR182-10.1	0.000029	0.0922	0.048	748	8.6	1484	30	1464	7	3.276	2.3	0.2588	2.3	0.987
mPR182-11.1	0.000011	0.0919	0.018	881	6.5	1526	41	1463	6	3.379	3.1	0.2670	3.1	0.995
mPR182-12.1*	0.000040	0.0916	0.065	718	11.0	1616	78	1447	12	3.576	5.5	0.2849	5.5	0.993
mPR182-13.1	0.000018	0.0921	0.028	618	11.3	1494	26	1465	7	3.304	2.0	0.2609	2.0	0.983
mPR182-14.1	0.000007	0.0917	0.012	580	8.4	1537	39	1458	7	3.400	2.8	0.2693	2.8	0.992
mPR182-15.1*	0.000013	0.0913	0.021	859	9.1	1493	32	1449	7	3.274	2.4	0.2606	2.4	0.990
mPR182-16.1*	0.000027	0.0913	0.044	603	8.5	1524	32	1445	7	3.342	2.4	0.2666	2.4	0.988
mPR182-17.1	0.000003	0.0922	0.005	782	11.8	1447	34	1471	7	3.198	2.7	0.2516	2.6	0.989
mPR182-18.1	0.000029	0.0924	0.047	744	9.8	1512	98	1467	10	3.354	7.3	0.2644	7.3	0.998

193488B coarse glassy monazite (hand-picked grains) from hard pipe

m193488B-1.1	0.000020	0.0919	0.032	777	13.1	1522	26	1459	5	3.363	1.9	0.2663	1.9	0.989
m193488B-2.1	0.000014	0.0915	0.023	1579	3.6	1479	21	1454	4	3.248	1.6	0.2579	1.6	0.990
m193488B-3.1	0.000014	0.0920	0.023	1060	3.5	1459	23	1463	9	3.215	1.8	0.2540	1.7	0.969
m193488B-4.1	0.000006	0.0923	0.010	929	3.4	1510	25	1472	5	3.356	1.9	0.2640	1.8	0.990
m193488B-5.1	0.000009	0.0918	0.014	1372	2.8	1504	21	1461	8	3.324	1.6	0.2628	1.6	0.963
m193488B-5.2*	0.000011	0.0919	0.018	1632	2.7	1567	22	1462	9	3.481	1.7	0.2752	1.6	0.958
m193488B-6.1	0.000011	0.0924	0.018	867	4.0	1458	24	1473	5	3.227	1.9	0.2537	1.9	0.989
m193488B-7.1	0.000014	0.0917	0.022	1219	8.0	1471	22	1458	8	3.235	1.7	0.2563	1.7	0.973
m193488B-7.2*	0.000011	0.0923	0.017	1085	8.2	1554	25	1470	5	3.463	1.8	0.2726	1.8	0.990
m193488B-8.1	0.000011	0.0923	0.018	822	11.5	1480	25	1471	9	3.280	1.9	0.2581	1.9	0.973
m193488B-8.2*	0.000029	0.0920	0.046	695	12.6	1464	27	1460	6	3.222	2.1	0.2550	2.1	0.989

m193488B-9.1	0.000014	0.0923	0.023	724	13.9	1449	26	1470	6	3.202	2.0	0.2521	2.0	0.989
m193488B-9.2*	0.000050	0.0919	0.081	520	18.2	1537	31	1451	7	3.387	2.3	0.2693	2.2	0.988
m193488B-10.1	-0.000001	0.0925	-0.002	1003	2.7	1451	23	1479	5	3.222	1.8	0.2525	1.8	0.990
m193488B-11.1	0.000025	0.0920	0.041	821	12.0	1512	25	1460	6	3.340	1.9	0.2644	1.8	0.988
m193488B-12.1	0.000007	0.0919	0.011	2057	2.2	1505	20	1464	7	3.330	1.5	0.2630	1.5	0.967
m193488B-12.2*	0.000005	0.0914	0.007	1777	2.3	1486	20	1453	10	3.264	1.6	0.2593	1.5	0.941
m193488B-13.1	0.000004	0.0918	0.007	949	4.1	1461	24	1462	5	3.218	1.9	0.2543	1.9	0.989
m193488B-14.1	0.000002	0.0921	0.003	1391	4.3	1496	34	1470	7	3.318	2.6	0.2612	2.5	0.988
m193488B-15.1	-0.000006	0.0913	-0.010	866	5.9	1476	25	1455	11	3.243	2.0	0.2573	1.9	0.956
m193488B-16.1	0.000011	0.0917	0.017	1306	2.7	1486	22	1458	4	3.273	1.7	0.2593	1.7	0.990
m193488B-17.1	0.000010	0.0913	0.016	1325	3.4	1508	22	1451	5	3.315	1.7	0.2636	1.6	0.989
m193488B-17.2*	0.000006	0.0919	0.009	1574	3.5	1505	21	1463	4	3.330	1.6	0.2630	1.6	0.991
m193488B-18.1	0.000018	0.0919	0.029	695	11.9	1484	27	1461	9	3.274	2.1	0.2589	2.0	0.973

PR-33C matrix monazite (hand-picked grains) from soft pipe

mPR33C-1.1	0.000053	0.0926	0.086	1035	15.9	1606	30	1464	10	3.583	2.2	0.2829	2.1	0.970
mPR33C-2.1	0.000050	0.0930	0.081	677	15.4	1513	31	1474	8	3.367	2.4	0.2645	2.3	0.983
mPR33C-3.1	0.000025	0.0919	0.041	1182	12.0	1545	29	1458	9	3.419	2.2	0.2708	2.1	0.976
mPR33C-4.1	0.000075	0.0933	0.121	787	15.3	1563	30	1472	7	3.489	2.2	0.2744	2.2	0.985
mPR33C-5.1	0.000031	0.0926	0.051	835	15.7	1539	30	1471	7	3.427	2.2	0.2697	2.2	0.986
mPR33C-6.1	0.000061	0.0928	0.099	794	14.8	1560	49	1466	7	3.471	3.5	0.2738	3.5	0.995
mPR33C-7.1	0.000034	0.0923	0.055	1006	9.7	1577	41	1464	5	3.510	2.9	0.2771	2.9	0.995
mPR33C-8.1	0.000000	0.0918	0.000	1035	16.3	1545	30	1462	6	3.427	2.2	0.2709	2.2	0.990
mPR33C-9.1	0.000024	0.0920	0.040	1055	14.0	1559	30	1461	6	3.460	2.2	0.2737	2.1	0.989
mPR33C-10.1	0.000048	0.0918	0.078	979	14.9	1569	30	1450	15	3.463	2.3	0.2755	2.2	0.942
mPR33C-11.1	0.000057	0.0920	0.092	709	15.8	1518	30	1451	7	3.338	2.2	0.2655	2.2	0.987
mPR33C-12.1	0.000043	0.0930	0.069	736	17.4	1524	30	1476	7	3.400	2.2	0.2668	2.2	0.987
mPR33C-13.1	0.000088	0.0936	0.143	1348	13.3	1544	24	1476	8	3.449	1.8	0.2706	1.8	0.975
mPR33C-14.1	0.000138	0.0938	0.224	517	22.3	1493	31	1465	9	3.303	2.4	0.2607	2.3	0.980
mPR33C-15.1	0.000075	0.0935	0.122	872	15.2	1513	28	1476	12	3.370	2.2	0.2645	2.1	0.960
mPR33C-16.1	0.000083	0.0924	0.134	815	15.9	1522	29	1453	7	3.353	2.2	0.2664	2.2	0.986
mPR33C-17.1	0.000031	0.0921	0.050	793	15.6	1473	29	1461	6	3.247	2.2	0.2568	2.2	0.988
mPR33C-18.1	0.000023	0.0925	0.037	801	16.5	1467	29	1472	7	3.248	2.3	0.2555	2.2	0.987
mPR33C-19.1	0.000118	0.0940	0.191	1155	13.7	1532	24	1475	11	3.416	1.9	0.2683	1.8	0.952
mPR33C-20.1	0.000067	0.0924	0.109	1018	11.4	1558	24	1457	7	3.448	1.8	0.2734	1.8	0.979

1 Prefix abbreviations: z (zircon), m (monazite), x (xenotime). Asterisk means rim analysis; all other analyses in cores.

2  $^{206}\text{Pb}/^{238}\text{U}$  and  $^{207}\text{Pb}/^{206}\text{Pb}$  ages corrected for common Pb using the  $^{204}\text{Pb}$ -correction method. Decay constants from Steiger and Jäger (1977).

3 1-sigma errors

4 Radiogenic ratios, corrected for common Pb using the  $^{204}\text{Pb}$ -correction method, based on the Stacey and Kramers (1975) model.

Table 2. TIMS Re-Os data for molybdenite from breccia pipe, Pea Ridge, St. Francois Mountains, Missouri.

sample	wt (g)	Re (ppm)	err <sup>1</sup>	<sup>187</sup> Re (ppm)	err <sup>1</sup>	<sup>187</sup> Os (ppb)	err <sup>1</sup>	in Ma			
								Age	err <sup>2</sup>	err <sup>1</sup>	err <sup>3</sup>
RO517-7	0.011	7.61	0.04	4.78	0.03	116.11	0.60	1440.6	1.2	8.0	9.2

1 Uncertainty including all sources of analytical error.

2 Uncertainty including only mass spectrometry error.

3 Uncertainty including all sources of analytical error plus decay constant uncertainty (0.35%).

Table 3.  $^{40}\text{Ar}/^{39}\text{Ar}$  data for minerals from breccia pipe, Pea Ridge, St. Francois Mou

CO <sub>2</sub> Laser Power (Watts)	Relative Isotopic Abundances (x 10 <sup>4</sup> )					
	$^{40}\text{Ar}$ ±1S	$^{39}\text{Ar}$ ±1S	$^{38}\text{Ar}$ ±1S	$^{40}\text{Ar}/^{39}\text{Ar}$ ±1S	$^{38}\text{Ar}/^{39}\text{Ar}$ ±1S	$^{40}\text{Ar}/^{38}\text{Ar}$ ±1S

*PR-182 muscovite,  $J = 0.0016208 \pm 0.0000003$*

1.0	182765.8	43.1	2418.4	11.1	30.8570	5.6437
1.2	1124292.0	66.4	14598.1	11.9	191.9466	5.3729
1.4	1725319.0	86.8	22592.0	13.0	302.7031	5.7017
1.6	1224695.0	68.0	15997.4	12.0	215.0850	5.4776
1.8	588656.1	63.3	7699.8	13.5	115.1803	5.8207
2	103100.0	42.4	1330.6	11.3	2.6626	5.4248
2.1	158879.1	42.8	2073.1	11.4	14.1081	5.4779
2.2	114035.0	42.4	1492.6	11.1	3.9583	5.5321
2.3	142859.5	42.8	1876.8	11.5	31.0933	5.4250
2.4	43492.0	41.2	562.3	11.3	0.0000	5.4251
2.5	96776.1	41.8	1282.8	11.3	15.9180	5.5878
2.6	53091.6	41.3	676.8	11.3	0.0000	5.5324
2.7	266010.5	44.8	3481.2	11.1	45.0808	5.5879
3.6	113783.7	41.8	1485.0	11.4	0.0000	5.3741
4.5	68947.2	41.5	907.9	11.9	25.2155	5.4789

Plateau age =  $1473 \pm 1$  Ma, steps 1.4-4.5 watts, 78.3% of  $^{39}\text{Ar}$ , MSWD = 1.04, integrated age = 1473 Ma

*PR-182 biotite,  $J = 0.0016208 \pm 0.0000003$*

1.0	34079.1	9.6	978.7	6.8	2.5706	4.7849
1.2	76372.8	11.5	1425.6	6.7	19.7345	4.5878
1.4	110212.1	14.2	1805.3	6.7	21.6229	4.7180
1.6	206624.0	17.9	2942.9	6.8	37.5409	4.5878
1.8	391878.4	26.6	5263.1	9.7	95.7259	4.6523
2.0	562537.2	27.6	7473.4	9.1	159.7443	4.6523
2.1	384502.7	23.7	5167.1	8.6	81.8545	4.5878
2.2	386225.8	23.7	5181.0	7.0	104.6737	4.6523
2.3	335589.1	21.8	4504.4	8.6	83.1991	4.7849
2.4	303953.6	21.8	4065.8	8.5	86.2740	4.7849
2.5	295375.7	20.8	3963.7	8.3	78.5226	4.5878
2.6	279885.4	19.8	3734.4	6.9	77.1483	4.5878
2.7	277773.5	18.9	3710.8	8.6	70.6624	4.5878

2.8	263794.7	19.8	3516.6	8.7	47.7542	4.6523
2.9	310779.9	21.8	4107.9	8.4	89.3785	4.5878
3.0	339687.6	22.7	4493.6	8.2	85.7796	4.5878
3.1	346541.3	21.8	4605.3	8.6	93.4124	4.6523
3.2	395826.8	24.7	5210.6	8.3	110.5960	4.6523
3.3	398560.4	24.7	5268.3	8.6	112.9985	4.5878
3.4	383000.4	22.7	5044.4	8.9	103.6355	4.7180
3.5	369885.7	20.8	4875.8	8.7	96.6949	4.4625
3.6	409761.9	25.6	5398.7	8.9	124.7838	4.7181
3.7	489226.9	27.6	6455.2	9.5	154.4448	4.7181
3.8	516670.9	26.6	6791.5	8.6	156.7386	4.7181
3.9	580640.6	31.5	7658.6	9.3	155.1468	4.6523
4	672030.7	35.5	8837.0	8.3	174.7033	4.4625
4.1	757871.4	34.5	9925.0	8.5	217.2174	4.4625
4.2	906955.3	41.4	11867.4	8.9	237.9010	4.8529
4.3	786974.3	40.4	10303.9	8.6	220.1044	4.8529
4.4	596639.9	33.5	7830.1	9.4	151.4985	4.7849
4.5	670228.5	35.5	8792.2	8.9	162.9279	4.6523
4.6	532401.5	26.6	6986.2	8.5	149.8573	4.5878
4.7	375092.7	24.7	4946.7	8.4	89.3785	4.9219
4.8	318197.3	20.8	4186.5	8.5	64.6214	4.6523
4.9	472843.8	27.6	6188.0	6.9	135.8078	4.7849
5.0	600594.0	30.5	7878.3	8.8	147.6821	4.9219
5.1	580777.0	30.5	7610.2	9.0	165.2513	4.7849
5.3	943897.6	41.4	12376.5	10.1	252.2371	4.6524
5.5	365264.2	22.7	4811.2	8.9	80.6483	4.7180
5.7	402670.2	24.7	5294.3	8.8	103.4180	4.5878
6.0	790174.6	39.4	10363.4	8.7	203.0790	4.5245
10.0	1318997.0	50.3	17278.3	9.2	362.2498	4.7850

Integrated age =  $1462 \pm 13$  Ma, no age plateau

*PR-182 K-feldspar,  $J = 0.0016208 \pm 0.0000003$*

1.0	49151.4	10.9	1714.8	7.7	73.0155	4.7107
1.1	50705.2	10.2	3027.1	7.3	80.5296	4.7817
1.2	30430.9	10.0	1864.9	5.4	32.7754	4.5716
1.3	64356.0	11.0	3224.9	7.4	76.1892	4.5716
1.4	35499.6	9.6	1497.8	5.2	21.0297	4.4371
1.5	73901.2	11.2	2376.0	7.3	52.7175	4.3074
1.6	56509.0	11.0	1805.6	7.9	45.8955	4.5038
1.8	94311.7	12.1	2671.9	5.2	42.4350	4.7817

2.0	144944.4	14.9	3817.5	7.2	63.1779	4.5038
2.2	161949.8	14.9	4083.3	7.8	70.6525	4.5038
2.5	217534.4	19.7	5313.4	5.5	108.1341	4.5038
2.8	230975.1	17.7	5615.5	7.4	87.4011	4.7107
3.0	203068.7	16.8	4903.3	8.2	66.2923	4.1831
3.5	334429.9	21.6	8026.6	7.8	124.4279	4.4371
4.0	4895283.0	180.1	87551.2	13.6	1773.1540	4.5053
4.5	682890.6	33.4	11596.9	8.1	221.7852	4.4371
5.0	691444.5	33.4	11737.2	7.9	232.8092	4.5717
5.5	261921.3	18.7	4355.4	5.7	103.8432	4.5038
6.0	107598.6	12.1	1777.8	8.0	62.7231	4.7107

Integrated age =  $1120 \pm 80$  Ma, no age plateau

Note: All data corrected for blanks, radioactive decay, nucleogenic interferences, mass discrimination Canyon sanidine (Kuiper et al., 2008). Argon isotope data acquired by simultaneous collection of :

ntains, Missouri

$(10^{-13} \text{ A})$				$^{39}\text{Ar Mol}$	$^{39}\text{Ar \%}$	$\text{Ca}$
$^{37}\text{Ar}$	$^{36}\text{Ar}$	$^{36}\text{Ar}$	$^{37}\text{Ar}$	$\infty 10^{-14}$	of total	$\pm 1$
$\pm 1\text{S}$	$\pm 1\text{S}$	$\pm 1\text{S}$	$\pm 1\text{S}$			
0.0000	7.1357	4.6572	0.2437	0.07	3.08	0.0000
0.0000	7.0537	6.2104	0.2623	0.45	18.60	0.0000
0.0000	7.1786	8.2721	0.2902	0.69	28.79	0.0000
0.0000	7.2225	7.3195	0.2675	0.49	20.39	0.0000
0.0000	7.2226	3.7502	0.2574	0.23	9.81	0.0000
0.0000	7.0947	0.6680	0.2378	0.04	1.70	0.0000
0.6082	7.1364	1.5222	0.2388	0.06	2.64	0.0051
0.0000	7.1365	0.7385	0.2378	0.05	1.90	0.0000
0.0000	7.0545	1.0254	0.2373	0.06	2.39	0.0000
0.0000	7.0546	0.5516	0.2356	0.02	0.72	0.0000
0.0000	7.0547	0.4871	0.2368	0.04	1.63	0.0000
0.0000	7.0548	0.6489	0.2350	0.02	0.86	0.0000
0.0000	6.9774	1.5799	0.2401	0.11	4.44	0.0000
0.0000	7.0959	0.8819	0.2375	0.05	1.89	0.0000
0.0000	7.2243	0.2383	0.2358	0.03	1.16	0.0000
74 $\pm$ 2 Ma						
6.9470	5.4053	3.6892	0.0766	0.03	0.38	0.6087
0.0000	4.2807	37.3717	0.1661	0.04	0.55	0.0000
0.0000	4.2134	14.2530	0.1111	0.06	0.70	0.0000
0.0000	5.6497	3.9780	0.0863	0.09	1.14	0.0000
0.0000	4.2807	8.3213	0.0994	0.16	2.03	0.0000
0.0000	4.2134	12.7109	0.1310	0.23	2.88	0.0000
7.4390	4.2134	4.5514	0.0912	0.16	1.99	0.1237
0.0000	4.2807	5.0833	0.0883	0.16	2.00	0.0000
0.0000	4.2134	4.2812	0.0951	0.14	1.74	0.0000
0.0000	4.4187	4.2065	0.0814	0.12	1.57	0.0000
0.0000	5.4862	2.4939	0.0737	0.12	1.53	0.0000
0.0000	4.3491	2.2258	0.0718	0.11	1.44	0.0000
6.7699	4.1474	1.8227	0.0823	0.11	1.43	0.1570

0.0000	5.3250	2.2861	0.0813	0.11	1.36	0.0000
0.0000	4.1474	2.6891	0.0804	0.13	1.59	0.0000
6.4354	5.4053	2.7391	0.0813	0.14	1.73	0.1234
0.0000	4.4187	1.6999	0.0862	0.14	1.78	0.0000
0.0000	5.8152	1.8558	0.0842	0.16	2.01	0.0000
3.0406	4.2807	1.8583	0.0746	0.16	2.03	0.0498
0.0000	4.1474	1.4313	0.0765	0.15	1.95	0.0000
0.0000	4.0827	1.3365	0.0852	0.15	1.88	0.0000
0.0000	4.0827	2.5114	0.0842	0.16	2.08	0.0000
0.0000	4.0827	1.7526	0.0813	0.20	2.49	0.0000
0.0000	4.4894	1.8872	0.0881	0.21	2.62	0.0000
0.0000	4.3491	2.0512	0.0832	0.23	2.96	0.0000
0.0000	5.8152	1.9938	0.0852	0.27	3.41	0.0000
0.0000	4.2134	2.9606	0.0970	0.30	3.83	0.0000
0.0000	4.0194	3.4189	0.1010	0.36	4.58	0.0000
0.0000	4.3491	3.4395	0.1100	0.31	3.98	0.0000
0.0000	4.2134	2.2744	0.0940	0.24	3.02	0.0000
0.0000	4.4187	2.1677	0.0921	0.27	3.39	0.0000
0.0000	4.2134	1.6617	0.0950	0.21	2.70	0.0000
0.0000	4.2807	1.4770	0.0784	0.15	1.91	0.0000
0.0000	4.1474	1.0578	0.0822	0.13	1.62	0.0000
4.9102	4.2134	1.4902	0.0823	0.19	2.39	0.0688
17.6333	5.4862	1.7182	0.0823	0.24	3.04	0.1940
0.0000	4.4187	1.7740	0.0970	0.23	2.94	0.0000
0.0000	4.2807	2.8706	0.1020	0.38	4.78	0.0000
0.0000	4.4187	1.0685	0.0813	0.15	1.86	0.0000
0.0000	4.2807	1.1450	0.0784	0.16	2.04	0.0000
6.6518	5.6497	2.3115	0.1010	0.32	4.00	0.0557
0.0000	4.2807	3.7222	0.1202	0.53	6.67	0.0000
13.2348	4.2807	1.2094	0.0557	0.05	1.03	0.6806
0.0000	5.8987	0.8027	0.0531	0.09	1.81	0.0000
0.0000	4.2134	0.3459	0.0506	0.06	1.12	0.0000
0.0000	4.3491	0.7064	0.0531	0.10	1.93	0.0000
0.0000	4.4187	0.2949	0.0498	0.05	0.90	0.0000
15.9014	5.1662	1.2688	0.0557	0.07	1.42	0.5910
0.0000	4.1474	0.1243	0.0498	0.06	1.08	0.0000
8.2853	4.2134	0.5778	0.0557	0.08	1.60	0.2740

0.0000	5.4053	0.5210	0.0584	0.12	2.29	0.0000
0.0000	4.2134	0.3334	0.0593	0.12	2.45	0.0000
0.0000	4.4187	0.5592	0.0629	0.16	3.18	0.0000
15.9310	4.0827	0.7645	0.0620	0.17	3.36	0.2510
0.0000	5.4053	0.5684	0.0638	0.15	2.94	0.0000
9.3086	4.2807	1.6857	0.0770	0.24	4.81	0.1027
15.6062	4.3491	28.5950	0.2770	2.67	52.44	0.0158
0.0000	4.3491	5.1450	0.1301	0.35	6.95	0.0000
0.0000	4.2807	5.0353	0.1098	0.36	7.03	0.0000
0.0000	4.2807	1.9547	0.0790	0.13	2.61	0.0000
23.3503	4.0827	0.7947	0.0685	0.05	1.06	1.1644

ation, and detector intercalibration. Ages calculated with decay constants in Min et al. (2000), ; all masses on faraday collectors (40-37) and ion counter (36) with a Thermo Scientific ARGUSVI n

Derived Results					
$\lambda/K$	$^{40}\text{Ar}^*/^{39}\text{Ar}$		$\%^{40}\text{Ar}^*$	Age (Ma)	
$1\sigma$	$\pm 1\sigma$			$\pm 2\sigma$	
0.0512	74.9	0.3	99.2	1454.9	9.3
0.0084	76.8	0.1	99.8	1480.1	1.7
0.0055	76.2	0.0	99.9	1471.8	1.2
0.0078	76.4	0.1	99.8	1473.9	1.5
0.0163	76.2	0.1	99.8	1472.4	3.6
0.0926	77.3	0.7	99.8	1486.0	17.4
0.0598	76.4	0.4	99.7	1473.9	11.2
0.0831	76.2	0.6	99.8	1471.5	15.1
0.0653	75.9	0.5	99.8	1467.7	12.4
0.2185	76.9	1.6	99.6	1481.7	41.1
0.0957	75.2	0.7	99.8	1459.2	17.8
0.1815	78.1	1.3	99.6	1496.4	34.4
0.0349	76.2	0.2	99.8	1472.0	6.5
0.0833	76.4	0.6	99.8	1474.2	15.6
0.1389	75.8	1.0	99.9	1466.3	26.5
0.4737	33.7	0.2	96.8	797.0	9.1
0.2577	45.6	0.2	85.3	1012.5	7.4
0.2003	58.6	0.2	96.1	1221.9	6.6
0.1648	69.7	0.2	99.4	1383.3	4.5
0.0698	73.9	0.1	99.4	1440.7	3.7
0.0484	74.6	0.1	99.3	1451.2	2.5
0.0701	74.1	0.1	99.7	1443.2	3.3
0.0710	74.1	0.1	99.6	1444.4	2.7
0.0804	74.1	0.1	99.6	1443.7	3.8
0.0935	74.3	0.2	99.6	1447.0	4.2
0.1191	74.2	0.2	99.7	1445.4	4.2
0.1002	74.6	0.1	99.8	1451.2	3.7
0.0962	74.6	0.2	99.8	1450.7	4.7

0.1304	74.7	0.2	99.7	1451.8	5.0
0.0870	75.3	0.2	99.7	1460.3	4.1
0.1036	75.3	0.1	99.8	1460.1	3.7
0.0827	75.0	0.1	99.8	1456.2	3.7
0.0962	75.7	0.1	99.9	1465.8	3.2
0.0701	75.4	0.1	99.9	1461.8	3.3
0.0709	75.7	0.1	99.9	1465.4	3.6
0.0722	75.7	0.1	99.9	1464.8	3.6
0.0653	75.6	0.1	99.8	1464.4	3.3
0.0546	75.6	0.1	99.9	1463.9	3.0
0.0571	75.9	0.1	99.9	1467.7	2.6
0.0491	75.6	0.1	99.9	1464.2	2.4
0.0569	75.8	0.1	99.9	1467.3	1.9
0.0367	76.2	0.1	99.9	1471.4	1.7
0.0293	76.2	0.1	99.9	1472.1	1.5
0.0365	76.2	0.1	99.9	1471.5	1.7
0.0466	76.0	0.1	99.9	1469.2	2.4
0.0435	76.0	0.1	99.9	1469.7	2.0
0.0522	76.0	0.1	99.9	1469.6	2.5
0.0749	75.6	0.1	99.9	1464.2	3.4
0.0858	75.8	0.2	99.9	1466.8	4.1
0.0590	76.2	0.1	99.9	1472.4	2.2
0.0604	76.1	0.1	99.9	1470.2	2.3
0.0503	76.1	0.1	99.9	1470.9	2.4
0.0300	76.1	0.1	99.9	1470.4	1.7
0.0797	75.7	0.1	99.9	1465.7	3.8
0.0702	75.9	0.1	99.9	1467.6	3.4
0.0473	76.1	0.1	99.9	1470.3	1.7
0.0215	76.2	0.0	99.9	1471.4	1.1

0.2201	28.4	0.1	99.4	693.9	5.2
0.1719	16.6	0.0	99.5	436.8	1.9
0.1994	16.2	0.0	99.4	426.2	2.3
0.1190	19.8	0.0	99.6	510.4	2.1
0.2605	23.5	0.1	99.5	591.4	3.6
0.1920	30.9	0.1	99.6	743.6	3.8
0.2029	31.2	0.1	99.9	749.0	5.4
0.1393	35.2	0.1	99.8	826.0	2.6

0.1252	37.9	0.1	99.9	875.8	2.6
0.0912	39.6	0.1	99.9	906.9	2.7
0.0735	40.8	0.0	99.9	929.8	1.5
0.0643	41.0	0.1	99.9	933.3	1.9
0.0976	41.3	0.1	99.9	938.2	2.5
0.0472	41.5	0.0	99.9	942.2	1.4
0.0044	55.7	0.0	99.8	1177.9	0.3
0.0332	58.7	0.0	99.8	1223.0	1.3
0.0323	58.7	0.0	99.8	1223.4	1.2
0.0871	59.9	0.1	99.8	1241.8	2.4
0.2037	60.4	0.3	99.9	1248.8	8.1

atmospheric  $^{40}\text{Ar}/^{36}\text{Ar}$  = 298.56 +/- 0.31 (Lee et al, 2006) and age of 28.201 +/- 0.046 for Fish nass spectrometer.

Table 4. Summary of geochronological data. Pea Ridge, St. Francois Mountains, Missouri.

Sample number	rock type	mineral <sup>1</sup>	primary age (Ma) <sup>2, 3, 4</sup>	older ages (Ma) <sup>2, 3, 4</sup>	younger ages (Ma) <sup>2, 3, 4</sup>
<b>SHRIMP U-Pb</b>					
PR-12	rhyolite (black)	zir	1473.6±8.0 (20)		
PR-91	rhyolite (pink)	zir	1472.7±5.6 (20)		
966-5	felsic dike	zir	1441±9 (12)	1455-1522	
PR-25	felsic dike	zir		1459-1500	
PR95-30	breccia pipe (hard)	mnz(c)	1464.1±3.6 (9)	ca. 1479 (1)	1454.6±9.6 (3)
PR95-30	breccia pipe (hard)	xnt	1468.0±8.0 (10)		
2275-15	breccia pipe (hard)	mnz(g)	1462.0±3.5 (17)		1448±7 (1)
2275-15	breccia pipe (hard)	xnt	1453±11 (5)		ca. 1405 (2)
PR-182	breccia pipe (hard)	mnz(g)	nd (high <sup>204</sup> Pb)		
PR-182	breccia pipe (hard)	mnz(c)	1464.8±2.1 (40)		1447.2±4.7 (9)
193488B	breccia pipe (hard)	mnz(g)	nd		
193488B	breccia pipe (hard)	mnz(c)	1461.7±3.7 (19)	ca. 1479 (1)	
PR-33C	breccia pipe (soft)	mnz(g)	1464.9±3.3 (20)		
PR-33C	breccia pipe (soft)	xnt	ca. 1469 (1)		
<b>Re-Os</b>					
2475-11	breccia pipe (hard)	mlb	1440.6±9.2 (1)		
<b><sup>40</sup>Ar/<sup>39</sup>Ar</b>					
PR-182	breccia pipe (hard)	mus	1473±1		
PR-182	breccia pipe (hard)	bio	~1440-1470		
PR-182	breccia pipe (hard)	ksp	~400-1200		

- 1 Abbreviations: zir (zircon), mnz(c) (monazite-coarse, glassy), mnz(g) (monazite-granular), xen (xenotime), mlb (molybdenite), mus (muscovite), bio (biotite), ksp (K-feldspar)
- 2 Two-sigma errors
- 3 Ages listed with uncertainties are calculated for sample sizes >3.
- 4 Value in parentheses is number of analyses.

Table 5. Trace element data for monazite and xenotime from breccia pipes, plus one whole-rock sample, Pea Ridge, St. Francois Mountains, Missouri

Sample <sup>1</sup>	La <sup>2</sup>	Ce <sup>2</sup>	Pr <sup>2</sup>	Nd <sup>2</sup>	Sm <sup>2</sup>	Eu <sup>2</sup>	Gd <sup>2</sup>	Tb <sup>2</sup>	Dy <sup>2</sup>	Ho <sup>2</sup>	Er <sup>2</sup>	Tm <sup>2</sup>	Yb <sup>2</sup>	Lu <sup>2</sup>	Th <sup>2</sup>	U <sup>2</sup>	Chondrite-normalized	
																	Eu/Eu*	La/Lu
PR-182 monazite																		
PR182cg-1.1	94768	184268	15491	55400	7950	883	4600	529	2580	285	630	66	445	44	8360	1028	0.445	254
PR182cg-2.1	113905	222441	18765	61639	9640	1103	5644	624	2947	289	591	53	303	28	8121	1073	0.456	478
PR182cg-3.1	104719	209675	16444	54926	8565	912	4991	610	3251	397	920	82	421	33	6318	786	0.425	375
PR182cg-4.1	120798	229506	19458	62429	9878	1127	6086	724	3690	440	1065	107	659	57	8648	1401	0.443	249
PR182cg-5.1	117349	231860	18711	60465	9225	1067	5626	652	3283	386	965	98	653	58	5369	928	0.451	239
PR182cg-6.1	130893	251732	19926	65080	10092	1108	5904	659	3043	316	641	55	331	31	9182	1236	0.438	503
PR182cg-7.1	146770	289251	22568	71563	11218	1225	6519	724	3424	367	801	81	551	57	5940	1159	0.437	306
PR182cg-8.1	94782	164831	12296	41717	5251	583	3077	353	1626	180	367	28	143	11	5143	3382	0.442	1039
PR182cg-9.1	122297	229238	19128	62632	9727	1074	5833	691	3594	439	1104	110	671	58	9678	1021	0.434	249
PR182cg-10.1	130837	259984	21370	67893	10626	1175	6348	747	3870	474	1194	125	805	75	9010	1043	0.436	207
PR182gm-1.1*																		
PR182gm-2.1	165936	394737	38211	123201	23519	121	14433	1198	4167	378	850	97	652	101	129020	3399	0.020	
PR182gm-3.1	171873	409245	34391	95088	17585	87	10258	798	1987	97	82	3	48	4	6958	10	0.020	4656
PR182gm-4.1	89690	211839	20839	72098	12161	62	6638	546	1403	69	65	4	27	3	3304	10	0.021	4236
PR182gm-5.1*	102966	243394	21371	74686	13294	65	7195	585	1530	83	92	5	34	3	6039	20	0.020	4567
PR182gm-6.1*	96140	227315	20944	72643	13270	64	6791	534	1536	97	173	18	120	19	11002	129	0.020	
PR182gm-7.1	76296	184668	16370	60159	12056	62	6642	759	3848	488	1253	172	1205	200	224831	5421	0.021	
PR182gm-8.1	72320	171744	17057	69385	11945	62	6490	487	1224	59	50	2	5	2	5690	3	0.021	4363
PR182gm-9.1	65319	149675	14386	61917	10286	50	5287	413	1039	52	49	2	13	2	7739	5	0.021	4395
PR182gm-10.1	94503	217178	20545	77190	13870	69	7698	605	1589	85	89	6	24	3	6281	30	0.020	4177
2275-15 monazite																		
2275gm-1.1	170295	335917	27258	79574	12734	1465	7841	915	4610	539	1234	117	688	60	11952	1026	0.447	335
2275gm-2.1	93358	172022	16108	60213	9008	1114	5604	606	3023	338	727	57	294	22	6843	757	0.478	505
2275gm-3.1	143950	291873	24415	75034	11665	1284	6884	821	4137	472	1013	87	460	36	12172	754	0.437	479
2275gm-4.1	139247	254033	21849	73932	11797	1357	7438	821	3894	418	828	65	315	25	8778	1290	0.442	656
2275gm-5.1	101646	196247	16334	55561	8394	979	5459	691	3744	441	941	76	402	32	10581	909	0.441	375
2275gm-6.1	91980	180022	13909	51703	7425	865	4505	547	2775	318	750	67	361	28	9367	1143	0.456	388
2275gm-7.1	125409	245274	21293	68728	10678	1267	6680	811	4093	442	917	76	388	30	10771	934	0.457	499
2275gm-8.1	108062	190299	15035	61636	9808	1231	6522	738	3560	407	905	74	391	29	2189	1069	0.469	435
2275gm-9.1	92230	183832	15402	54968	8070	944	4959	583	3015	329	810	73	415	31	3997	630	0.455	349
2275gm-10.1	231236	454439	39532	118384	18349	1982	10470	1177	5199	541	1055	88	476	40	18089	3197	0.436	690
2275gm-11.1	110584	193516	16041	50696	8798	788	5757	604	2612	250	445	30	135	10	6806	683	0.337	1257
2275gm-12.1	163743	314478	26809	91528	14442	1680	8810	1057	5279	572	1168	96	472	37	16844	1205	0.454	521
2275gm-13.1	134005	235744	20635	68650	10952	1234	7100	787	3821	441	906	72	366	31	7604	4610	0.427	505
2275gm-14.1	72975	131111	10561	63495	9861	969	6051	643	2998	321	612	48	243	18	4515	438	0.382	466
2275gm-15.1	110470	208533	17736	61180	9463	1076	5684	655	3401	403	882	77	408	34	10864	920	0.447	384
PR33C monazite																		
PR33Cgm-1.1	136524	263739	22642	70155	10179	1127	5995	667	3266	366	790	72	433	43	18842	1309	0.440	374
PR33Cgm-2.1	135775	262824	24040	76848	11492	1304	7052	823	4177	489	1052	90	482	38	18253	1346	0.441	425
PR33Cgm-3.1	154470	298968	25050	74406	10765	1210	6243	716	3444	386	829	75	436	46	21680	1437	0.450	394

PR33Cgm-4.1	116355	223198	18564	64205	9378	991	5529	607	2897	321	677	60	342	33	14833	1343	0.419	419
PR33Cgm-5.1	140292	273035	22851	73242	10640	1176	6215	688	3329	373	792	69	410	42	19498	1292	0.441	397
PR33Cgm-6.1	149792	293034	25439	79969	11491	1280	6790	752	3665	409	881	80	494	50	20807	1424	0.442	354
PR33Cgm-7.1	141497	265775	23105	71639	10380	1124	6078	677	3279	369	790	71	426	41	19522	1387	0.431	403
PR33Cgm-8.1	130175	251646	21230	72287	10223	1188	6023	682	3364	375	788	71	413	40	17590	1448	0.462	386
PR33Cgm-9.1	104541	203541	18839	64974	9431	979	5376	568	2716	314	673	60	360	34	15684	987	0.419	365
PR33Cgm-10.1	103738	202685	16595	57038	8449	917	4732	508	2538	286	600	56	332	34	15834	1075	0.442	363
2275-15 xenotime																		
2275gx-1.1**	3049	5850	804	4132	3132	981	11088	3929	38948	10856	37890	6980	49681	6767	752	663	0.507	
2275gx-2.1**	447	1364	321	3006	3900	1315	14991	5355	54116	14539	54990	9860	70119	10615	404	616	0.524	
2275gx-3.1	35	414	191	2125	3139	1078	13208	5226	56877	15502	57702	10822	77781	11544	265	449	0.510	0.000
2275gx-4.1**	524	1564	344	3134	4146	1355	15642	6030	62651	16340	60354	11104	80731	11944	1414	873	0.513	
2275gx-5.1	27	353	145	1487	2124	691	8632	3110	33606	9297	35388	6726	46459	6064	144	532	0.492	0.001
2275gx-6.1	71	780	353	4060	5499	1832	19889	6847	62036	15729	56087	9386	64593	9681	4243	1208	0.534	0.001
2275gx-7.1	34	413	187	2092	3206	1119	13794	5736	61504	16466	60528	11215	81463	11843	199	535	0.513	0.000
2275gx-8.1**	2364	5935	945	6036	5649	1836	18973	6430	62342	15898	55328	9749	67797	9862	2083	743	0.541	
2275gx-9.1**	4666	9037	1212	5517	3777	1072	11748	4334	41629	10422	38070	7052	51748	7567	5993	518	0.491	
2475-11-169.0†	13300	17800	1850	6670	1170	101	695	84.3	395	64.8	173	23.1	143	21				

1 Abbreviations: cg (coarse glassy monazite), gm (granular matrix monazite), gx (granular matrix xenotime)

2 All values are ppm

\* Elevated HREE due to overlap on adjacent xenotime. Not plotted on Fig. 14.

\*\* Elevated LREE due to overlap on adjacent monazite.

† Molybdenite-bearing whole-rock hard pipe sample

Table 6. Gd in coexisting monazite and xenotime  
(sample 2275-15)

Analysis	Gd (mona.) (ppm)	Gd (xeno.) (ppm)	Temp. (°C) <sup>1</sup>
1.4	5143	6966	834 ± 33
9.2	6903	7427	954 ± 41
3.1	4810	7516	772 ± 28
14.1	5554	7759	820 ± 32
5.1	5668	6896	887 ± 37
6.1	6851	4716	1283
14.2	9184	7225	1169
6.2	5246	7768	794 ± 30

1 after Gratz and Heinrich (1998). 1-sigma error, propagated by assuming 5% analytical error based on measurement of Gd in standards.